UNCLASSIFIED

AD NUMBER
AD075184
NEW LIMITATION CHANGE

TO
Approved for public release, distribution
unlimited

FROM
Distribution authorized to U.S. Gov't.
agencies and their contractors;
Administrative/Operational Use; Jul 1954.
Other requests shall be referred to the
Director, Wright Air Development Center,
Wright-Patterson AFB, OH 45433.

AUTHORITY

AFWAL ltr, 5 Jul 1984

AD 075184

rmed Services Technical Information Agenc

Reproduced by

DOCUMENT SERVICE CENTER

KNOTT BUILDING, DAYTON, 2, OHIO

This document is the property of the United States
Government. It is furnished for the duration of the contract and
shall be returned when no longer required, or upon
recall by ASTIA to the following address:
Armed Services Technical Information Agency, Document Service Center,
Knott Building, Dayton 2, Ohio.

THE JET PUMP AS A LUBRICATION OIL SCAVENGE PUMP FOR AIRCRAFT ENGINES

RICHARD G. CUNNINGHAM

DEPARTMENT OF ENGINEERING RESEARCH
THE PENNSYLVANIA STATE UNIVERSITY

JULY 1954

WRIGHT AIR DEVELOPMENT CENTER

ABSTRACT

A study was made of the oil jet pump, in particular the possibility of application as a scavenge pump for aircraft engines. Three major problems treated in the theoretical and experimental investigations are: (a) effect of high viscosity; (b) cavitation and altitude ceiling characteristics; and (c) behavior with an air-oil mixture inducted at the suction port.

An analytical expression is developed which describes pump performance in dimensionless terms: a flow ratio, a pressure-difference ratio, the nozzle to throat area ratio; and two friction loss coefficients.

Oil jet pump efficiency is of the order of 25 per cent at high jet Reynolds numbers (R_N = 10,000 to 30,000) and decreases only slightly as R_N approaches 3,000. Below this point performance drops rapidly; at 1,000, efficiency is about 10 per cent.

Pump capacity is limited by cavitation under certain conditions. Based on a correlation of test results an equation is developed expressing altitude ceiling as a function of cavitation-limited flow ratio, nozzle pressure drop, and design area ratio. Operation at altitudes of 60,000 feet and over is possible, but at reduced pump efficiency.

The jet pump can be oversized to provide the excess capacity needed in the dry-sump system. Equations are developed for use in predicting the air consumption rate of a jet scavenge pump; as a function the primary and secondary oil flow rates and the pressures on the pump. Agreement with test results is good.

Variables in the laboratory program include nozzle to throat area ratio (eight pumps), b = 0.1 to 0.6; nozzle diameter 0.100 to 0.177 inch; nozzle pressure drop 20 to 200 psi; discharge pressure up to 60 psig; primary flow rate 10 to 60 lbs/min; flow ratio 0 to 4.6; pressure-difference ratio 0 to 2.6. Altitude pressures were simulated to over 70,000 feet. Oils used were MIL-L-6081A, Grade 1005; MIL-L-6082A, Grade 1100; and MIL-L-7808 synthetic oil. Oil temperatures were 80 to 190F, for a viscosity range 2 to 100 centistokes. Nozzle and throat-diffuser friction coefficients are correlated versus Reynolds number from 400 to 30,000.

PUBLICATION REVIEW

This report has been reviewed and is approved.

FOR THE COMMANDER:

NORMAN C. APPOLD
Colonel, USAF
Chief, Power Plant Laboratory
Directorate of Laboratories

WADC TR 55-143

iii

LIST OF ILLUSTRATIONS

LIST OF TABLES

INTRODUCTION

The jet pump or eductor, ejector, injector, is a device by means of which one fluid stream is pumped by the action of a high velocity jet of the same or other fluid. The pumping process is a result of transfer of momentum from the jet fluid of the pumped stream. The most familiar applications are the steam-jet air ejector (compressible flow) and the water jet pump. The latter is widely used as a booster for water-well centrifugal pumps.

Oil supplied to aircraft engines is usually removed from the sumps under the lubrication zones by one or more scavenge pumps, and returned to the oil tank. This is usually termed a "dry-sump" system: The volumetric capacity of the scavenge pumps is 1.5 to 6 times the oil rate into the engine, thus maintaining a "dry" engine. Some air is normally pumped from the sump with the oil as a result of the excess pump capacity. Turbojet aircraft engines contain from two to as many as a dozen scavenge pumps. Each pump normally requires an individual mechanical drive arrangement, usually involving one or more gears to take power from the main shaft.

The Objective. - This investigation was undertaken to determine the feasibility of replacing the usual gear-type scavenge pump with the jet pump. Three major problems must be answered: (a) the effect of viscosity, or low Reynolds number on performance; (b) the upper limit of operating pressures and velocities (cavitation); and (c) behavior with a two-phase mixture of air and oil inducted at the suction port, as in the dry-sump system.

CHAPTER I

JET PUMP THEORY

A jet pump is a device by means of which a fluid may be pumped by the action of a high velocity jet of the same, or other fluid. The pumping action is a result of a transfer of momentum from the jet fluid to the fluid being pumped.

Because of the complex nature of the problem, development of the theory of jet pumps has been slow, particularly for compressible flow. There are a large number of references on the subject, but the contributions of Fluegel (1) and Keenan and Newmann (2) (3) are probably the most significant.

In the case of incompressible flow, the analyses by Gibson (4), Gosline and O'Brien (5), Fluegel (1), and Hussmann (6) are of interest in the present problem, that of pumping lubricating oil.

The objectives of the theoretical study, presented in detail in Appendix I, were:

    a. To include the effects of friction in the form of dimension-less coefficients that could be established as some function of viscosity, probably by means of the Reynolds criteria.

    b. To simplify otherwise cumbersome relations through use of "total head" pressures, as opposed to use of static pressure terms.

    c. To clearly differentiate between unavoidable mixing losses and friction losses.

<u>Mechanism of Pumping Action.</u> - As a jet of fluid penetrates a stagnant or slowly moving fluid, a dragging action occurs on the boundary of the jet between the high- and low-velocity particles. Mixing occurs between the jet fluid and the low velocity fluid; and transfer of momenta accelerates the latter in the direction of the flow. As the two flows progress, the mixture stream spreads. The un-disturbed high velocity core progressively decreases in diameter until it disap-pears. (See Fig. 1). Confined by parallel throat walls, the secondary fluid enters a region of decreasing area, that area being the annulus between the mixture stream and the throat wall. At the throat entrance the annular area is the differ-ence between jet and throat area. At the throat exit the mixture stream has spread until it touches the wall of the throat. Then all of the side fluid has been mixed with the primary jet.

<u>Assumptions</u>. - In common with other solutions, the approach may be termed an "approximate" theory, since the details of the mixing process are avoided by use of impulse-momentum relations.

1. The flow streams are one-dimensional at throat entrance and exit.
2. Mixing is completed in the constant area throat, against an adverse pressure gradient.

Derivations of the theoretical relations describing the behavior of the liquid/liquid jet pump are given in Appendix I. These results are summarized as follows.
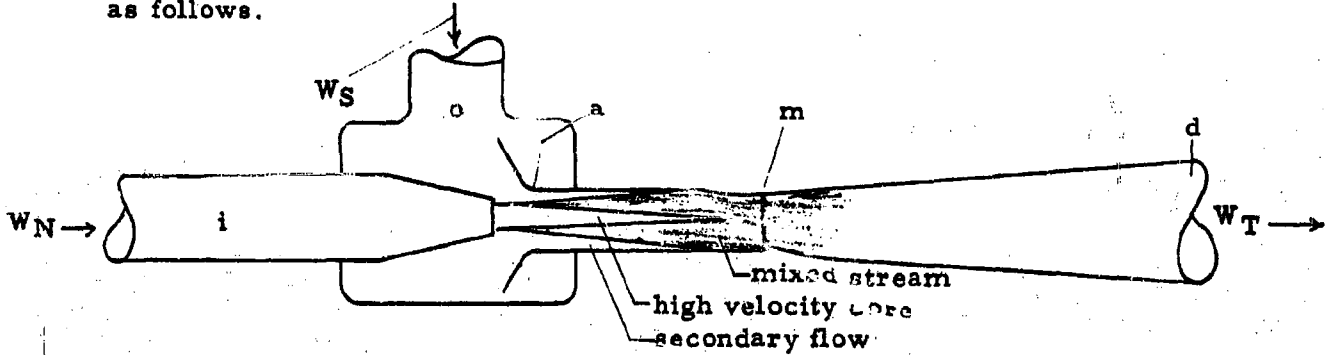
Fig. 1

<u>Nomenclature.</u> - A more complete list is given with the derivation in Appendix I

P	static pressure, lb_f/ft^2
$\bar{P}$	total pressure, lb_f/ft^2
V	velocity, ft/sec
g_c	gravitational constant, $lb_m ft/lb_f sec^2$
ρ	density, lb_m/ft^3
W	mass flow rate, lb_m/sec
A	cross sectional area, ft^2

Subscripts. -

i	nozzle entry
o	side flow entry
d	discharge, diffuser exit
m	throat section
N	nozzle
S	secondary or pumped fluid
a	throat entry
mep	maximum efficiency point on η vs ϕ plot.

Dimensionless Ratios. -

b	nozzle to throat area ratio, A_N / A_m
ϕ	flow ratio, W_S / W_N
N	pressure ratio $\bar{P}_d - \bar{P}_o / \bar{P}_i - \bar{P}_d$
R	Reynolds number
η	efficiency, ϕN.

Friction Loss Coefficients. -

K_1	nozzle
K_2	throat-entry
K_3	throat wall friction
K_4	diffuser
K_{34}	throat-diffuser, $K_3 + K_4$

Nozzle Pressure Drop. -

$$\bar{P}_i - \bar{P}_o = \frac{\rho V_N^2}{2g} \left[1 + K_1 \right] \tag{20}$$

Output Pressure Rise, Suction to Discharge. -

$$\bar{P}_d - \bar{P}_o = \frac{\rho V_N^2}{2g} \left[2b + \frac{2\phi^2 b^2}{1-b} - (1+K_{34}) b^2 (1+\phi)^2 \right.$$
$$\left. - (1+K_2) \frac{\phi^2 b^2}{(1-b)^2} \right] \tag{21}$$

Overall Pressure Drop, Inlet to Discharge. -

$$\bar{P}_i - \bar{P}_d = \frac{\rho V_N^2}{2g} \left[1 + K_1 - 2b - \frac{2\phi^2 b^2}{1-b} + (1+K_{34}) b^2 (1+\phi)^2 \right.$$
$$\left. + (1+K_2) \frac{\phi^2 b^2}{(1-b)^2} \right] \tag{22}$$

Jet Pump Efficiency. - Pump efficiency, η, is defined as the ratio of energy output to energy input:

$$E_{out} = \frac{W_S}{\rho} (\bar{P}_d - \bar{P}_o) \frac{ft\ lb_f}{sec}$$

$$E_{in} = \frac{W_N}{\rho} (\bar{P}_i - \bar{P}_d)$$

$$\eta = \frac{E_{out}}{E_{in}} = \frac{W_S}{W_N} \frac{\bar{P}_d - \bar{P}_o}{\bar{P}_i - \bar{P}_d} = \phi N \qquad (12)$$

where ϕ is the flow ratio and N is the pressure ratio.

Dimensionless Pressure Ratio, N. -

$$N = \frac{\bar{P}_d - \bar{P}_o}{\bar{P}_i - \bar{P}_d} = \frac{2b + \frac{2\phi^2 b^2}{1-b} - (1+K_{34})b^2(1+\phi)^2 - (1+K_2)\frac{\phi^2 b^2}{(1-b)^2}}{1 + K_1 - \text{numerator}} \qquad (23)$$

Note that, $\dfrac{N}{N+1} = \dfrac{\bar{P}_d - \bar{P}_o}{\bar{P}_i - \bar{P}_o}$; and $N + 1 = \dfrac{\bar{P}_i - \bar{P}_o}{\bar{P}_i - \bar{P}_d}$

The dimensionless ratios ϕ and N define the performance of the jet pump.

Energy Analysis

Included in Appendix I is a study of the energy relations in the jet pumping process. It is shown that the losses consist of the following:

A. **Mixing Loss.** A loss of energy occurs when two streams of dissimilar velocity mix, as in the throat of the jet pump. This loss decreases as the velocity of the pumped stream approaches that of the jet and theoretical efficiency is 100 per cent when the velocities are equal.

B. **Jet Loss.** Experimentally it was found that the pressure at the nozzle tip was effectively P_o, the side port pressure, not P_a the (lower) throat entry pressure. A loss of energy, here termed the "jet loss" results from the flow of the free jet from P_o to P_a. The fact that the nozzle-tip pressure is evidently P_o is attributed in large part to practical pump design configuration: (a) side-port entry passage is large in area, and unrestricted (Figs. 8, 9); (b) the nozzle tip is invariably withdrawn a distance "S" from the throat entry proper (Chapter V). It is possible that the contour of the throat entry could be designed so as to partially utilize the jet loss energy. It is quite real, however, for pumps used herein, efficiencies of which (20 to 30 per cent) are representative of practical jet pumps in general use.

C. **Friction Losses.** These consist of nozzle, throat entry, throat, and diffuser losses and are accounted for with coefficients K_1, K_2, K_3, and K_4. Because of minor effect, and the difficulty of measuring it, K_2 is assumed zero. K_3 and K_4 are both based on throat velocity V_m, and are conveniently combined as K_{34}. Friction losses are thus expressed by K_1 and K_{34} only.

Expressions for mixing, jet, and friction losses are included, Eqs. 26, 27, 19, as well as an equation for total losses in the jet pump, Eq. 28, Appendix I. Theoretical pressure ratio N, and efficiency η, are plotted versus flow ratio ϕ, in Fig. 2. Three sets of curves are included for operation under conditions A, B, and C above. Efficiency is of course highest under assumption A. With the jet loss included the efficiency reaches a maximum of 42 per cent. Inclusion of friction losses reduces peak efficiency to 20 to 30 percent, range common in practice.

Design Selection of Area Ratio b

As shown by the C curves in Fig. 2 for b = 0.5, the pressure ratio (and hence discharge pressure) decreases with flow ratio ϕ. This and the corresponding efficiency curve are similar to the performance curves for a centrifugal pump. As the discharge pressure is increased, the quantity pumped decreases, until at the cut-off point, secondary flow ceases ($\phi = 0$).

The design area ratio b determines the discharge pressure versus flow ratio characteristic. In Fig. 3 theoretical characteristic curves are given for assumed friction loss coefficients of $K_1 = 0.1$ and $K_{34} = 0.3$, (approximately the minimum encountered in testing oil jet pumps). At a particular value of ϕ, several b values will function, but only one yields optimum performance, i.e., maximum efficiency. All of the N vs. ϕ curves are bounded by an envelope curve which is the locus of maximum N values at any ϕ. Similarly, an envelope curve across the top of the efficiency curves is the locus of maximum efficiencies with the assumed friction factors 0.1 and 0.3. An envelope curve may be computed directly, as shown below.

Optimum Area Ratio b. - This is found from Eq. 23 for N and,

$$\frac{\partial N}{\partial b} = 0$$

The result is a fifth order equation in b, with only one friction coefficient, K_{34}. With $y = (1+K_{34})$, and $K_2 = 0$, this equation for optimum b is:

$$
- b^5 \left[y \,(1+\phi)^2 \right] + b^4 \left[1 - \phi^2 + 4y \,(1+\phi)^2 \right]
$$
$$
- b^3 \left[4 - 4\phi^2 + 6y \,(1+\phi)^2 \right]
$$
$$
+ b^2 \left[6 - 4\phi^2 + 4y \,(1+\phi)^2 \right]
$$
$$
- b \left[4 - \phi^2 + y(1+\phi)^2 \right] + 1 = 0 \tag{30}
$$

For the special case of no side flow, $\phi = 0$, Eq. 30 reduces to

$$b_{opt} = \frac{1}{1+K_{34}} \tag{30a}$$

6

Differentiation of Eq. 21 to find optimum b for maximum energy output,

$$\frac{\partial (P_d - P_o)}{\partial b} = 0$$

yields the same Eq. 30 for b. In other words, selection of b via Eq. 30 will yield both maximum N and maximum energy output* for given $\emptyset$ and K values.

To avoid the laborious calculations of b from Eq. 30, the solution is presented graphically (vs. $\emptyset$) in Fig. 4. This clearly demonstrates that (a) the design area ratio decreases as desired flow ratio W_S/W_N increases, and (b) at any flow ratio the optimum area ratio decreases as the friction increases. For example, the optimum area ratio at $\emptyset = 1.0$ is b ≈ 0.293, but for high friction losses, say $K_{34} = 1.0$ (as with very viscous oils) the optimum area ratio is only b = 0.142. Of course the corresponding pump efficiency will be lower in the case of high friction, but it will be the highest available, i. e., no other b value would improve efficiency at the subject flow ratio, $\emptyset = 1.0$, with $K_{34} = 1.0$.

The heavy line, $K_{34} = 0.3$, is recommended for general (high Reynolds number) use. Example: what value of b should be used to handle a flow ratio of $\emptyset = 1.0$, with $K_{34} = 0.3$? Answer: $b_{opt} = 0.227$.

Optimum Flow Ratio, $\emptyset_{mep}$

For any given area ratio b and friction factors K_1 and K_{34}, pump efficiency versus flow ratio $\emptyset$ (or quantity pumped, for constant W_N), passes through a maximum. This particular value of flow ratio $\emptyset_{mep}$ is found from

$$\frac{\partial \emptyset N}{\partial \emptyset} = 0$$

and the result is, with $(1 + K_1) = s$, $K_2 = 0$, and $(1 + K_{34}) = y$:

---

* If the jet loss is not recognized, $\partial N / \partial b = 0$, using Eq. 13 for N, will produce a fifth order equation for b_{opt} dependent on K'_1 as well as K_{34}. Justification for the simpler form, (including jet loss) is that it predicts actual performance far better.

$$\phi^4_{mep} b^4 \left[- \frac{1}{(1-b)^4} + \frac{4}{(1-b)^3} - \frac{2(y+2)}{(1-b)^2} + \frac{4y}{1-b} - y^2 \right]$$

$$+ \phi^3_{mep} b^4 \left[\frac{-4y}{(1-b)^2} + \frac{8y}{1-b} - 4y^2 \right]$$

$$+ \phi^2_{mep} b^2 \left[\frac{-2yb^2}{(1-b)^2} + \frac{4b}{(1-b)^2} - \frac{3z}{(1-b)^2} + \frac{4yb^2}{1-b} - \frac{8b}{1-b} + \frac{6z}{1-b} - 6y^2 b^2 \right.$$

$$\left. + 4yb - 3yz \right]$$

$$+ \phi_{mep} b^2 \left[-4y^2 b^2 + 8yb - 4yz \right]$$

$$-y^2 b^4 + 4yb^3 - yzb^2 - 4b^2 + 2zb = 0 \tag{31}$$

The maximum efficiency flow ratio is dependent on K_1, K_{34} and b.

Theoretical ϕ_{mep} values calculated from Eq. 31 were compared with test values for eight jet pumps with good correlation.

Approximate Solution for ϕ_{mep}. - In previous work (12) it has been noted that maximum efficiency occurs when the mixture momentum equals the jet momentum, $W_T V_m = W_N V_N$. In dimensionless terms this yields

$$\phi_{mep} = \frac{1}{\sqrt{b}} - 1 = \frac{d_m}{d_N} - 1 \tag{32}$$

That this simple equation does predict maximum efficiency ϕ quite well was confirmed by the tests in this work. Eq. 32 gives approximately the same values as Eq. 31 for low friction flows, i.e., $K_{1,34}$ less than about 0.35. (See Table 3.)

Maximum Flow Ratio, ϕ_o

In plotting theoretical characteristic curves, or in selecting a pump for an application, it is helpful to determine the maximum capacity. As shown by Figs. 2 or 3, this occurs at N = 0. By equating energy out, $\phi(P_d-P_o)$, or P_d-P_o Eq. 21, or N, Eq. 23, to zero and solving for ϕ, a quadratic equation is obtained permitting direct calculation of ϕ_o, as follows ($K_2 = 0$):

$$\phi_o = \frac{(1+K_{34})(1-b)^2 - \sqrt{(1-b)^2 - K_{34}(3b^2 - 8b + 7 - 2/b)}}{- \left[b^2 + K_{34}(1-b)^2 \right]} \tag{33}$$

A graphical solution to Eq. 33 is presented (vs. b) in Fig. 5 for K_{34} values from 0 to 1.0. Incidentally for frictionless flow Eq. 33 reduces to $\phi_0 = 1 - b/b$, which will be recognized as the condition for zero mixing loss.

Envelope Curves

The family of characteristic curves in Fig. 3, for $K_1 = 0.1$ and $K_{34} = 0.3$, shows that peak efficiency declines somewhat at extreme low, and high, b values. The relations between N, η, ϕ, and b for the jet pump are shown in Fig. 6. These curves were constructed as follows:

1. Assume $K_1 = 0.1$ and $K_{34} = 0.3$.
2. For a series of fixed values of ϕ, calculate b_{opt} from Eq. 30 (or see Fig. 4).
3. Calculate N and $\eta = \phi N$ for each pair of ϕ - b_{opt}, with Eqs. 23 and 12.

The results appear in Table 1. and Fig. 6.

Table 1. N and η versus ϕ for Optimum b Value
$K_1 = 0.1$, $K_{34} = 0.3$, $K_2 = 0$

Flow Ratio ϕ	Optimum b b_{opt}	N	$\eta = \phi N$ Per Cent
0.24	0.500	0.840	20.3
0.3	0.435	0.722	21.6
0.5	0.350	0.493	24.7
1	0.227	0.269	26.9
2	0.127	0.132	26.4
5	0.0461	0.0434	21.7

This η vs. ϕ curve is the envelope curve for the family of efficiency curves in Fig. 3. The N vs. b and N vs. ϕ curves show the maximum obtainable pressure ratio under the given friction condition. The latter is the envelope curve for the family of N curves in Fig. 3.

Dual Optimum. - Note that two optimizing equations between b and ϕ have been presented: Eq. 30 (Fig. 4) for b_{opt} at a particular ϕ; and Eq. 31 for optimum ϕ_{mep} at a particular b value. Optimization at one friction condition is a function of two variables, thus forming a three dimensional surface. For $K_1 = 0.1$ and $K_{34} = 0.3$ the optimum combination is very nearly b = 0.2 operating at $\phi = 1.2$. The corresponding efficiency is $\eta = 27$ per cent, with N = 0.225. For

this case alone, $b_{opt} - \emptyset$ and $\emptyset_{mep} - b$ are identical. Note that the η curve for b = 0.2 is tangent to the envelope curve at its maximum point, whereas larger b value curves are tangent at $\emptyset < \emptyset_{mep}$, and smaller values at $\emptyset > \emptyset_{mep}$.

Similar analyses were made at other friction conditions with the results tabulated below. The pump with area ratio b = 0.2 operating at $\emptyset = 1.2$ remained the best "dual optimum" condition.

Table 2 Envelope Curve Study

Assumed Friction	Max. η
$K_1 = 0.05$ $K_{34} = 0.10$	37.5
$K_1 = 0.10$ $K_{34} = 0.20$	30.5
$K_1 = 0.10$ $K_{34} = 0.30$	27.0
$K_1 = 0.20$ $K_{34} = 0.40$	22.0

Approximate Theory

It has been suggested previously (5, 11) that the N vs. $\emptyset$ characteristic curve be approximated with a straight line. Inspection of Figs. 3, 10 to 14, shows that the N - $\emptyset$ line is slightly concave down, at b = 0.1, linear at b = 0.2, and concave up for larger b values. Thus, particularly for b < 0.3, this linearity approach is quite useful. A straight line on N vs. $\emptyset$ coordinates is drawn between $\emptyset_0$ (Eq. 33 or Fig. 5) on the abscissa and N_0 on the ordinate. N_0 is calculated from Eq. 23, which reduces to the following at $\emptyset = 0$.

$$N_0 = \frac{2b - (1+K_{34}) b^2}{1 + K_1 - \text{numerator}} \tag{23 a}$$

The efficiency curve, $\eta = \emptyset N$ will be a parabola; the following relations also apply, if N vs. $\emptyset$ is linear:

$$N = N_0 - e\emptyset \tag{34}$$

where $e = \dfrac{N_0}{\emptyset_0}$, the slope

$$\emptyset_{mep} = \frac{\emptyset_0}{2} \tag{35}$$

$$\eta = \emptyset N_o - e\emptyset^2 \tag{36}$$

$$\eta_{max} = \frac{N_o \emptyset_o}{4} \tag{37}$$

In Appendix 3 this approximation is compared with N_o and $\emptyset_o$ values versus b from Reference 11.

CHAPTER II

TREATMENT OF EXPERIMENTAL DATA
COMPARISON WITH THEORY

In the course of this work eight jet pumps of varying design and with area ratios from b = 0.1 to 0.6 have been tested. Performance testing included jet Reynolds numbers from 500 to 30,000, nozzle pressures 20 to 200 psig, viscosity 5 to 100 centistokes, nozzle diameters 0.100 to 0.177 inch.

Test Procedure. - Testing a jet pump consists of measuring three pressures, P_i, P_o, P_d, and the two flow rates, W_N and W_S. Generally a test is made at a selected nozzle flow rate W_N and side port pressure P_o. There exists for each pump a unique relationship between back pressure P_d and side flow rate W_S -- much the same as for a centrifugal pump, discharge of which is similarly dependent on back pressure. The test is made by varying P_d from the "cutoff" pressure where $W_S = 0$, to the minimum obtainable (back pressure valve wide open). At a number of operating points, usually about 10 to 15 for each performance curve, these three pressures and two flow rates are recorded. Fig. 7 shows the test stand flow circuit. Primary flow was supplied with a positive displacement pump driven by a variable-speed D.C. motor.

Experimental Jet Pumps. - In order to investigate design variables, primarily area ratio b and spacing S, the pump shown in Fig. 8 was designed. It consists of one body with three interchangeable nozzles and three throat-diffuser sections of similar design. Thus up to nine jet pumps can be assembled in the one body. Additional throat-diffuser sections were made to check effect of throat length and throat entry shape. All diffuser angles were 8 degrees, total included angle.

A commercial pump of conventional conic nozzle and throat design was also employed, with two nozzle sections and provisions for varying the spacing S. See Fig. 9.

All pumps are identified by three numbers, e.g., No. 141/318/308. The numbers refer to nozzle diameter, throat diameter, and nozzle-to-throat spacing in thousandths of an inch.

Calculations. - Pressures are converted to psig units, flows to lb/min rates. The pressure ratio N is then calculated from

$$N = \frac{P_d - P_0}{P_i - P_d}$$

which is the experimental counterpart of the theoretical Eq. 23. The pressures are supposed to be total heads, but in all of the work velocity heads have been negligible, thus permitting substitution of static pressures.

In Fig. 10 these measured N values are plotted versus flow ratio ϕ for pump No. 173/224/020, b = 0.6. Test conditions are included on the curve sheet. The solid N and $\eta = \phi N$ curves are theoretical, and are discussed below.

Similar performance curves (at high Reynolds numbers) are presented for b = 0.534, 0.4, 0.2, and 0.1 in Figs. 11, 12, 13, and 14. Results with b = 0.133, 0.1736, and 0.30 were virtually identical with those given, and are omitted to conserve space. (Numerical results are given later in Table 3.)

Calculation of Friction Coefficients. - From measured values of W_N, W_S, P_i, P_o, and P_d, friction coefficients K_1 and K_{34} were calculated from the theoretical relations, repeated below:

$$K_1 = \frac{\bar{P}_i - \bar{P}_o}{\frac{\rho}{2g} V_N^2} - 1 \tag{17}$$

$$K_{34} = \frac{2}{b(1+\phi)^2} + \frac{1-2b}{(1-b)^2} \frac{\phi^2}{(1+\phi)^2} - 1 - \frac{(\bar{P}_i - \bar{P}_o) \frac{N}{N+1}}{\frac{\rho V_N^2}{2g} b^2 (1+\phi)^2} \tag{14}$$

From continuity, $V_N = W_N / \rho A_N$, or

$$\frac{\rho V_N^2}{2g} = \frac{0.002326 \, W_N'^2}{sg \, d_N^4}$$

where W_N' is the primary flow, lb/min, sg is fluid specific gravity, and d_N is nozzle diameter, inches. Note in Eq. 14 that $P_d - P_o$ is obtained from

$$\frac{N}{N+1} (P_i - P_o) = P_d - P_o$$

where N is read from a smoothed curve at the selected ϕ. Of course $P_d - P_o$ could also be obtained from a plot of directly measured values, at the ϕ in question.

The throat-diffuser coefficient was calculated for each test at the "operating flow ratio". This was taken as $\phi \simeq 2/3\, \phi_{mep}$, from inspection of each experimental N - ϕ plot. So far as K_1 is concerned, flow ratio was immaterial, since P_1-P_o was in general unaffected by ϕ*. Sample calculations of K_{34} and K_1 appear in Appendix 2.

<u>Theory versus Experiment</u>. - The validity of the theoretical analysis was tested by calculating N - ϕ curves for each test, using measured K_1 and K_{34} values. This of course ensured agreement at the one flow ratio. If the theoretical curve and data agree at <u>other flow ratios</u>, the theory is verified. Success or failure is evidenced by the agreement of data with the theoretical curve at ϕ greater and less than the "match point" ϕ, where K_{34} was calculated from experiment.

Discussion of Theory vs. Experimental Results

Examination of Figs. 8 to 12 shows that the theory agrees quite well with actual test results, i. e., the experimental points agree with theory curve over a wide range of flow ratios. The sudden break in the data points, and departure from theory, at high flow ratios is the result of cavitation. This phenomenon is covered in detail in a later chapter.

It will be noted that the experimental data points fall above the theory at flow ratios approaching zero, for the smallest area ratios, b = 0.2 and 0.1, Figs. 11 and 12. This behavior was also noted for pumps No. 141/387/311 (b = 0.133) and No. 100/240/445 (b = 0.1736).

The difference at low flow ratios, a maximum at ϕ = 0, is attributed to departure from the theoretical assumptions. Separation of the jet from the throat wall, or rather failure of the flow to conform with the throat wall until well beyond the entrance, could reduce friction and account for the fact that actual performance slightly exceeds theoretical prediction at ϕ values near zero.

The error is small, and on the conservative side. (Comparison of measured and theoretical <u>efficiency</u> curves shows practically no difference, since both approach zero with ϕ (η = ϕN).

Summary of Basic Performance Tests

In Table 3, below, the results of performance tests of the eight jet pumps are summarized. All tests are at high Reynolds numbers and probably represent maximum efficiency performance, i. e., minimum fraction factors for the size

---

*In one test only (No. 183) where spacing was sub-normal, P_i did decrease by about 5 per cent at the maximum flow ratio. Otherwise, with constant P_o, P_i was always unaffected by W_S or ϕ.

of pump in question. As is the case with turbulent flow in pipes, friction factors decline toward minimum values at high Reynolds numbers. (See next Chapter.)

Effect of Area Ratios. - Whereas the theoretical analysis (Chapter I) showed $b = 0.2$ to be optimum for maximum efficiency with fixed K_1 and K_{34} values, Table 3 indicates that $b = 0.3$ is superior. Furthermore, efficiency does not decline at high b values as the analysis with constant K values shows. Examination of the K_{34} column reveals that measured K_{34} values decrease as b increases, for these tests at high Reynolds numbers.

Table 3 Basic Performance Data, Experimental Jet Pumps

Norm. Area Ratio b	Pump No.	Test	Oil+	Temp. F	Vis.**	Sp. Grav.	Primary Flow W_N LB/min	Nominal Nozzle Pressure P_1, psig	Jet Reynolds No. R_N	K_1	Throat Reynolds No. R_m	K_{34}	q_{mep}	η max per cent
0.1	100/316 /307	173	C	180	7.2	0.836	20.72	100	13,075	0.208	10,760	0.294	2.4	22.8
0.133	141/387 /311	129	1005	100	5.34	0.863	28.0	40	16,350	0.0846	15,540	0.446	1.6	22.8
0.174*	100/240 /445	12	1005	81	7.0	0.869	21.0	100	13,413	0.189	13,413	0.386	1.4	22.4
0.20	141/316 /308	179	C	180	7.2	0.836	43.1	100	19,300	0.100	17,240	0.358	1.2	25.3
0.30	173/316 /216	153	1005	100	5.34	0.863	66.2	100	31,500	0.0895	21,350	0.206	0.8	29.8
0.40	141/224 /291	148	1005	100	5.34	0.863	44.3	100	25,840	0.0677	24,400	0.272	0.55	26.0
0.544*	177/240 /255	166	C	80	7.2	0.836	60.0	80	21,970	0.114	19,400	0.154	0.3	25.5
0.60	173/224 7020	164	C	80	7.2	0.836	58.6	80	21,370	0.0762	19,800	0.176	0.24	23.6

* Conical nozzle and throat entry, Fig. 9. Other pumps Fig. 8.
+ Properties of oil blends appear in Appendix 2.
** Centistoke

CHAPTER III

CORRELATION OF MEASURED FRICTION COEFFICIENTS

One of the primary questions to be answered in judging the feasibility of using a jet pump in a lubrication system is that of the effect of viscosity. As developed below, tests show that pump efficiency is affected relatively little by viscosity down to a jet Reynolds number of about 3,000. Below this, performance decreases so rapidly that operation in the laminar region should be avoided.

The Effect of Viscosity. - To simulate low temperature operation, blends of Grades 1005 and 1100 oil (identified as A, B, C) were used at controlled temperatures from 80 to 200 F. Viscosity and specific gravity data are given in Figs. 43 and 44. In Fig. 15, N characteristic curves are given for two jet pumps at several viscosities. The uppermost N - $\emptyset$ line for each pump is the "normal" pressure ratio characteristic. The depression of the 31 centistoke curve is quite different between the 100/240/445 and 141/316/408 pumps. The reason of course is the difference in Reynolds numbers, which are noted at the right of the curves. As shown below, performance declines rapidly with Reynolds number when $R_N < 3,000$. (Loss in efficiency due to lowering of N values is quite evident, since $\eta = \emptyset N$).

Additional tests with different velocities soon confirmed that Reynolds number, not viscosity, governed performance when viscous effects are large.

Reynolds Numbers

The jet pumping process, a momentum interchange, depends upon turbulent mixing on the primary and secondary streams. Turbulence can persist only when the viscous stresses in the flow are insufficient to damp out local fluctuations in velocity.

Reynolds Similitude. - By means of dimensional analysis it can be shown that in the nozzle, and in the throat and diffuser, the dynamic pattern of flow will depend upon the value of the Reynolds number. The Reynolds number expresses the relative importance of viscous action, being a ratio of inertial to viscous forces. In any two flows in which viscosity plays an important role, dynamic

similitude exists when the boundaries are geometrically similar, and the Reynolds numbers are the same.

Apart from the simpler flows in the nozzle and diffuser, the complex jet mixing process itself depends upon a "stability parameter" (7), which resembles a Reynolds number. Whether or not turbulent mixing occurs between a free jet and the surrounding fluid depends on the value of the stability parameter. As in the case of the transition from turbulent to laminar pipe flow at a Reynolds number of about 2100, a critical value exists for the free jet.

The case of the jet pump is complicated by the fact that the mixing occurs in an adverse pressure gradient, and is confined by the parallel walls of the throat. The latter will be a stabilizing influence, tending to delay the onset of turbulent flow (8).

Since both the mixing process and the nozzle, side entry, and diffuser flows may be expected to depend upon Reynolds number, measured values of loss coefficients have been correlated versus either the jet Reynolds number R_N or the throat Reynolds number, R_m.

Calculation of Reynolds Numbers. - Reynolds numbers are calculated from test data as follows:

$$R_N = \frac{V_N D_N}{\nu} = \frac{4}{\pi} \frac{W_N}{\rho D_N \nu}$$

where V_N, D_N, and W_N are in units of lb_m, ft, and seconds. This may also be written

$$R_N = \frac{379.1 \; W_N'}{sg \; \nu \; d_N} \tag{38}$$

With $W_N' = lb_m/min$

sg = specific gravity of fluid

ν = kinematic viscosity, centistokes

d_N = nozzle diameter in inches

By continuity the throat Reynolds number is,

$$R_m = \sqrt{b}(1 + \emptyset) \; R_N \tag{39}$$

It is interesting to note that $R_m = R_N$ for $\emptyset = \dfrac{1}{\sqrt{b}} - 1$, which is the condition for equality between throat and jet momentum. As mentioned in Chapter II this forms a good approximation to $\emptyset_{mop}$. At high Reynolds numbers at least,

the throat Reynolds number R_m at the experimental $\emptyset_{mep}$ was always found to be quite close in value to the jet Reynolds number R_N.

Experimental Results

Values of nozzle coefficient K_1 calculated from test results are plotted vs. nozzle Reynolds number R_N in Fig. 16. These data consist of K_1 values from 42 performance test on eight jet pumps plus a few nozzle tests. Included are coefficients for (a) three nozzles with elliptical profile (Fig. 8): $d_N = 0.100$, 0.141, 0.173 in.; and (b) for two nozzles with conical approach profile: $d_N = 0.100$, 0.177 in. (Fig. 9).

In general K_1 varies inversely as R_N to about the one-half power, from 500 to 20,000. Although these data are insufficient to show it, it would be expected that this relation would fail at very high Reynolds numbers; where K_1 probably approaches a constant value (independent of R_N). $K_1 = 0.1$ is probably a good general assumption for this case.

Size Effect. - As would be expected, the smallest nozzle exhibits the highest loss coefficient, i.e., has the lowest efficiency, at any one value of R_N.

If coefficients are available in the literature for a particular nozzle selected for a jet pump design, these may be applied directly.

K_1 values may be taken from Fig. 16 for design use. These curves will be somewhat conservative for application to larger nozzles ($d_N > 0.177$ in.).

Throat-Diffuser Coefficient. - K_{34} values are plotted versus throat Reynolds number R_m in Fig. 17. These values are based on some 42 tests on eight jet pumps, using three mineral oil blends and a synthetic oil.

Referring to Fig. 17 the following points of interest are noted:

1. Friction increases rapidly for $R_m < 3,000$, where $K_{34} \approx 900/R_m$.

2. A horizontal line, $K_{34} = 0.3$, best represents results for $R_m > 3,000$.

3. There is an indication that K_{34} vs. R_m dips to a minimum (0.2) at about 5,000 and then rises again to 0.34 or 0.4 at $R_m = 15,000$. Data are insufficient to warrant a conclusion, however.

4. At high Reynolds numbers (15,000-20,000) pumps with large area ratios, b = 0.3, 0.4, 0.534, 0.6 showed $K_{34} < 0.3$. For pumps of small area ratios, 0.2, 0.174, 0.133, 0.10, $K_{34} > 0.3$.

Table 4. Measured Friction Coefficients vs. Reynolds Numbers

Area Ratio b	Jet Pump No.	Test No.	Oil	Temp. F	Vis. centistoke	Sp. Grav.	W_N lb/min	Nom. P_i psig	R_N	K_1	$\emptyset$	R_m	K_{34}
0.1	100/316/307	94	B	200	6.7	0.824	12.7	40	8,720	0.273	2.40	9,380	0.276
		98	B	145	14.8	0.843	11.9	40	3,620	0.483	2.10	3,550	0.274
		97	B	125	21.0	0.850	11.65	40	2,480	0.560	1.90	2,270	0.382
		99	B	80	60.0	0.865	10.32	40	754	1.024	0.60	382	5.58
		173	C	180	7.2	0.836	20.72	100	13,080	0.208	1.50	10,760	0.294
		175	C	110	23.0	0.859	17.75	83	3,410	0.414	1.80	3,020	0.291
0.133	141/387/311	82	A	160	16.0	0.841	26.45	40	5,290	0.264	1.60	5,030	0.356
	141/387/411	86	A	100	57.0	0.861	39.2	100	2,180	0.422	1.15	1,710	0.450
	141/387/311	129	1005	100	5.3	0.863	28.0	40	16,350	0.0846	1.60	15,450	0.446
	141/387/411	187	C	180	7.2	0.836	43.4	100	19,300	0.104	1.40	16,900	0.400
0.174	100/240/445	38	1005	86	6.5	0.867	15.0	40	10,340	0.218	1.40	10,340	0.347
		57	A	160	16.0	0.841	12.15	40	3,420	0.391	1.35	3,350	0.286
		58	A	150	19.0	0.844	12.0	40	2,840	0.411	1.40	2,840	0.352
		60	A	135	25.0	0.850	11.9	40	2,120	0.462	1.05	1,810	0.505
		55-56	A	125	31.0	0.853	12.7	40	1,720	0.444	0.80	1,290	1.69
		62	A	79	100	0.869	10.0	40	437	1.08	0.50	273	2.26
		12	1005	81	7.0	0.869	21.0	100	13,410	0.189	1.40	13,410	0.386
		65	A	160	16.0	0.841	19.9	100	5,610	0.300	1.35	5,490	0.182
		64	A	150	19.0	0.844	19.8	100	4,680	0.322	1.35	4,580	0.207
		63	A	135	25.0	0.850	19.5	100	3,490	0.365	1.25	3,273	0.232
		61	A	125	31.0	0.853	19.4	100	2,790	0.378	1.20	2,560	0.258
		67	A	80	100	0.868	17.4	100	760	0.773	0.35	427	3.80
0.20	141/316/308	179	C	180	7.2	0.836	43.1	100	19,300	0.100	1.0	17,240	0.358
		190	7808	150	6.7	0.890	44.6	100	20,150	0.096	0.9	17,100	0.337
		178	C	180	7.2	0.836	43.1	100	19,300	0.106	0.9	16,380	0.322

Table 4. Continued

Area Ratio b	Jet Pump No	Test No.	Oil	Temp. F	Vis. centistoke	Sp. Grav.	W_N lb/min.	Nom. P_i psig	R_N	K_1	β	R_m	K_{34}
		91	A	200	9.0	0.827	26.1	40	9,530	0.158	1.15	9,140	0.315
		90	A	180	12.0	0.834	26.2	40	7,160	0.202	1.1	6,710	0.282
	141/316/408	72	A	160	16.0	0.841	25.8	40	5,160	0.246	1.2	5,060	0.318
		73	A	125	32.0	0.853	24.7	40	2,510	0.372	1.1	2,350	0.372
		74	A	80	100	0.868	21.2	40	656	0.878	0.4	410	2.71
0.30	173/316/237	153	1005	100	5.3	0.863	66.2	100	31,500	0.0895	0.7	29,350	0.206
		156	C	180	7.2	0.836	58.1	80	21,200	0.0958	0.7	19,700	0.220
		157	C	125	17.0	0.854	50.0	62	7,550	0.196	0.7	7,040	0.254
		161	C	100	28.0	0.863	43.1	49	3,920	0.275	0.7	3,650	0.229
	173/316/337	132	C	100	28.0	0.863	53.0	100	5,720	0.208	0.4	4,380	0.185
0.40	141/224/291	148	1005	100	5.3	0.863	44.3	100	25,840	0.0677	0.5	24,400	0.272
		169	C	96	30.0	0.864	43.5	113	4,510	0.255	0.35	3,830	0.235
		170	C	96	30.0	0.864	30.7	60	3,180	0.332	0.35	2,700	0.196
0.534	177/240/255	166	C	180	7.2	0.836	60.0	80	21,970	0.114	0.2	19,400	0.154
		168	C	96	30.0	0.864	43.2	45	3,580	0.252	0.2	3,170	0.395
0.6	173/224/020	164	C	180	7.2	0.836	58.6	80	21,370	0.0762	0.2	19,800	0.176

Efficiency versus Reynolds Number. - Rapid estimates of maximum pump efficiency may be made using the approximate solution in Chapter I, Eqs. 23a (N_o), 33 ($\emptyset_o$) and Eq. 37, $\eta_{max} = N_o\emptyset_o/4$. (This approximation is based on the assumption that N vs. $\emptyset$ is a straight line. It is quite accurate for area ratios in the vicinity of b = 0.2).

With K_1 and K_{34} values taken from the heavy line curves in Figs. 16 and 17, efficiencies were calculated via Eq. 37 at R values from 500 to 20,000. (at $\emptyset_{mep}$, $R_m \approx R_N$.) Results appear in Table 5 and are plotted vs. R_m in Fig. 17.

Table 5. Calculated Efficiencies vs. Reynolds Number

$R_{N, m}$	K_1*	K_{34}	$\emptyset_o$	N_o	$\eta = N_o\emptyset_o/4$ Per Cent
20,000	0.10	0.30	2.49	0.463	28.8
7,000	0.20	0.30	2.49	0.409	25.4
3,000	0.33	0.30	2.49	0.354	22.0
2,000	0.43	0.45	2.14	0.314	16.8
1,000	0.66	0.9	1.54	0.242	9.32
700	0.82	1.3	1.20	0.218	6.55
500	1.0	1.8	0.96	0.168	4.04
300	1.4	3.0	0.60	0.111	1.66

* K_1, K_{34} values from heavy line curves, Figs. 16 and 17.

The efficiency curve in Fig. 17 is representative of the actual test results. As the Reynolds number is increased above 3,000, only a slight gain in performance results; this is due to the decline in nozzle coefficient K_1. Below 3,000, both K_1 and K_{34} are increasing, and efficiency drops off rapidly. Operation here should be avoided if possible.

Effect of Oil Used. - As shown by Table 4, these measurements of K values involved the use of MIL-L-6801A Grade 1005 oil, three blends of Grade 1005 plus MIL-L-6802A, Grade 1100 oil, and MIL-L-7808, a synthetic oil. At similar viscosities (through temperature control) all oils gave essentially the same performance. (As shown in Chapter IV, oil composition did affect cavitation slightly.)

The importance of the synthetic oil to future lubrication systems warrants a special comparison. Experimental N values vs. $\emptyset$ were the same for blend C and MIL-L-7808 synthetic oil, within experimental accuracy. Test data and calculated K values for blend C and for synthetic oil (under similar conditions, $R_N \approx 20,000$) appear as Tests 179 and 190 in Table 4. K_1 values were 0.100 and 0.096, K_{34} values were 0.358 and 0.337, for the mineral blend and the synthetic oil, respectively.

Effect of Altitude. - The theoretical developments in Chapter I and Appendix 1 show that pump performance is dependent on pressure differences, and not on absolute or gage pressures. All of the data cited so far in this report was taken with side port or suction pressure P_0 within one psi of tank pressure. The tank was normally vented to the atmosphere (except when cavitation testing was underway). Local ambient pressure corresponds to about 1,200 to 1,400 feet altitude in the NACA table (Ref. 13.).

Fig. 18 compares performance of pump No. 141/316/308, at 1,400 and at 12,000 feet altitude (tank pressure 10 inches Hg. below atmospheric). The two N curves are identical except for the cavitation - limited flow ratio, ϕ_L, which is lower for the altitude test. This test, as well as many performance tests at altitudes to 70,000 feet made in the cavitation study, confirm the theoretical independence of the jet pump from altitude, providing the pump is not cavitating.

Effect of Pump Size. - Pipe friction factors are dependent on the relative roughness of the wall, as well as on Reynolds number (14). Size also affects nozzle coefficients (8,9). This effect has already been demonstrated by Fig. 16 for nozzle diameters from 0.100 to 0.177 inch. To investigate the effect of size on the overall pump performance the interchangeable Tee jet pump was assembled and tested with b = 0.20, with three different sizes of nozzle and throat-diffusers. Results are summarized in Table 6. Note from the pump code numbers that nozzle diameters are 0.100, 0.141, and 0.173 inch, with proportional throat diameters. Conclusion: In range tested, size exerts essentially no effect.

Table 6. Size Effect on Jet Pump Performance
Area Ratio, b = 0.20
Oil MIL-L-7808, Synthetic, 190,150,135F.
Nominal, R_N = 20,000

Jet Pump No.	Test No.	W_N lb/min	Nom. P_i psig	N_0 at $\phi=0$	N at $\phi = 0.9$	ϕ_{mep}	η max per cent
100/224/190	208	20.78	92	0.50	0.28	1.1	26.2
141/316/308	190	44.6	100	0.48	0.28	1.1	25.6
173/387/219	206	66.8	100	0.50	0.29	1.1	26.8

Effect of Nozzle-to-Throat Spacing. - This design variable "S" is not included in the theory; it must be determined experimentally. Although this subject is covered in some detail in Chapter V the effect of S on the measurement of K_{34} should be mentioned here in connection with the $K_{34}-R_m$ correlation study. Particularly for larger area ratios (b > 0.3), the agreement between test and theory with change in ϕ is affected to some extent by the spacing S.

The K_{34} data in tables 3 and 4, plotted in Fig. 17, are only from tests for which there was good agreement at high Reynolds number between theoretical and experimental N - $\emptyset$ curves, i.e., S was at or near optimum for every test. (Adjusting S for maximum efficiency, also yielded the best match between theory and experimental results. This agreement is important, since the correlation sought is K_{34} vs. R_m: $\emptyset$ should not affect K_{34}.)

24

CHAPTER IV

CAVITATION IN THE OIL JET PUMP

A second major question to be answered in evaluating the jet pump as an aircraft engine scavenge pump is that of the upper limit of practical operating pressures and velocities.

From the standpoint of size and weight of the pump and associated plumbing, it would be desirable to operate at very high flow ratios, i.e., pump a large amount (W_S) from the engine with a small primary flow (W_N). As shown in Fig. 3, large ratios may be had by using small design area ratios of the order of b = 0.1 or 0.2.

The price paid for a high ϕ characteristic (high relative capacity) is loss of output pressure capacity: N values for small b pumps are low. Since

$$P_d - P_o = \frac{N}{N+1} (P_1 - P_o), \qquad (40)$$

progressively higher inlet pressures P_1 must be used to obtain a given output in pressure P_d, as b is reduced. The use of high nozzle pressures of course means high jet velocities.

As shown below, high jet velocities and/or low suction-port absolute pressure results in cavitation. This disturbance places definite limits on pump capacity. An experimentally determined cavitation function is established, permitting the design of jet pumps for high-altitude operation.

A. Evidence and Consequences of Cavitation

Assume, for ease of discussion, a pump operating with fixed W_N and P_o. The amount of fluid pumped, W_S, is then controlled entirely by the discharge or back pressure P_d. (In this way the performance tests reported herein were conducted.) As P_d is reduced, W_S and hence ϕ, normally increases to the limit, ϕ_o, determined by the design area ratio b. Conversely, raising P_d will reduce W_S and ϕ toward zero flow. An increase in P_d above "cut-off" will result in rejection of primary fluid from the side port.

The relation between the three pressures P_i, P_o, and P_d, and the two flows W_N and W_S is uniquely determined by the N - ϕ characteristic curve, whether primary flow or side port pressure are constant or varying. Note again that N, which fixes ϕ on the applicable characteristic curve, is a ratio of pressure differences, $N = (P_d-P_o)/(P_i-P_d)$: it is independent of absolute pressures.

The Cavitating Jet Pump. - Under certain conditions of high jet velocity the normal experimental, and theoretical response of W_S to change in P_d fails. Below a critical value of back pressure, W_S attains a fixed value independent of P_d, termed "limiting flow", W_{SL}. The corresponding "limiting flow ratio" is ϕ_L.

Fig. 19 shows several performance tests with limiting flow. In Fig. 19 A it was caused by raising the nozzle pressure drop from 39.5 to 99 psi. P_o was atmospheric in both cases. In Fig. 19 B limiting flow was caused by throttling the side port pressure below atmospheric. These oil jet pump curves bear marked resemblance to cavitating water jet pump curves (5).

Further examples of limiting flow were presented earlier in Fig. 10 through 14 covering jet pumps with b = 0.1 to 0.6. All of these high Reynolds number tests were made with P_i = 80 to 100 psi; all exhibited limiting flow. As shown by the vertical dashed line, efficiency $\eta = \phi N$, drops toward zero.

B.   Observations with Transparent Jet Pump

In order to determine where cavitation occurs in the jet pump and how it results in limiting flow, a "two-dimensional" jet pump was constructed from sheets of clear plastic as shown in Fig. 20.

The nozzle and throat areas were selected to approximate jet pump No. 100/240/445. The throat of the lucite pump is square, 1/4 by 1/4 inch, with a diffuser divergence angle of 10 degrees. The nozzle approach consists of a metal cylindrical "nose" which projects between the one-inch outer lucite slabs. The hole in the tip is a slit 0.050 inch wide by 0.230 inch; which forms a ribbon-shaped jet perpendicular to the plane of the pump.

Performance. - At p_i = 150 psig, the transparent pump behaved quite like the conventional cylindrical pump, including limiting flow. Maximum efficiency was of the order of only 10 to 15 per cent. This is attributed to the unusual nozzle shape, and the large internal surface area in contact with the flow stream.

Visual Evidence of Cavitation. - Limiting flow was accompanied by the presence of a "front" in the throat of the pump. From the point of mixing to the front the fluid appeared as a gray foam. Across the well defined front a sudden change to a lighter color occurred.

Figs. 21 and 22 consist of photographs of the pump in four stages of cavitation, caused by progressively lowering the back pressure (labeled p_b in these pictures). The second picture shows the cavitation front near the throat entry, p_b = 22.5 psia. As p_b is reduced to 21 and 17 psia in the last two pictures, the front moves deeper into the throat; but W_{SL} = 40 lb/min for all cases with the front in the throat. Onset of limiting flow coincided with the appearance of the cavitation front at the throat entry.

High-Speed Flash Lighting. - The use of a high-speed electronic flash tube (General Radio Corp. Strobolux) operated at about 30 flashes per second considerably aided interpretation of cavitation phenomena. Although the light was not, of course, "synchronized", to the human eye, it froze the action momentarily. Color change across the cavitation front was reversed: from light foam to dark liquid oil.

Incipient Cavitation. - Under stroboscopic lighting the nozzle or primary flow rate was gradually increased. Up to a nozzle pressure of about 30 psig, primary and secondary streams were clear. At 33 psig (jet velocity about 50 ft/sec) the first signs of cavitation appeared at the jet boundary: small bubbles which grew and collapsed. At the same time (a) a distinct cavitation whistle was detected, and (b) bubbles were first found in the diffuser. The latter is evidently a result of air evolved in cavitation and not yet re-dissolved in passage through the diffuser of the jet pump.

Choking Flow. - Further increase in jet velocity increased the width and length of the cavitation disturbance; more and more air bubbles could be seen in the diffuser. Not until the cavitation "void" filled the throat entrance, did "choking" flow occur.

High-Speed Flash Pictures of Cavitation. - Four stages of cavitation are shown in Fig. 23. These pictures were made with a miniature camera at f4.5 lens opening on Super XX film. "Open-flash" technique was used. The high-speed flash (40 microseconds) was obtained with a General Radio Corp. "Strobolux" unit, wired for push-button single-flash use.

In the top picture the jet velocity is slightly above that corresponding to incipient cavitation. The air cavities, although slightly blurred, are quite evident.

The gray cast in the diffuser is the result of the air released in cavitation and not yet completely redissolved.

The second picture was taken at the point of choking or limiting flow. The cavitation disturbance has grown sufficiently to fill the throat entrance. No change in the cavitation whistle was noted at this point.

Further increase in cavitation intensity moves the cavitation front downstream as shown in the two bottom pictures. The increasing amount of fine air bubbles released from solution as cavitation intensity increases, is indicated by the gradual change in gray shading of the diffuser fluid, from the top to the bottom picture. Both primary and secondary streams enter the pump free of entrained air. A sight glass in the discharge line several feet from the diffuser showed clear oil again. The air had redissolved in the oil.

Pressure Jump at Cavitation Front. - The transparent jet pump was provided with three static-pressure taps in the throat section. See Figs. 20 to 23. By controlling the back pressure the cavitation front could be positioned between two of the taps. With a total flow of the order of 50 lb/min., the pressure was observed to suddenly increase by as much as 11 or 12 psi across the front.

This jump is apparently the result of a sudden deceleration of the liquid oil particles at the front. It is suggested that primary and secondary oil particles travel from throat entrance to the cavitation front in "free flight", surrounded by air, vapor, and foam. At the cavitation front the "void" collapses and the liquid decelerates, filling the throat section. Calculations of pressure recovery based on this hypothesis agree well with the observed pressure jumps. The pressure relations are also affected to some extent by the evolution and solution of dissolved air. Cavitation is known to be effective in releasing air from solution. Also, air dissolves relatively more slowly than it evolves (15).

Other work with the transparent jet pump included control of primary flow air content, operation without side flow, operation on water, and use of the pump body as a cavitating venturi. Results are summarized below.

Summary and Conclusions

1. Cavitation first occurs at the jet boundary near the nozzle exit. Upon visual appearance of cavitation,

     a. A whistle is detected, and
     b. Air bubbles appear in the diffuser.

2. An increase in jet velocity, or a decrease in mixing zone pressure causes the region of disturbance to spread and extend downstream toward the throat. Oil in diffuser becomes increasingly cloudy from air bubbles.

3. Limiting or choking flow occurs when the throat entry is blocked by the cavitation disturbance.

    a. At lower jet velocities or higher mixing zone pressures limited cavitation may occur but with small effect on pump performance. Limiting flow is not present, i.e., W_S responds to variation in P_d.

    b. Higher jet velocities or lower mixing zone pressures cause the cavitation front to move downstream in the throat.

    c. The side flow W_S is independent of P_d whenever the cavitation front is present in the throat regardless of its position.

4. A sudden increase in static pressure occurs across the cavitation front of the order of 11 psi for the transparent jet pump. This can be accounted for as the pressure rise accompanying a rapid deceleration of the liquid phase.

5. Dissolved air content of the primary or jet stream has little or no effect on the inception of cavitation, nor on the pumping performance. An increase in air content does cause a slight receding of the front when cavitation is present in the throat.

6. Cavitation fronts were observed in the throat without side flow ($\emptyset = 0$) under conditions of high jet velocity and low back pressure. The pressure jump was similar in magnitude to that with secondary flow.

7. In appearance and performance the cavitating water jet pump seems to be identical with the oil pump. A pressure increase occurs across the cavitation front, and released air content in the diffuser increases as cavitation intensity increases.

8. The cavitation disturbance in a venturi with parallel throat is similar to that in the jet pump: the appearance is the same, and the pressure jump across the cavitation front is again observed.

    It is believed that satisfactory explanations of limiting flow, the appearance of the cavitating zone, and the pressure jump across the cavitation front have been established. Of course, the mechanism of cavitation remains a complex problem -- particularly so when dealing with a non-pure substance such as a hydrocarbon. What triggers the collapse of the cavitation zone in a sharply defined front remains unknown.

C. Limiting-Flow Theory and Tests

From the continuity relation and the side flow energy equation (4) in Appendix I,

$$W_S = \rho A_{Sa} V_{Sa}$$

$$V_{Sa} = \sqrt{\frac{2g(\overline{P}_0 - P_a)}{\rho (1 + K_2)}} \tag{40}$$

Eq. 40 refers to the throat-entry where the secondary flow stream area is assumed* to be $A_{Sa} = A_m - A_N$, the pressure is P_a, and the velocity of W_S is V_{Sa}. Thus, $\underline{W_S \text{ is determined by } P_0 - P_a}$. Limiting flow W_{SL} would occur if the throat entry pressure reached a fixed minimum, $P_a = P_c$. If this conjecture is correct, Eq. 40 shows that

$$V_{SL}^2 \text{ and/or } W_{SL}^2 \text{ values plotted versus } P_0 - P_c \text{ should be linear.}$$

This linearity was shown to be true for the cavitating water jet pump (5), where P_c was taken to be the vapor pressure of water, P_v.

<u>Oil Cavitation.</u> - Compared with water, oil cavitation is complicated by two differences:

1. Lubricating oil contains up to 15 per cent by volume of dissolved air which evolves in proportion to a decrease in absolute pressure. Water contains about one tenth the amount.

2. A hydrocarbon lubricating oil is a mixture of many fractions of different vapor pressure. In general, oil vapor pressures are quite low (15).

<u>Limiting Flow versus p_0, absolute Pressure.</u> - In the absence of a known critical pressure, limiting flow data for cavitating oil jet pumps were plotted against absolute suction port pressure.+ W_{SL}^2 vs. p_0. Such curves for several pumps formed essentially straight lines, usually passing through the origin of coordinates. The magnitude of W_{SL} at any one pressure, of course, depends on the size of the pump, and the area ratio b.

---

* The primary stream, or jet, is assumed to enter the throat with area equal to nozzle area A_N. Jet spreading or mixing <u>before</u> throat entry is ignored.

\+ L o w e r case p refers to psi units, capital P is lb_f/ft^2

Limiting-Flow Function, Y. - Converting limiting flow data to a velocity basis by dividing by flow stream area, A_{Sa}, eliminates pump size and reduces all data to a common basis as shown below. By definition the limiting or "choking" velocity of the secondary fluid entering the throat is,

$$V_{SL} = \frac{W_{SL}}{\rho A_{Sa}} = \frac{W_{SL}}{\rho A_N} \frac{b}{1-b} \qquad (41)$$

The Limiting-Flow Function, Y, is:

$$Y = \frac{\rho V_{SL}^2}{144 \; 2g} = \frac{W_{SL}^2 \; b^2}{144 \; \rho \; 2g \; A_N^2 \; (1-b)^2} \quad psi \qquad (42)$$

The theoretical value of Y is,

$$Y = \frac{Po - Pc}{1 + K_2}$$

Test Procedure. - Limiting flow is indicated by the sharp break in the N - ϕ or η - ϕ experimented curve. Once limiting flow is reached, further reduction in back pressure P_d, hence N, has no effect on W_{SL} or ϕ_L. This simplifies test procedure: pumps are operated at fixed primary flows, W_N, with back pressure valve opened wide to provide minimum P_d. Limiting flows W_{SL} are then read from the sideflow rotameter versus the independent variable p_o.

W_{SL} values were converted to Y functions (in psi) with Eq. 42 and plotted against suction port pressure. Fig. 24 shows the results for tests on three pumps of area ratios, 0.20, 0.30 and 0.534. (Pump details Figs. 8 and 9.) The oil was MIL-L-6081A, Grade 1005. Y values for b = 0.30 are lowest, b = 0.20 in the middle, and points for b = 0.534 are highest. This is attributed primarily to effect of nozzle-to-throat spacing S. As shown in the next chapter, an extra large spacing suppresses the onset of limiting flow, at low p_o values. The relation Y = 0.68 p_o appears to represent the general experimental correlation.

In this test p_o values were obtained by evacuating the entire (closed) oil circuit, including the overhead oil tank. Tank pressure and suction port pressure are essentially equal (the gravity head compensates flow losses). The results in Fig. 24 simulate high-altitude oil system operation. Dissolved air is reduced as the tank pressure is reduced.

Control by Throttling Side Flow. - Suction port pressure can, of course, be depressed simply by closing a valve between the tank and the pump. Fig. 25 shows Y values for tests made this way. The oil tank was vented to atmospheric pressure at all times. Consequently the oil may be regarded as saturated with air at one atmosphere. Comparison of the line, $Y = 0.68\ p_O$, with the curve in Fig. 25 shows how higher dissolved air content aggravates cavitation. At $p_O = 4$ psia, Y is about 25 per cent below that for the "altitude" tests, Fig. 24, where air was removed by maintaining the tank under vacuum. This difference shows why high-altitude operation should be simulated with the entire system under altitude pressure, not by throttling the pump. This applies to conventional rotary pumps, and to lube and fuel system tests in general as well as to the problem at hand.

Effect of Oil Properties. - As shown above the maximum or critical inflow velocity depends on $p_O - p_C$, where p_C is some minimum value, (the vapor pressure in the case of water). Y, as divorced from pump size, would be expected to be a function of fluid properties such as vapor pressure, air-solubility constant, viscosity and perhaps surface tension. As shown by Figs. 24 and 25, temperatures of 100 and 150 F gave the same results.

The currently approved synthetic (diester) oil MIL-L-7808 has an extremely low vapor pressure* that should suppress cavitation (raise Y) if "vapor" cavitation causes limiting flow.

Vapor pressure apparently exerts little effect on cavitation: In Fig. 26 Y vs. p_O data for Grade 1005 oil are compared with similar data taken with MIL-L-7808 oil. These tests, as well as other, here omitted, show essentially no difference between the two oils. Release of dissolved air or "air cavitation" is apparently the mechanism of limiting flow, not vapor cavitation.

Temporary Cavitation Suppression by Air Removal. - By operating the entire oil system under high vacuum for a prolonged period, most of the air can be stripped out of solution. Y values are nearly doubled by this procedure as shown by Fig. 27, at B. The C to D portion of the test consisted of taking a series of W_{SL} readings as tank and p_O pressure was increased in a rapid "dive" to sea level conditions. The top of the loop shows that a Y value of over 15 psi was reached. After a few minutes operation, air solubility equilibrium was again established and Y dropped to 10 psi, closing the loop. Synthetic oil was used in this test. This hysteresis loop effect was also noted for Grade 1005

---

* Vapor pressure of the synthetic oil at 300 F is only 0.1 compared to 80 mm Hg. for Grade 1010 oil (16). Vapor pressure of Grade 1005 oil is not available, but is well above 80 mm Hg.

oil--but to a lesser degree. Here the difference in vapor pressures probably plays a more important role.

<u>Note.</u> - The displacement of Y in Fig. 27 is a transient effect: after several minutes at one p_o value, limiting flow returns to the normal or equilibrium value. With the exception of Fig. 27 care was exercised in all limiting-flow tests to obtain reproducible data. W_{SL} values were measured in both directions, i.e., while slowly reducing p_o, and again during return of p_o to atmospheric pressure. Identical values of W_{SL} were obtained both ways.

D. Significance of the Limiting-Flow Function·

Limiting flow is important to jet pump design when it curtails the operating flow ratio, ϕ_{op}. Usual procedure calls for pump operation at a flow ratio near ϕ_{mep}, the maximum efficiency point. If $\phi_L < \phi_{mep}$, special consideration must be given to the cavitation problem. Given Y, ϕ_L can be predicted for any pump.

Combined with $\phi_L = W_{SL}/W_N$, Eq. 42 may be rearranged as follows:

$$\phi_L = \frac{1-b}{b} \sqrt{\frac{144\,Y}{\rho\,v_N^2/2g}} \tag{43}$$

This relation describes the limiting flow problem: ϕ_L is dependent on b, Y, and jet velocity. Theoretically,

$$Y = \frac{P_o - P_c}{1 + K_2},$$

and the limiting-flow tests (Fig. 24) show that $Y = 0.68\,p_o$, approximately. The jet velocity term may be replaced with the nozzle pressure drop by (Eq. 20). These changes produce:

$$\phi_L = \frac{1-b}{b} \sqrt{\frac{(1+K_1)\,0.68\,p_o}{p_1 - p_o}} \tag{44}$$

where pressures are psia.

<u>Limiting-flow ratio ϕ_L can be improved by:</u>

    a. Increasing suction-port absolute pressure p_o. Entrance velocity depends on $p_o - p_a$; and p_a is at a minimum under cavitating conditions.

b. Increasing the relative area of the secondary flow stream, $A_{Sa}/A_N = (1-b)/b$, by enlarging the throat (reduce b).

c. Reducing the jet velocity (reduce p_i-p_o).

Effect of Jet Velocity. - If the jet pump is operating under limiting flow conditions, the throat-entrance velocity of the secondary fluid is at a maximum. Increasing jet velocity, as by increasing W_N, will not affect W_{SL}. Limiting flow ratio will decrease inversely to W_N.

Fig. 28 is a plot of performance versus nozzle flow rate, pump suction at 14.1 psia. At about $W_N = 15$ lb/min, limiting flow was reached: the throat entrance pressure was reduced to "p_c" the critical value. Beyond this point W_{SL} is constant, ϕ decreases. In this case limiting flow first occurred at a nozzle pressure drop of about 70 psi. As shown below, this depends on p_o, and will occur at lesser pressure drops as the altitude is increased.

The function $Y = 0.68\, p_o$ is of concern only if the jet velocity is sufficiently high to depress the throat entrance pressure to the critical. This can be checked by calculating Y_{op} for the design condition of the pump, assuming no cavitation. From Eq. 44, but with Y_{op} in place of $Y = 0.68\, p_o$:

$$Y_{op} = \rho\, \frac{V_{Sa}^2}{2g} = \frac{p_i-p_o}{1+K_1}\, \frac{\phi_{op}^2 b^2}{(1-b)^2}$$

If this value is less than $Y = 0.68\, p_o$, the pump is not at the critical condition. Performance will be independent of absolute suction-port pressure, and affected only by pressure ratio N. Fig. 29 shows Y vs. p_o for a pump with low jet velocity: $(p_i-p_o) = 40$ psi. Note that at $p_o = 10$ psia, experimental Y values become constant at 7.0 psi. This is predicted by the equation above. Under the test conditions (at sea level) the flow ratio was $\phi_{op} = 1.78$. With $K_1 = 0.1$, $b = 0.2$,

$$Y_{op} = \frac{40}{1.1}\, (1.78)^2 \left(\frac{0.2}{1-0.2}\right)^2 = 7.1\ \text{psi}$$

The jet velocity is so low, that at sea level limiting flow does not occur. At $p_o = 10$ psia limiting flow starts.

E.   Altitude Ceiling

As a scavenge pump in an aircraft engine, the suction port absolute pressure may be assumed equal to the altitude pressure. Thus p_o will be 14.7 psia at sea level and only 1.047 psia at 60,000 feet (13).

Equation 44 may be arranged to express minimum suction port, hence altitude, pressure:

$$p_o = \frac{\phi_L{}^2 \, b^2 \, (p_i - p_o)}{(1-b)^2 \, 0.68 \, (1+K_l)} \tag{44a}$$

At the "altitude ceiling" the operating flow ratio ϕ_{op} equals the limiting flow ratio: $\phi_{op} = \phi_L$, by definition. Assuming that normal design procedure provides for $\phi_{op} \approx 2/3 \, \phi_{mep}$, then $\phi_L = 2/3 \, \phi_{mep}$. In Chapter I a useful (approximate) relation between ϕ_{mep} and b was presented:

$$\phi_{mep} = \frac{1 - \sqrt{b}}{\sqrt{b}} \tag{32}$$

Under these conditions,

$$\phi_L{}^2 = \frac{4}{9} \, \frac{(1-\sqrt{b})^2}{b} \quad \text{and Eq. 44a becomes}$$

$$p_o = \frac{4 \, (1-\sqrt{b})^2 \, b \, (p_i - p_o)}{9 \, (1-b)^2 \, 0.68 \, (1+K_l)} \tag{45}$$

Minimum p_o is expressed only in terms of area ratio b and the nozzle pressure drop. Eq. 45 is expressed graphically at the top of Fig. 30 for area ratios b = 0.1 to 0.6 and nozzle pressure drops of 20 to 200psi. The nozzle coefficient was assumed to be $K_l = 0.1$. The dashed portion below 40 psi and above 150 psi indicate extrapolation beyond the range covered in establishing $Y = 0.68 \, p_o$.

Even for b = 0.1 the altitude ceiling is seen to be only 35,000 ft for $p_i - p_o =$ 100 psi; and 50,000 feet for $p_i - p_o = 50$ psi. Larger area-ratios are even more limited.

Reduced Flow Ratio. - A considerable reduction in minimum p_o is obtained by reducing the operating, hence limiting, flow ratio. For example if $\phi_{op} = 1/4$ ϕ_{mep}, instead of $2/3 \, \phi_{mep}$, Eq. 45 becomes

$$p_o = \frac{1}{16} \, \frac{(1-\sqrt{b})^2 b \, (p_i - p_o)}{(1-b)^2 \, 0.68 \, (1+K_l)} \tag{45a}$$

Note that p_o is proportional to $(\phi_{op}/\phi_{mep})^2$, which appears as the coefficient $(2/3)^2 = 4/9$ in Eq. 45, and $(1/4)^2 = 1/16$ in Eq. 45a. Altitude ceiling with the lower flow ratio expressed in Eq. 45a is considerably improved, as shown at the bottom of Fig. 30. Here the ceiling on a pump with b = 0.1 is over 60,000 feet, even with $p_i = p_o = 200$ psi.

Inspection of Fig. 3 or Figs. 10 to 14 shows that at $\emptyset_{op} = 1/4 \, \emptyset_{mep}$, efficiency is about 10 to 12 per cent. This compares with 21 to 22 per cent at $\emptyset_{op} = 2/3 \, \emptyset_{mep}$. Obviously the procedure followed above could be reversed: values of $\emptyset_{op}/\emptyset_{mep}$ could be calculated as a function of altitude, b, and $p_i - p_o$.

Jet Pump Characteristics at 60,000 Feet. - If a minimum value of p_o is set, as by selecting 60,000 feet as the altitude ceiling, maximum allowable nozzle pressure drop can be calculated directly as a function of area ratio b. Eq. 44 may be arranged as follows:

$$p_i - p_o = \frac{(1-b)^2 \, (1+K_1) \, 0.68 \, p_o}{\emptyset_L^2 b^2} \tag{44b}$$

Again, $\emptyset_L = \emptyset_{op}$ could be found by the approximate relation for $\emptyset_{mep}$ as a function of b. Since high Reynolds number performance curves, N and η vs. $\emptyset$, are available from this work (see Figs. 10 to 14) they will be used instead. Let $\emptyset_{op} = 1/4 \, \emptyset_{mep}$ where $\emptyset_{mep}$ is the flow ratio at peak efficiency. For example, Fig. 13 shows that $\emptyset_{mep} = 1.2$ for b = 0.2, hence let $\emptyset_L = \emptyset_{op} = 1/4 \times 1.2 = 0.3$. At $\emptyset = 0.3$, N = 0.4, $\eta = 12$ percent. Following this procedure, Eq. 44b was calculated for b = 0.1 to 0.6, with $p_o = 1.047$ (60,000 feet), and $K_1 = 0.1$. The limiting nozzle pressure drop is plotted versus b in Fig. 31. It declines from 208 psi at b = 0.1 to 89 psi at b = 0.6. Using the N values from the experimental curves at $\emptyset_{op} = 1/4 \, \emptyset_{mep}$, maximum discharge pressures were calculated for each maximum nozzle pressure drop:

$$p_d - p_o = \frac{N}{N+1} \, (p_i - p_o)$$

The maximum discharge pressure rise, $p_d - p_o$, is plotted versus b in Fig. 31. Note that it is much less sensitive to area ratio: Maximum $p_d - p_o = 31.8$ psi at b = 0.1 and 59.4 psi at b = 0.6. The reason for this is the fact that N, hence N/N+1, increases rapidly with b, while maximum $r_i - p_o$ decreases with b. The two changes compensate each other.

Under "ceiling" conditions, pump discharge pressure is increased at the expense of $\emptyset$, by increasing b. The top curve in Fig. 31 shows that $\emptyset_{op}$ declines from 0.55 at b = 0.1 to only 0.0625 at b = 0.6. It would be advantageous to minimize back pressure to permit use of the smallest possible area ratio.

CHAPTER V

NOZZLE-THROAT SPACING, AND THROAT DESIGN

The theory developed in Appendix 1 and Chapter I permits design of a jet pump for any desired capacity and performance characteristic. The theoretical analysis does not predict what the distance from nozzle tip to throat entry should be, nor does it prescribe the correct throat profile.

A. Nozzle-Throat Spacing

The experimental jet pump, Fig. 8, was specially designed to permit study of the nozzle-throat spacing, termed S here. The nozzles were mounted in sections of No. 16 thin-wall tubing, which were inserted into the pump body through an O-ring seal (Fig. 8). By loosening the nut, the nozzle could be moved axially, allowing wide adjustment of S even while the pump was in operation. Scribe marks on the nozzle tube at intervals of 0.1 in. indicated the internal spacing S.

Experimental Results. - To find the optimum value of S, the spacing was set at approximately one nozzle diameter and the subject pump was set at a flow ratio of $\phi_{op} \approx 2/3 \; \phi_{mep}$ by adjusting the back pressure to the proper value. (Primary flow rate and suction port pressure were held constant. Cavitation was avoided by avoiding high jet velocities. Except where Reynolds number effect was being studied, R_N was kept high, usually over 20,000.) Optimum S was then found by varying the nozzle position in steps of 0.1 in. to obtain maximum secondary flow, W_S, with W_N and all three pressures held constant. The slight change in operating flow ratio was neglected.

Results are listed in Table 7 as S values, and as a ratio to nozzle diameter, S/d_N. Where more than one "optimum" S value is listed, W_S, hence efficiency, was essentially the same over the range of S values, i.e., there was low sensitivity to variation in S.

Discussion. - The S/d_N column in Table 7 reveals a consistent decrease with increase in b. It will be recalled that a large b means a small flow ratio, e.g., see Figure 3. Thus S decreased with flow ratio, as a result of varying b. (For each pump $\phi_{op} \approx 2/3 \; \phi_{mep}$). This suggests that the exposed area of the free jet before throat entry, $A_j = \pi d_N S$, decreases with ϕ as does the annular area A_{Sa} available for W_S at the throat entry (again, as a result of increasing b). A_{Sa} is defined as $A_m - A_N$ or $A_N (1-b)/b$, by assuming that the jet enters the throat with area equal to that at nozzle discharge, A_N. (See Appendix 1.)

TABLE 7 OPTIMUM NOZZLE-THROAT SPACINGS
(See Fig. 32)

Nominal Area Ratio, b	Pump No.	Test Nos.	S in.	S/d_N
0.1	100/316/	92	0.307	3.07
			0.407	4.07
0.133	141/387/	83, 128	0.311	2.21
			0.411	2.92
0.2	141/316	75,178	0.208	1.48
		179	0.308	2.18
0.2	100/224/	207	0.190	1.90
0.2	173/387/	205	0.219	1.26
0.3	173/316	152, 156	0.137	0.79
		158, 159	0.237	1.37
			0.337	1.95
0.4	141/224/	147	0.091	0.64
			0.191	1.35
			0.291	2.06
0.6	173/224/	163	0.120	0.69
			0.020	0.12

Assuming that $A_j = CA_{Sa}$, where C is a constant, let

$$\frac{A_j}{A_N} = \frac{CA_{Sa}}{A_N} = C\frac{1-b}{b} \qquad (46)$$

Substituting for the areas A_j and A_N in Eq. 46 results in,

$$\frac{S}{d_N} = C'\frac{1-b}{b} \qquad (47)$$

That such a proportionality exists is apparently verified by Fig. 32.

S/d_N values from Table 7 are plotted versus b, and compared with 1-b/b. The relation

$$\frac{S}{d_N} = \frac{1}{3}\frac{1-b}{b} \qquad (48a)$$

agrees well with the minimum spacings, and

$$\frac{S}{d_N} = \frac{1-b}{b} \qquad . \qquad (48b)$$

represents a sort of upper boundary. Multiple points at one b value show the range of S/d_N values over which performance was essentially constant. For this design, in which throat lengths were four times the throat diameters[*] $(L = 4d_m)$ the mean results for optimum spacing are well represented by,

$$\frac{S}{d_N} = \frac{1}{2} \quad \frac{1-b}{b} \tag{48c}$$

over a range of area ratios b = 0.1 to 0.6. Thus, for b = 0.2, S/d_N should be 2.0: the nozzle should be withdrawn from the throat entry by two nozzle diameters.

Optimum Spacing vs. Flow Ratio. - Results presented above were obtained at $\emptyset_{op} \cong 2/3 \, \emptyset_{mep}$. Experience showed that the optimum spacing increased some what with the flow ratio at which the given pump was operating. (at zero side flow, optimum spacing was redefined as that producing maximum discharge pressure for given fixed nozzle flow and side port pressure.) This trend confirms earlier findings (6).

Importance of S in Theory-Experiment Comparison. - Experimental values of N plotted versus $\emptyset$ were compared with theoretical N - $\emptyset$ characteristic curves in Chapter II. As explained there, K_{34} and K_1 values for use in the theoretical equations were calculated from the experimental data at $\emptyset_{op} \cong 2/3$ $\emptyset_{mep}$. This procedure of course resulted in exact matching of theory and experiment at the flow ratio $\emptyset_{op}$, where the K's were evaluated. Validity of the theory was judged on the basis of how well it predicted N at flow ratios below and above $\emptyset_{op}$.

As shown by Figs. 10 to 14, good agreement was found between theoretical and experimental N - $\emptyset$ curves, over a wide range of flow ratios. In the case of the two highest area ratios pumps, 177/240, b = 0.544, and 173/224, b = 0.6, this agreement resulted only after an appreciation of the importance of spacing S. The theoretical N - $\emptyset$ curve was found to agree with experimental results best when the spacing S was adjusted to optimum (best efficiency). Effect of changing S is to alter the slope of the experimental N - $\emptyset$ curve: an increase in S decreases the slope, moving the maximum efficiency point to the right, (increases $\emptyset_{mep}$). This sensitivity of slope and hence of agreement between theory and test results was noticeable only at the two highest area ratios. At b = 0.1 to 0.4, theory-test data agreement was affected slightly, if at all, by S.

Cavitation Limited Flow and Spacing. - A study of N - $\emptyset$ performance curves (sea level conditions) for several spacings indicated a slight tendency for large S values to suppress cavitation: $\emptyset_L$ could be increased slightly by increasing S. This was most noticeable at high b values. However, the gain is

---

[*] The effect of throat length on S/d_N is discussed in Part B, below.

small and since efficiency under normal conditions suffers as a result of the over-large S, the method is probably of no practical value, at least at sea level.

As the suction port absolute pressure is depressed (by evacuating the oil system including the tank) the effect of S on cavitation is somewhat greater. The limiting-flow function Y appears in Fig. 33 for three nozzle-to-throat spacings: optimum and less and greater than optimum. Y values are generally highest for the large S values. See Chapter IV for the relation between Y, W_{SL}, ϕ_L etc.

Effect of Low Jet Reynolds Number on Optimum Spacing. - Comparison tests at low Reynolds numbers (1800 to 3500) showed that optimum S was about the same as at high Reynolds numbers. This was true for pumps with b = 0.1 to 0.4. However, pump 177/240 with b = 0.544 showed best results at R_N = 3,580 when the spacing was made larger.

TABLE 8
EFFECT OF SPACING AT LOW JET REYNOLDS NUMBERS
Pump 177/240, b = 0.544, R_N = 3,580
Nominal W_N = 42 lb/min., p_o atmospheric

Test No.	S in.	N_o	N at ϕ = 0.2	ϕ_{mep}	η max %
168	0.255*	1.46	0.64	0.28	15.4
105	0.455	1.47	0.80	0.28	17.7

* Yields best efficiency at high R_N, where 0.455 in. is too large.

A tentative conclusion is that low Reynolds number performance can be improved by using large nozzle-to-throat spacing, but only at high b values. It may be that the short throat of this pump (about 2 diameters, see Fig. 9) influences these results.

B. Throat Length and Entrance Shape

In the literature on jet pumps, recommended values for the length of the parallel-wall throat section range from 4 diameters up to 10 diameters. With compressible flow little departure from optimum performance has been noted for lengths from 4 to 14 diameters. The value of S/d_N = 7 to 7.5 has been recommended by three investigators, cited by Kroll (10).

Several oil jet pumps purchased some time ago from Schutte and Koerting Co., Philadelphia, were designed with throat lengths which averaged about 2 diameters (0.48 < b < 0.62). Previous tests on oil jet pumps here, reported by Hussmann (6) showed that 4 diameters was slightly better than 2 diameters. For this work it was decided to adopt 4 diameters as the "standard" length (Fig. 8).

To check the effect of a short throat, particularly as regards cavitation limited flow, the throat-diffuser section for pump No. 141/316/307 was duplicated except with $L = 2d_m$ instead of $4d_m$. This part is denoted as 316-S in the table of dimensions, Fig. 8. The optimum nozzle-to-throat spacing was determined and a performance test at a high jet Reynolds number was made. Results are summarized in Table 9.

TABLE 9
COMPARISON OF TWO- AND FOUR-DIAMETER THROAT LENGTHS
Pump Nos. 141/316/308, 141/316-S/548; b = 0.2.
MIL-L-7808 Synthetic Oil at 150 F
Nominal $p_i - p_o$ = 100 psi, R_N = 20,000.

Test No.	L/d_m	ϕ_{mep}	η max %	K_1	K_{34}*	ϕ_L	S, in.
190	4	1.1	25.5	0.0956	0.337	1.27	0.308
199	2	1.05	23.3	0.0954	0.448	1.27	0.548

* Evaluated at ϕ = 0.9. Theory agreement with test results equally good with both throat lengths.

As shown in Table 9, the maximum efficiency was reduced slightly from 25.5 to 23.3 per cent in halving the throat length. This is also reflected in the throat-diffuser friction coefficient: K_{34} = 0.448 vs. 0.337 for the "standard" throat length of 4 diameters. Confirming the previous comparison (6), a four-diameter throat length is better - at least for b = 0.2, the area ratio involved here. The limiting-flow ratio ϕ_L was unaffected by changing L.

Throat Length and Optimum Nozzle Spacing. - The value of S was approximately doubled, from 0.208 - 0.308 in. for L/d_m = 4 (see Table 7) to 0.548 for the short throat pump. Mixing length along the jet is S + L, assuming completion of mixing at the diffuser entrance. Evidently the reduction L resulted in the increase in optimum S value: S and L are interdependent.

As was previously shown in Fig. 32, the trend of optimum spacings with b can be expressed approximately as

$$\frac{S}{d_N} = \frac{1}{2} \frac{1-b}{b} \tag{48c}$$

for the series of pumps from b = 0.1 to 0.6, all with four-diameter throat
lengths. This trend, and the relation between S and L shown by the comparison of two- and four-diameter throats, suggests that probably S + L
should vary with b through change in L, not in S, as was the case here.
Longer mixing lengths along the jet are required as b is reduced (hence ϕ_{op}
increased). If the throat lengths were progressively-increased as b was decreased, it is quite possible that optimum S would be essentially the same for
every b value. Further theoretical and experimental study of the relation between b, L, and S is recommended. Only limited work on jet mixing length
in an adverse pressure gradient has been reported (1, 18).

As reported in Chapter II, the pump with b = 0.3 gave best maximum efficiency, nearly 30 per cent. Efficiencies at b = 0.1 and 0.6 were
lowest, about 23 per cent. It is possible that this variation in efficiency is
in part a result of the fixed throat length. At or near b = 0.3, an L of four
diameters was perhaps "Optimum", while at lower b values L = 4 d_m was
inadequate. At b > 0.3, the four-diameter throats were probably too long for
best results. Through proper adjustment of throat lengths it should be possible to reduce the variation of efficiency with design area ratio.

Throat Entrance Shape. - The throat entry profile for the experimental jet
pump was selected as a short cone with an included angle of about 120 degrees.
A small radius at the entrance eliminated the sharp edge. (Fig. 8). A longer
conical entry with an angle of 60 degrees, was present in the "conventional"
pumps, Fig. 9. Comparison of performance curves reveals no advantage
from using the longer cone; this confirms previous findings (6).

Converging nozzles of high efficiency are obtained from a profile
consisting of a quarter of an ellipse (used for the nozzles in the experimental
jet pump). A throat-diffuser, part 0.317-E, was machined with such a profile
at the throat entry, and compared with the simpler conical entry. Area ratio
was b = 0.2 in both cases. Results are summarized in Table 10.

TABLE 10
EFFECT OF THROAT ENTRY SHAPE
Pump Nos. 141/316/308 and 141/317 -E/438, b = 0.2
Throat Lengths: L = 4d_m

R_N	Test No.	Throat -Diffuser	ϕ_{mep}	η_{max}%	K_1	K_{34}	ϕ_L
20,000*	190	0.316	1.1	25.5	0.096	0.337	1.27
20,000*	201	0.317-E	1.1	26.4	0.096	0.314	1.3
5,000**	72	0.316	1.2	22.8	0.246	0.318	—
5,000**	103	0.317-E	1.15	23.4	0.302	0.243	—

* MIL-L-7808 Synthetic Oil at 150 F. (p_i-p_o) = 100 psi, nominal
** Oil blends A and B. (p_i-p_o) = 40 psi, nominal

At both high and moderate Reynolds numbers the rounded throat entrance produced better results. But the small gain hardly justified the added difficulty of machining. The gain in ϕ_L indicates that cavitation was suppressed slightly by the gradual entrance curvature. Conclusion: The short conical entrance, with rounded corner at the throat bore, is recommended over a longer cone, or the ellipse shape

CHAPTER VI

THE JET PUMP AS A SCAVENGE PUMP
The Effect of Entrained Air in Oil

In the dry-sump lubrication system, used on most aircraft engines, oil supplied to the gears, bearings, etc., is collected at low points in pockets or sumps. This oil is usually removed by gear type scavenge pumps having a volumetric capacity 1.5 to 6 times the oil rate into the engines. This excess capacity is necessary for several reasons:

    a. To permit rapid removal of excess oil accumulated during maneauvers.

    b. To remove oil that is highly aerated in the sump, hence occupying a large volume.

    c. To maintain oil flow at high altitudes where the scavenge pump volumetric efficiency declines due to low absolute inlet pressure.

Items (a) and (b) still apply if the positive displacement pump is replaced with a jet pump. Regarding (c), it has been demonstrated (Chapter IV) that in order to reach extreme altitudes the jet pump must be operated at flow ratios considerably less than the maximum efficiency point (ϕ_{op} 1/4 ϕ_{mep}). This is simply a case of "oversizing" the pump to avoid cavitation-limited flow, and is analogous to gear pump practice.

As a result of the excess capacity the scavenge pump (gear or jet) handles a two-phase, two-component fluid: air mixed in oil. In Part A below the consequences of this departure from the clear oil side-low condition are examined.

As developed in Chapter I and Appendix 1, jet pump performance is described by the pressure ratio,

$$N = \frac{P_d - P_o}{P_i - P_d}$$

Pump efficiency is the product of N and the secondary-to-primary flow ratio $\phi = W_S/W_N$. The ratio of discharge - side port pressure difference to the nozzle pressure drop may be expressed in terms of N as

$$\frac{P_d - P_o}{P_i - P_o} = \frac{N}{N+1}$$

In the usual application of a liquid jet pump, the nozzle and side fluids are similar. If instead of a liquid, a two-phase two-component mixture is "picked-up" at the pump suction, the mixing process and the diffuser flow will be altered. The nozzle flow, on the other hand, will be unaffected. The expression for $p_d - p_o$ is derived below to include the effect of air.

Nomenclature:

W	mass flow rate, lb/sec
W'	mass flow rate, lb/min
Q	volumetric flow rate, ft^3/min
P	static pressure lb_f/ft^2
$\overline{P}$	total pressure, lb_f/ft^2
p	static pressure, psi
V	velocity ft/sec
ρ	density, lb_m/ft^3
η	efficiency
g	gravitational constant $\dfrac{lb_m ft}{lb_f sec^2}$
b	area ratio A_N/A_m
N	dimensionless pressure ratio p_d-p_o/p_i-p_d
ϕ	flow ratio W_S/W_N
ω	volumetric flow ratio, aerated oil to nozzle flow
$K_{1,2,3}...$	friction loss coefficients, see Chapter I.

Subscripts:

N	primary fluid at nozzle discharge
S	secondary or pumped fluid
A	air
AO	aerated oil
o	side flow entry to pump
i	nozzle entry
a	throat entry
m	throat exit, diffuser entry
d	pump discharge, diffuser outlet
mep	maximum efficiency point on the η vs ϕ plot
op	operating point on ϕ axis

Side-Flow Pressure Drop at Throat Entry. - It is assumed that a mixture of air and oil flows from the side port entry region at p_o pressure into the throat at a, entering the annular area between jet and throat walls. Assuming isothermal flow, the enthalpy change in air phase is zero (6). Air evolved from

the oil due to the pressure drop is ignored. The energy equation is,

$$\frac{P_o}{\rho_o} + \frac{V_{So}^2}{2g} = \frac{P_a}{\rho_a} + \frac{V_{Sa}^2}{2g} + \frac{P_{fl}}{\rho_a} \qquad (49)$$

where the density $\rho_{o,a}$ is that of the air-oil mixture. It is not independent of pressure as ρ for clear oil is. Let

$$P_{fl} = K_2 \frac{\rho_a V_{Sa}^2}{2g}$$

and multiply both sides by the downstream density:

$$\frac{\rho_a P_o}{\rho_o} + \frac{\rho_a V_{So}^2}{2g} = P_a + (1 + K_2) \frac{\rho_a V_{Sa}^2}{2g}$$

Let $\quad \overline{P}_{oA} \quad \frac{\rho_a P_o}{\rho_o} + \frac{\rho_a V_{So}^2}{2g}$

which for small changes in density is satisfactory, particularly since the inlet velocity head is usually negligible.

Eq. 49 then becomes

$$\overline{P}_{oA} - P_a = (1 + K_2) \frac{\rho_a V_{Sa}^2}{2g} \qquad (50)$$

By continuity,

$$V_{Sa} = \frac{W_S + W_{air}}{\rho_a A_{Sa}} \qquad (51)$$

Neglecting the air mass flow rate, and with $\phi = W_S/W_N$,

$A_{Sa} = Am - A_N = A_N \dfrac{1-b}{b}$, and $W_N = \rho V_N A_N$

Eq. 51 becomes,

$$V_{Sa} = \frac{\rho V_N \; \phi \; b}{\rho_a \; (1-b)} \qquad (52)$$

Neglecting the air mass flow rate, the mixture density at a, the throat entry, is defined as,

$$\rho_a = \frac{W'_S}{Q_S + Q_{As}} = \frac{\rho Q_S}{Q_S + Q_{Aa}} = \frac{\rho \; \phi}{\omega_a} \qquad (53)$$

where $\omega_a = \dfrac{Q_S + Q_{Aa}}{Q_N} = \emptyset + \dfrac{Q_{Aa}}{Q_N}$.

Combining Eqs. 50, 52, and 53,

$$\overline{P}_{oA} - P_a = (1+K_2) \frac{\rho}{2g} V_N^2 \left(\frac{b}{1-b}\right)^2 \emptyset \, \omega_a \qquad (54)$$

If no air is present, $\omega_a = \emptyset$, and Eq. 54 reduces to Eq. 4, Appendix 1.

Momentum Relations in Throat. - As previously developed, the pressure rise
in the throat is the change in momentum between entry and exit less the wall-
friction drag loss. Again the weight of the air will be dropped, as a neg-
ligible contribution to the input momentum. *

$$\frac{W_N V_N}{g} + \frac{W_S V_{Sa}}{g} - \frac{W_T V_m}{g} - F_{fl} = A_m (P_m - P_a) \qquad (55)$$

Following the procedure for the clear oil case, let

$$F_{fl} = K_3 A_m \frac{\rho_m}{2g} V_m^2$$

The throat exit velocity V_m is related to the nozzle velocity as

$$V_m = \frac{W_T}{\rho_m A_m} = \frac{\rho V_N b (1+\emptyset)}{\rho_m} \qquad (56)$$

By definition the mixture density at m is,

$$\rho_m = \frac{\rho Q_N + \rho Q_S}{Q_N + Q_S + Q_{Am}} = \frac{\rho(1+\emptyset)}{1 + \omega_m} \qquad (57)$$

where $\omega_m = \dfrac{Q_S + Q_{Am}}{Q_N} = \emptyset + \dfrac{Q_{Am}}{Q_N}$

As before the air mass flow rate is neglected.

---

* Folsom, Chemical Engineering Progress, v. 44, Oct. 1948, p 765
  derived the momentum equation for a liquid-jet air pump consisting of
  a straight tube without diffuser. For no oil side flow ($\emptyset = 0$) and with no
  diffuser, the above relations become similar to Folsom's.

Q_{Am} is the volumetric air flow rate at the pressure (P_m) and temperature (i.e., oil temperature) at the throat outlet.

Inserting the continuity relations, the momentum equation becomes,

$$P_m - P_a = \frac{\rho}{2g} V_N^2 \left[2b + \frac{2\phi \, \omega_a b^2}{1-b} - (2+K_3) b^2 (1+\phi)(1+\omega_m) \right] \quad (58)$$

For no entrained air this reduces to Eq. 7.

Diffuser Energy Equation. - The equation is similar to that developed for oil flow only, except that density is no longer a constant:

$$\frac{P_m}{\rho_m} + \frac{V_m^2}{2g} = \frac{P_d}{\rho_d} + \frac{V_d^2}{2g} + \frac{P_{fl}}{\rho_m} \quad (59)$$

Multiply by ρ_m and let

$$\overline{P}_{dA} \quad \frac{\rho_m P_d}{\rho_d} + \rho_m \frac{V_d^2}{2g}$$

which is satisfactory except for large changes in density. The velocity head in the outlet pipe from the jet pump is generally negligible: $\overline{P}_d \approx P_d$. With

$$P_{fl} = \frac{K_4 \rho_m V_m^2}{2g}$$

and the expression for ρ_m developed above, Eq. 59 becomes

$$\overline{P}_{dA} - P_m = (1-K_4) \frac{\rho V_N^2}{2g} b^2 (1+\phi)(1+\omega_m) \quad (60)$$

Side Port to Discharge Pressure Rise. - By combining Eqs. 54, 58, and 60, $\overline{P}_d - \overline{P}_o$ is found to be,

$$\overline{P}_{dA} - \overline{P}_{oA} = \frac{\rho}{2g} V_N^2 \left[2b + \frac{2\phi \omega_a b^2}{1-b} - (1+K_2)\phi \omega_a \frac{b^2}{(1-b)^2} \right.$$

$$\left. -(1+K_3 + K_4) b^2 (1+\phi)(1+\omega_m) \right] \quad (61)$$

Similarly, combining the nozzle energy equation

$$\overline{P}_i - P_a = \frac{\rho}{2g} V_N^2 (1+K'_1) \quad (3)$$

with Eq. 54,

$$\bar{P}_i - \bar{P}_{oA} = \frac{\rho}{2g} V_N^2 \left[1 + K'_1 - (1+K_2) \frac{\phi \omega_a b^2}{(1-b)^2} \right] \quad (62)$$

Finally, by combining Eqs. 61 and 62 the overall pressure drop $\bar{P}_i - \bar{P}_{dA}$ may be found. Comparison of these basic equations with their counter-parts developed in Appendix 1 for side inlet flow without air, reveals that ϕ^2 has been replaced by $\phi \omega_a$ and that $(1+\phi)^2$ has been replaced by $(1+\phi)$ $(1+\omega_m)$. For no air flow $\omega_a = \omega_m = \phi$, and the relations reduce to identity with the original equation. The effect of the air is to reduce the density of the fluid, thus increasing the velocities (for the same oil flow).

Relation to N - ϕ Characteristic Curve. - The above relations describe approximately the relations between pressure differences and air content. The effect of air is to cause the pump to operate at a higher pressure drop, hence a lower N value. It is postulated that with aerated secondary flow the corresponding pressure ratio, N_{Ao}, is related to ω in the same manner that N is related to ϕ when no air is present: N_{Ao} vs ω is identical with N vs. ϕ. ω is the volumetric ratio of an air-oil mixture to the nozzle oil flow rate, and N_{Ao} is the dimensionless ratio of pressures $(\bar{P}_d - \bar{P}_o)/(\bar{P}_i - \bar{P}_d)$.

The mass rate of air flow corresponding to ω depends upon what pressure the volumetric air rate is evaluated at, such as P_a or P_m. As shown below, evaluation at P_a leads to rather satisfactory agreement of this approximate theory with the experimental results.

Air Flow Rate. - By definition of ω_a,

$$Q_{Aa} = \omega_a Q_N - Q_S = \frac{W_N}{\rho} (\omega_a - \phi) \quad (63)$$

and

$$Q_{Ao} = Q_{Aa} \frac{p_a T_o}{p_o T_a} \quad, \quad Q_{A,NTP} = Q_{Aa} \frac{p_a 520}{14.7 T_a} \quad (64)$$

Q_{Ao} and $Q_{A,NTP}$ are the volumetric air flow rates at the side port pressure and temperature and at NTP conditions, respectively. By assuming that the air temperature at a, the throat entry, is equal to the oil temperature, solution of Eqs. 63 and 64 for the air rate requires only that P_a be known. ω_a is found from the N - ϕ characteristic curve of the pump in question at N_{Ao}. This may either be the theoretical curve (eq. 23) or an experimental curve measured with a clear-oil side flow, i.e., without air.

Evaluation of P_a. - The throat entry pressure is found from Eq. 54 as follows:

$$P_a = \bar{P}_{oA} - \frac{\rho}{2g} V_N^2 \frac{b^2}{(1-b)^2} \phi \omega_a \quad (65)$$

As with the clear oil case, side flow velocity-head is neglected: $\bar{P}_{oA} \cong P_oA$. The throat entry coefficient K_2 has been dropped as negligible. All of the above terms are known if the oil flows W_N and W_S are given, and the three pressures at inlet, suction, and discharge of the pump. The aerated-flow volume ratio ω_a is obtained from the N characteristic curve at the N_{A_o} value represented by the three pressures $\bar{P}_1$, $\bar{P}_{oA}$ and $\bar{P}_{dA}$ for the aerated secondary flow operation.

Experimental Results, Two Phase Flow

The amount of secondary fluid pumped by a jet pump with a given jet velocity, or W_N rate, is governed by the discharge pressure $\bar{P}_d$. Just as with a centrifugal pump, an increase in back pressure will decrease the pump capacity until at the "shut-off head" the flow of pumped fluid becomes zero.

A fixed relation N vs $\emptyset$, exists between pressure ratio and flow rate. If the side fluid is restricted to a fixed rate (as scavenge oil is in an engine) and the discharge pressure P_d is then lowered, one or a combination of the following result:

(a) <u>With restricted suction line</u>: The side port pressure P_o will decrease until the balance between N and $\emptyset$ has been restored.

(b) <u>With vented suction</u>: Air will be drawn in at a rate dependent upon the back pressure. The lower P_d is, the greater the air rate. The "starved" pump makes up for an inadequate secondary oil flow by drawing in air.

Case (b) above is that existing in the scavenge pump application of the jet pump. The "scavenge ratio" for a given pump is determined to some extent by the back pressure. Again, note the similarity to the centrifugal pump: capacity is determined by discharge pressure.

<u>Test Procedure</u>. - Fig. 34 shows the flow diagram for two-phase flow. The side port, normally connected to a supply of oil, was fed from the bottom of a "sump". The secondary oil flow at rate W_S was admitted to the side of the sump as shown; and the top of the sump was vented to the atmosphere through a rotameter used for air measurement. Several pumps were operated at $\emptyset_{op}$ values selected by examination of their characteristic curves (See Figs. 10 to 14), ranging from 1/3 to 2/3 of $\emptyset_{mep}$. Nozzle flow rates were such as to yield p_i values of 40 psig or 100 psig. Suction port pressures were atmospheric.

As a back pressure p_d corresponding to N at the operating $\emptyset$ value, no air was drawn in. With any reduction of p_d below this value, air was inducted and measured by rotameter. Measured air rates are converted to NTP conditions (14.7 psia and 60 F) and compared with calculated $Q_{A, NTP}$ values.

<u>Test Results.</u> - From the N - ϕ characteristic curve for the pump under test ω_a is obtained as that corresponding to N_{AO}, the air test pressure ratio. p_a is then calculated with the ϕ and ω_a values using Eq. 65, leading to calculation of Q_{Aa} and/or $Q_{A,NTP}$.

<u>Operating Conditions for Test No. 100, Pump No. 100/316/307</u>

b, nominal	0.1
$\left(\dfrac{b}{1-b}\right)^2$	0.0124
oil	blend "B"
oil temp.	200 F
viscosity	6.7 centistokes
ρ	51.5 lbs/ft^3
W'_N	12.6 lb/min
P_i	40 psig, nominal
P_o	-0.10 psig, (14.13 psia)
W'_S	19.9 lb/min
ϕ	1.58 $\Big\}$ no air flow
N	0.131

When operated at any pressure ratio below N = 0.131, air was inducted at the side port: W_S was held constant at 19.9 lb/min. To obtain mixture flow ratios ω_a, the N - ρ characteristic curve is used, either experimental or theoretical. Fig. 35 is the curve for Pump No. 100/316/307. Assuming N_{AO} = 0.05, ω_a is read as 3.11.

Hence,

$$Q_{Aa} = \frac{W'_N}{\rho}(\omega_a - \phi) = \frac{12.6}{51.5}\left(3.11 - 1.58\right) = 0.374 \text{ ft}^3/\text{min}$$

$$P_a = P_{oA} - \frac{\rho V_N^2}{2g \times 144}\omega_a \rho \left(\frac{b}{1-b}\right)^2 \quad \text{psia}$$

where p_{oA} is expressed in psia units.

By continuity, $W_N = A_N V_N \rho$, and

$$\frac{\rho V_N^2}{2g \times 144} = \frac{0.1451}{\rho}\frac{W_N^2}{d_N^4 \times 144} = \frac{0.1451 (12.6)^2}{0.0001 \times 51.5 \times 144} = 31.0 \text{ psi}$$

$$p_a = 14.13 - 31.0 \times 3.11 \times 1.58 \times 0.01238 = 12.25 \text{ psia}$$

In correcting Q_{Aa} to NTP conditions, 14.7 psia and 60 F, it is assumed that the air in the throat has been heated to oil temperature, 200 F.

Hence $Q_{A,NTP} = Q_{Aa} \dfrac{P_a \, 520}{14.7 \, T_a} = 0.374 \, \dfrac{12.25 \times 520}{14.7 \times 660} = 0.246 \text{ ft}^3/\text{min}$

This value for air flow at $N_{AO} = 0.05$ is one point comprising the theoretical air flow curve plotted versus N_{AO} in Fig. 36. The points and dashed line represent the experimental results from Test No. 100.

By definition the theory and test results agree at $Q_A = 0$. At higher air flows the two differ by as much as 10 to 20 per cent for this test. In view of the complexity of this flow process and the necessarily approximate nature of the solution the agreement is surprisingly good.

Fig. 37 compares theory and experiment for the same pump but at a higher jet velocity ($p_i = 100$ psig versus 40 psig in Fig. 3). Again the trend is satisfactorily predicted.

Test with b = 0.20. - Air tests have been made with Pump No. 141/316/308 (see Fig. 8) and typical results appear in Fig. 38 along with the theoretical curve. The agreement is similar to the pump with b = 0.1. The operation was at higher N_{AO} values, of course, because of the change in pump area ratio.

Test with b = 0.544. - To further test the validity of the solution air tests were made using Pump No. 177/240/455, a pump with a relatively high area ratio, b = 0.544. (See Fig. 9). This means that the pump operates at high N values, but only at very low flow ratios. (The maximum efficiency flow ratio is about $\emptyset_{mep} = 0.35$).

Fig. 39 shows the result of a test at $\emptyset = 0.10$. The agreement with the theory is similar to the other two pumps tested.

Conclusion. - Three jet pumps have been tested with a two-phase two-component mixture of air and oil inducted at the side port. This simulates the condition under which a jet pump would function as a scavenge pump. When coperated at a pressure ratio below that corresponding with the oil flow ratio $\emptyset$, and with a vented "sump", air is drawn into the pump. The air rate is found to vary in a nearly linear manner with N_{AO}, the air test pressure ratio.

The hypothesis that the jet pump will pump air at a rate equal to the oil "deficiency" (as indicated by the departure from the basic characteristic curve of the pump), is borne out by agreement with measured air rates. Within rather narrow limits the scavenge ratio of a given jet scavenge pump may be decreased by raising the back pressure, and conversely. In general, however, the pump capacity, hence scavenge ratio, is a question of energy input, i.e., nozzle flow and pressure, and the design area ratio of the pump.

B. Aerated Primary Flow

The jet scavenge pump would be "powered" hydraulically by a supply of lubricating oil from an engine-driven positive displacement pump. This might be a separate pump, or one or more added elements inside the body of the main pressure pump. The oil delivered to the nozzle of the jet scavenge pump would normally be free of entrained air. However, under conditions conducive to poor separation of air from the oil in the tank or deaerator, the primary flow at the jet pump might contain entrained air.

It has been shown theoretically and experimentally (6) that air entrained in the nozzle fluid increases the nozzle pressure drop, P_i-P_o, and the output pressure rise, P_d-P_o, compared with the same flow rate of clear oil. The approximate theoretical relations developed above in Part A serve to illustrate the approach; further derivations will be omitted here.

Nozzle Pressure Drop. - In the nomenclature of this report the nozzle pressure drop for aerated primary flow may be expressed (6) as,

$$(P_i-P_o)_A \approx (1+X_o) \ \frac{\rho V_N^2}{2g} \ (1+K_1)$$

thus
$$\frac{(P_i-P_o)A}{P_i-P_o} \approx 1 + X_o \tag{66}$$

where
$$X_o = \frac{Q_{Ao}}{Q_N} \tag{67}$$

is the aeration of the nozzle fluid at the nozzle discharge pressure; ρ is the oil density. As explained in Appendix 1, present experimental results have demonstrated that within experimental accuracy, effective discharge pressure at the nozzle tip is P_o; for all of the pumps tested in this program.

The earlier report compared experimental results with the approximate relation, Eq. 66; agreement was good. Since the tests were confined to relatively low pressure drops, of the order of 10 psi or less, it was deemed advisable to check the behavior of the jet pump under the higher pressure-drop conditions to be encountered in the scavenge-pump application. The test stand circuit shown in Fig. 7 was modified to permit aeration of the primary stream. Room air was metered through a wet-test gas meter into the suction side of the variable speed oil pump at a tee in the oil supply line from the tank. (The oil rotameter was located upstream from the tee.) A throttle valve in the oil line between the tee and rotameter was used to control the amount of air drawn in; by slightly depressing the gage pressure at the air bleed point.

Air Content at Nozzle Discharge. - Lubricating oil contains approximately 10 per cent by volume of dissolved air at one atmosphere pressure under equilibrium conditions. This changes directly as the absolute pressure over the oil. The nozzle discharges to pressure P_O, which was nearly atmospheric in the following tests. Hence, the volume of entrained air at P_O was essentially the same as that metered into the system, corrected, however, for the temperature change. Let Q_{AM} ft^3/min be the volumetric air rate at barometric pressure and room temperature indicated by the air meter. Then the air rate at the nozzle discharge pressure P_O is:

$$Q_{Ao} = Q_{AM} \frac{T_O}{T_M} \tag{68}$$

from which
$$X_O = \frac{Q_{Ao}}{Q_N} \tag{67}$$

The absolute temperature of the air, T_O, is assumed equal to that of the oil. Air temperature, T_M, at the meter is room absolute temperature. Q_N is the volumetric primary oil flow rate.

Test Results. - Pump No. 141/316/308, b = 0.2, was operated at oil rates corresponding to nozzle pressure drops of 40 and 80 psi (with clear oil) P_O was atmospheric and P_d was controlled to obtain an operating flow ratio of $\emptyset_{op} \cong 2/3 \ \emptyset_{mep}$, which is 0.8 for this particular pump. In addition a test at 40 psi was made with zero side flow; $\emptyset = 0$. Air was added to the primary oil stream and resultant pump behavior noted. In Fig. 40 the ratio of measured nozzle pressure drop with aerated primary fluid to pressure drop with clear oil (same W_N) is plotted versus $1 + X_O$. The approximate theoretical expression, Eq. 66, is shown for comparison.

At these high nozzle pressure drops, the actual increase of $P_i - P_O$ due to entrained air is considerably less than predicted, as shown by Fig. 40. The curve for the 80 psi pressure drop (clear oil) condition falls below that for 40 psi. (Note that the points at 40 psi fall on the same line for $\emptyset = 0.8$ and $\emptyset = 0$.) Reference (6) reported that experimental values of

$$\frac{(P_i - P_O)A}{P_i - P_O} \quad \text{were}$$

predicted quite well by $1 + X_O$; where the pressure drops were only of the order of a few psi. This indicates that the effect of entrained air is a maximum at very low pressure drops, and decreases considerably as pressure drop goes up. For example, at $X_O = 50$ per cent aeration, the nozzle pressure drop is increased by 50 per cent for $P_i - P_O \cong 2$ psi (reference 6), but is increased only 40 per cent for $P_i - P_O = 40$ psi and about 30 per cent for an 80 psi nozzle pressure drop; reading from the curves in Fig. 40 at $(1 + X_O) = 1.5$. This could well be an air-in-oil solubility effect. At high pressures appreciable portions of the entrained air probably are dissolved in the oil by the time the turbulent mixture arrises at the nozzle. At the high jet velocities the air-

oil mixture may leave the nozzle in a metastable condition: The time interval is too short to permit evolution of the dissolved air as the static pressure on the oil drops rapidly. The entrained air content is thus actually less than assumed under equilibrium conditions, suppressing the volume-increase effect of the air.

Output Pressure Rise and Efficiency. - The output pressure rise P_d-P_o also increases with nozzle fluid aeartion as shown in Fig. 41, where the ratio of $(P_d$-$P_o)_A$ to P_d-P_o for clear oil is plotted for the same tests as Fig. 40. Output pressure increases almost as fast as nozzle pressure drop, and as a result pump efficiency declined very little with nozzle aeration for these tests at 40 and 80 psi. Note that the efficiency loss was greatest for the lowest pressure drop. (At very low pressure drops, the decrease in efficiency would be greater.)

Effect on Performance Curve. - A performance test (No. 212) was made on the b = 0.2 pump with W_N = 40 lb/min (80 psi nozzle pressure drop with clear oil). Air was bled into the primary stream to produce a (theoretical) aeration (at discharge pressure and oil temperature) of 37 per cent. This amount of aeration raised the nozzle pressure drop to 86.2 psi. The N vs. $\emptyset$ and η vs. $\emptyset$ characteristic curves were virtually identical with those for clear oil, (see Fig. 13.) : $\emptyset_{mep}$ was 1.2 and η_{max} was 26.2 per cent. One difference was noted: Limiting-flow ratio was $\emptyset_L$ = 1.28 whereas $\emptyset_L \approx 1.4$ for clear oil with similar nozzle pressure drop (86.2 psi) and side port pressure (atmospheric). (See Chapter IV). The added air thus aggravated the cavitation tendency somewhat.

Conclusion. - At nozzle pressure as high as 40 and 80 psig aeration of the primary oil stream exerts very little effect on pump behavior. Nozzle pressure drop and output pressure rise both increase with aeration. This nozzle pressure drop response to air entrainment is considerably less than at very low pressure drops of the order of 2 psi. Primary stream aeration would apparently cause no particular problem in the jet scavenge pump application.

CHAPTER VII

DESIGN PROCEDURE AND EXAMPLES

Jet pump performance is described by the primary and secondary flow rates W_S and W_N and the nozzle, side port, and discharge total pressures $\overline{P}_i$, $\overline{P}_o$ and $\overline{P}_d$. The latter may usually be replaced with static pressures P_i, P_o, P_d. These operating variables comprise the flow rates, $\emptyset = W_S/W_N$, and the pressure rates, $N = P_d-P_o/P_i-P_d$. Physically the pump is characterized by the nozzle and throat areas A_N and A_m; dimensionlessly, $b = A_N/A_m$.

The three factors N, $\emptyset$ and b are related by the analytical Eq. 23, including friction loss coefficients, K_1, K_2 and K_{34}:

$$N = \frac{2b + \dfrac{2\emptyset^2 b^2}{1-b} - (1+K_{34}) b^2 (1+\emptyset)^2 - \dfrac{\emptyset^2 b^2}{(1-b)^2}}{1 + K_1 - \text{numerator}} \qquad (23)$$

The optimum relation between b_{opt} and $\emptyset$ was found from $\partial N/\partial b = 0$, producing Eq. 30 and Fig. 4 ($K_{34} = 0$ to 1.0, and with $K_2 = 0$).

General Procedure, High Reynolds Number Case. - In the usual situation with light oils and high jet velocities, the Reynolds number will probably exceed 15,000 or 20,000. Here it may be assumed that $K_1 = 0.1$ and $K_{34} = 0.3$; for design use, Fig. 42 relates b_{opt}, $\emptyset$, and N. Given one of the three factors, the other two can be read directly from the curves. For comparison, the experimental values of $\emptyset_{mep}$ and N_{mep} for eight jet pumps are shown in Fig. 42 (see Table 3, Chapter II). In general, K values were less than $K_1 = 0.1$ and $K_{34} = 0.3$ for large b values, and slightly larger at $b = 0.1$. Thus there is some departure from the solid line curves.

Procedure Example 1. - Given secondary flow rate and discharge pressure*, and the requirement for a high flow ratio: Design the pump.

Given: W_S, P_d-P_o
Find: b, W_N, P_i-P_o, d_N, d_m.

The requirement for high flow ratio dictates the choice of a small area ratio (Fig. 42). This work extended to a minimum value of $b = 0.1$, which will be selected here. Fig. 42 shows that $\emptyset_{th} = 2.5$ and $N_{th} = 0.1$. Hence, efficiency

---

* Since suction port pressure is usually atmospheric, discharge gage pressure is essentially equal to P_d-P_o lb_f/ft^2 or p_d-p_o, psi. Similarly p_i-p_o approximately equals nozzle gage pressure.

56

$\eta = \phi_{th}N_{th}$, is 25 per cent.[*] This is at a flow ratio essentially equal to the maximum efficiency point. (This value, ϕ_{mep}, can be calculated directly with Eqs. 31 or 32.) It is recommended that pumps be designed conservatively to operate at $\phi_{op} = 2/3\ \phi_{mep} \approx 2/3\ \phi_{th}$; (but ϕ_{op} will be dictated by cavitation limits for high altitude use - see below). Correspondingly, $N_{op} \approx 4/3\ N_{th}$, which results from the linear N-ϕ approximation, Eq. 34, Chapter I. The pump will be operated at $\phi_{op} \approx 2/3 \times 2.5 = 1.67$ and $N_{op} = 4/3 \times 0.1 = 0.133$, $\eta = 22.3$ per cent. Nozzle flow is $W_N = W_S/\phi_{op}$; and the nozzle pressure drop (P_i-P_o) is found from

$$\frac{P_d-P_o}{P_i-P_o} = \frac{N}{N+1}$$

Nozzle diameter is found from the nozzle equation

$$P_i-P_o = \frac{\rho V_N^2}{2g}\ (1+K_1) \qquad (20)$$

and the continuity relation

$$W_N = \rho A_N V_N$$

yielding,

$$d_N^4 = 16.15 \times 10^{-6}\ \frac{(1+K_1)\ W_N'^2}{s.g.\ (p_i-p_o)} \qquad (69)$$

where, d_N = nozzle diameter, inches

K_1 = nozzle coefficient, usually 0.1

W_N' = nozzle flow rate, lb_m/min

s.g. = oil specific gravity

$P_i - P_o$ = nozzle pressure drop, psi

The throat diameter is found from b and d_N,

$$d_m = \frac{d_N}{\sqrt{b}}$$

Nozzle-to-throat spacing is found from (Chapter IV):

$$S = d_N\ \frac{1}{2}\ \frac{1-b}{b} \qquad (48c)$$

[*] Subscript refers to the theoretical values from Fig. 42.

Recommended pump design is that in Fig. 8: The throat entrance is a short cone of about 120 degrees included angle; diffuser angle is 8 degrees; throat length is four diameters. The adjustable nozzle-spacing feature can, of course, be omitted.

Procedure Example 2. Given secondary flow rate and (high) discharge pressure. Design the pump for maximum recovery of nozzle pressure.

Given: W_S, P_d-P_o
Find: b, W_N, P_i-P_o, $d_N d_m$.

Here a large b value is indicated in order to obtain a high N. Select b = 0.5: From Fig. 42 N_{th} = 0.94, ϕ_{th} = 0.23. Following the procedure above ϕ_{op} = 2/3 x 0.23 = 0.153, N_{op} = 1.24, etc. These two examples illustrate the procedure and use of Fig. 42. Note that in addition to the pump "duty", i.e., capacity and discharge pressure, some information must be had as to the desired pump characteristics. This may be the need for (a) High flow ratio, or (b) High discharge pressure relative to nozzle pressure, or (c) Maximum efficiency. If the latter is the case, choose b = 0.2 to 0.3. Selection of b is the first step, in any case.

Scavenge Pump Design

Application of the jet pump as an oil scavenge pump in an aircraft engine requires consideration of the following:

1. The effect of viscosity, or better, Reynolds number.
2. The cavitation characteristics, or more directly, the altitude ceiling.
3. Pump behavior with two-phase, two-component, secondary flow.

To illustrate the use of the material in this report, a design example is presented which includes treatment of each of these problems in the course of the solution.

The Problem

Substitute a jet pump for the aft or midframe scavenge pump of a model J-47 turbojet engine. The oil rate to be handled by the jet scavenge pump in 3.5 gal/min; the back pressure on the pump is 25 psig, with Grade 1005 oil at 100 F. The flow ratio is to be a maximum in order to conserve weight (pump the 3.5 gpm with a minimum nozzle or primary flow rate). Find pump size and operating characteristics.

Pump Size. - The procedure in Example 1 above will be followed. To obtain a high flow ratio, use $b = 0.1$; from Fig. 42, $\phi_{th} = 2.5$ and $N_{th} = 0.1$. Let

$$\phi_{op} = \frac{2}{3} \phi_{mep} \qquad \frac{2}{3} \phi_{th} = \frac{2}{3} 2.5 = 1.67$$

$$N_{op} = \frac{4}{3} \times 0.1 = 0.133$$

Alternately, these values can be found from the "linear" or approximate $N - \phi$ characteristic curve. (Chapter I):

$$N = N_0 - \frac{N_0}{\phi_0} \phi \tag{34}$$

$$N_0 = \frac{2b - (1+K_{34})b^2}{1+K_1 - numerator} \tag{23a}$$

$$\phi_{mep} = \frac{\phi_0}{2} \tag{35}$$

The maximum flow ratio ϕ_0, a function of $K_{34} = 0.3$, and $b = 0.1$, is conveniently found from Fig. 5, as $\phi_0 = 4.6$. Hence $\phi_{mep} = 2.3$ (compared with 2.5). A function of $K_1 = 0.1$ as well as K_{34} and b, N_0 is

$$N_0 = \frac{2 \times 0.1 - (1.3) \times 0.01}{1.1 - numerator} = 0.205$$

and $N_{mep} = N_0/2 = 0.102$, compared with 0.1 from Fig. 42. At $\phi_{op} = 2/3 \phi_{mep}$, and $\phi_{mep} = \phi_0/2$, Eq. 34 reduces to,

$$N_{op} = \frac{2}{3} N_0 = 0.137, \text{ compared with } 0.133.$$

The former values, derived from Fig. 42, will be used below.

Note. - The simplified linear $N - \phi$ characteristic curve is quite accurate at low b values, 0.1 to 0.2. As b increases the actual $N - \phi$ line becomes increasingly concave (up). As a result the approximate $N - \phi$ curve will err on the high side, at high b values. The full theoretical N Eq. 23 should be used for better accuracy.

With $N_{op} = 0.133$, and $p_d - p_o = 25$ psi,

$$p_i - p_o = \frac{(N+1)25}{N} = \frac{1.133}{0.133} \times 25 = 214 \text{ psi}$$

Upon determination of the nozzle pressure drop, the limiting-flow ratio ϕ_L should be checked. If less than ϕ_{op}, modification will be necessary. From Chapter IV,

$$\phi_L = \frac{1-b}{b} \sqrt{\frac{(1+K_1)\, 0.68\, p_0}{p_1-p_0}} \qquad (44)$$

$$\phi_L = \frac{1-0.1}{0.1} \sqrt{\frac{1.1 \times 0.68 \times 14.7}{214}} = 2.04$$

Since $2.04 > 1.67$, the design is satisfactory at $p_0 = 14.7$ psia, or sea level. Following discussion of the Reynolds number effect below, the altitude ceiling will be covered.

At 100 F, the specific gravity of Grade 1005 oil is 0.863, see Fig. 43.

$$W'_S \frac{lb}{min} = \frac{gal}{min} \times s.g. \times \frac{62.4}{7.48}$$

$$W'_S = 3.5 \times 0.863 \times \frac{62.4}{7.48} = 25.2 \ lb/min$$

With the flow ratio $\phi_{op} = 1.67$,

$$W'_N = \frac{25.2}{1.67} = 15.1 \ lb/min$$

The nozzle diameter is

$$d_N^4 = \frac{0.1615 \times 10^{-4} \times 1.1 \times (15.1)^2}{0.863 \times 214} = 0.219 \times 10^{-4}$$

$$d_N = 0.0684 \ in.$$

The throat diameter is,

$$d_m = \frac{d_N}{\sqrt{b}} = \frac{0.0684}{0.316} = 0.216 \ in.$$

The throat length is four diameters,

$$L = 4 \times 0.216 = 0.865 \ in.$$

Nozzle-to-throat spacing, from Chapter V,

$$\frac{S}{d_N} = \frac{1}{2} \quad \frac{1-b}{b} = 4.5$$

$$S = 0.0684 \times 4.5 = 0.308 \text{ in.}$$

The Effect of Low Reynolds Number. - For the conditions above, the jet Reynolds number is,

$$R_N = \frac{379.1 \; W'_N}{s.g. \; \nu \; d_N} \tag{38}$$

$$R_N = \frac{379.1 \times 15.1}{0.863 \times 5.2 \times 0.0684} = 18,700$$

where the viscosity, ν = 5.2 centistokes, was obtained from Fig. 44 at 100 F. This value is sufficiently high to justify the assumed (minimum) friction coefficients K_1 = 0.1 and K_{34} = 0.3. It should be noted, however, that K_1 is likely to be larger than 0.1 with such a small nozzle diameter. The plot of K_1 values versus R_N in Fig. 16 reveals a definite size effect, comparing K_1 for d_N = 0.100 versus the 0.177 or 0.173 inch nozzles.

If R_N = 1,000, what effect will it have on design? Assuming R_m is also 1,000, Figs. 16 and 17 yield, K_1 = 0.66 and K_{34} = 0.9. Entering Fig. 5 with this throat-diffuser coefficient and b = 0.1: $\emptyset_o$ = 2.8 (compared with 4.6 at K_{34} = 0.3).

$$N_o = \frac{0.2 - 1.9 (0.01)}{1.66 - \text{numerator}} = 0.122$$

Assuming that the N - $\emptyset$ curve is linear, for purpose of rapid evaluation, Eq. 37 shows that,

$$\eta_{max} = \frac{N_o \emptyset_o}{4} = \frac{0.122 \times 2.8}{4} = 0.086$$

or 8.5 per cent, compared with about 25 per cent for the high Reynolds number case. The operating flow ratio is estimated from

$$\emptyset_{op} = \frac{2}{3} \; \emptyset_{mep}, \quad \emptyset_{mep} \approx \frac{\emptyset_o}{2}$$

$$\emptyset_{op} = \frac{2}{3} \; \frac{2.8}{2} = 0.934$$

$$N_{op} = \frac{4}{3} \; N_{mep} \approx \frac{2}{3} \; N_o = 0.0814$$

The nozzle pressure drop is, assuming $p_d - p_o$ remains 25 psi,

$$p_i - p_o = \frac{1 + 0.0814}{0.0814} \,(25) = 333 \text{ psi}$$

For the same secondary flow rate, $W'_S = 25.2$ lb/min (neglecting any change in specific gravity), the new nozzle flow is approximately,

$$W'_N = 15.1 \,\frac{1.67}{0.934} = 27 \text{ lb/min}$$

$$d_N^4 = \frac{0.1615 \times 10^{-4} \,(1.66)\,(27)^2}{0.863 \times 333} = 0.68 \times 10^{-4}$$

and $\qquad d_N = 0.099$ in.

For the assumed $R_N = 1,000$, and the corresponding calculated W'_N and d_N values, the viscosity (from Eq. 38) is found to be 120 centistokes. This corresponds to Grade 1005 oil at -17 F, as shown by the viscosity chart, Fig. 44.

Low Reynolds number depresses the $N - \phi$ characteristic line, e.g., see Fig. 15, reducing both ϕ_{op} and N_{op}, hence efficiency. To produce the same energy output (flow rate and discharge head) the additional friction losses require an increase in energy input. This appears above as an increase in both primary flow rate and nozzle pressure.

Complete analysis of the behavior of the jet pump versus temperature requires information on the effect of temperature on the associated oil system; in particular, how W_N, W_S and p_d respond.

Altitude Ceiling Analysis. - Returning to the original case of high Reynolds number, the design will now be checked from the standpoint of altitude ceiling, heretofore neglected in the sizing of the pump. At the altitude ceiling, $\phi_L = \phi_{op}$, by definition. The minimum suction port pressure is

$$p_o = \frac{\phi_L^2 \, b^2 \,(p_i - p_o)}{(1-b)^2 \, 0.68 \,(1 + K_1)} \qquad\qquad (44a)$$

$$p_o = \frac{(1.67)^2 \,(0.1)^2 \,(214)}{(1-0.1)^2 \, 0.68 \,(1.1)} = 9.86 \text{ psia}$$

From the altitude-pressure tables (13), the maximum altitude is 10,700 feet. Obviously the original design, based on $\phi_{op} = 2/3 \, \phi_{mep}$, must be revised if the pump is to function at high altitudes. As shown in

Chapter IV, the ceiling can be increased by reducing the operating flow ratio. For $\phi_{op} = 1/4 \times 2.5 = 0.625$,

$$N_{op} = \frac{0.205}{4.6} (4.6 - 0.625) = 0.177$$

compared with 0.133 at $\phi_{op} = 2/3 \, \phi_{mep}$. The efficiency ($\phi N$) is now about 11 per cent, or half of the former value. At this N_{op} value,

$$p_i - p_o = \frac{1 + 0.177}{0.177} \times 25 = 177 \text{ psi}$$

which is lower than before by virtue of the increase in N_{op}. The minimum suction port pressure is now,

$$p_o = \frac{(0.625)^2 (0.1)^2 \times 166}{(1-0.1)^2 \times 0.68 \times 1.1} = 1.07 \text{ psi}$$

which corresponds to a maximum altitude of 59,500 feet. Higher altitude can be reached by a further reduction in ϕ_{op}. The nozzle flow rate will be $25.2/0.625 = 40.3$ lb/min. A new nozzle diameter is now calculated for this flow and the nozzle pressure drop of 166 psi; leading to recalculation of nozzle to throat spacing, and throat diameter and length.

Air Induction at Suction Port. -   The design layout so far has been based on a one-to-one scavenge ratio. If the back pressure drops below the design value of 25 psig, air will be drawn in the suction port. Also, if the nozzle flow rate is increased (with no change in W_S), air will be inducted. Such changes result in the pump operating at an N value below that on the N-ϕ characteristic curve at the existing flow ratio. The resultant over-capacity of the pump is satisfied by air, in much the same way it is in a positive displacement pump. In Chapter VI an approximate theoretical equation was presented, permitting direct calculation of the air rate; hence, the scavenge ratio and discharge aeration of the oil.

It will be necessary to design for some over-capacity, i.e., with a scavenge pump-to-pressure pump capacity ratio greater than one. This may be accomplished at the same time that the altitude ceiling is set. If in the example above, the N_{op} value had been held at 0.133 as ϕ_{op} was reduced to 0.625, the nozzle pressure drop would have remained at 214 psi. This N_{op} value is below that on the N-ϕ characteristic curve (0.177), effecting an over-capacity. In Chapter VI sample calculations were included to demonstrate the method of finding air capacity, hence, need not be repeated here. By starting the design at the selected ceiling, (with no over-capacity), decrease in altitude will raise p_o and the capacity of the pump; air will be inducted at lower altitudes, and will be a maximum at sea level. If this yields too high a "scavenge-ratio" at low altitudes, the

air rate can be reduced by increasing the back pressure on the pump, thus raising N_{op}. An altitude-responsive back-pressure valve might be the answer if excessive air handling at low altitudes should prove troublesome.

CHAPTER VIII

CONCLUSIONS AND RECOMMENDATIONS

Should the jet pump be employed as an oil scavenge pump in aircraft engines? It is not possible to give a clear-cut yes or no answer to the problem. The theoretical and experimental analyses reported herein revealed no reason prohibiting such an application. To win approval, the jet scavenge pump must successfully compete with the positive displacement (usually gear-type) pump now used. The two types are compared below.

Weight. - An aluminum jet pump with a No. 12 AN aluminum tee as a body weighs about 0.7 lbs. This body size should serve to scavenge a 3.5 gal/min oil flow. The midframe scavenge pump (Model NC 193) on the J-47 engine handles 3.5 gal/min at a nominal scavenge ratio of 10/3.5. This pump weighs about 2.7 lbs. With the driving gears, brackets etc, unavailable for measurement, it is impossible to estimate such added weight with an accuracy. The total is probably two or three times the gear pump weight along.

To the 0.7 lbs jet pump weight must be added that of the primary flow supply line and contained oil, and a primary supply pump. * This might be a separate pump driven at a take-off pad, or an element added to an existing oil pump. As a crude guess, the weight of the jet pump, five feet of No. 12 hose, fittings, and a supply pump, might be of the order of 5 or 6 lbs. There is probably some weight advantage to the jet pump, but not decisively so.

Physical Installation. - This comprises the chief advantage of the jet scavenge pump: It can be produced at a fraction of the cost of a precision high-speed gear pump. Powered hydraulically, precise mounting for gear alignment is avoided. The primary fluid supply pump could be driven at any convenient power take-off point; the jet pump location would be unrestricted by need for access to a mechanical drive point.

The pumps tested in this work were equipped with the usual body surrounding the nozzle-throat junction, or mixing point. Secondary fluid enters at a tee inlet on one side. This body portion could be eliminated in the scavenge pump application, affording full radial entry of secondary fluid.

---

* Two or more jet scavenge pumps could be "powered" by one primary supply pump.

An optimum arrangement should obtain by installing the pump vertically in the bottom of the sump; the wall faired into the throat entry. The nozzle could be supported above on struts, discharge downward into the open throat.

Engineering Design. - Unquestionably the process of originally designing a jet scavenge pump installation would be more complex than the selection of a positive-displacement gear pump. Experience would probably point the way to simplier methods than the step-by-step method followed in this work. The jet pump must be finally selected in the light of temperature effects (Reynolds number), and altitude effects. The latter largely dictates pump design for air craft use.

Suggestions for Improvement, and Future Work

1. The problem of low efficiency at low Reynolds number might respond to changes in configuration of the jet pump. Turbulence inducing devices in the nozzle could lower the useful limit of jet Reynolds number, now about $R_N = 3,000$.

2. The use of a variable-area nozzle (19) might offer advantages both as regards viscous effects and cavitation-limited flow.

3. There is a need for further basic work in determination of optimum de-design. Present experimental results indicate that optimum nozzle-to-throat spacing and throat length are interrelated with area ratio. Proper matching of all three variables might bring about an appreciable gain in oil pump efficiency, possibly to 35 per cent, compared with the 25 to 30 per cent attained in these tests. (Although area ratio is included in the theory, mixing length is not.)

4. The cavitation-limited flow phenomenon warrants further study; also Y measurements should be extended to other oils and other fluids such as water, fuels, and hydraulic fluids.

   Limiting-flow responds somewhat to nozzle spacing. Other design changes might help. The two-stage mixing zone design (4) should effect a marked improvement. A portion of the secondary flow could be mixed with the high velocity primary jet; the (slowed) stream would then entrain the remainder of the secondary flow at a point downstream. Thus, the combination of high flow ratio and high jet velocity at one point of mixing, is avoided.

REFERENCES

1. "The Design of Jet Pumps", Flugel, G., NACA T.M. 982, 1939.

2. "A Simple Air Ejector", Keenan, J. H., and Newmann, *Journal of Applied Mechanics* vol. 69, 1942, pp A-317 to A-336.

3. "An Investigation of Ejector Design by Analysis and Experiment" Keenan, J. H., Newmann, E. P., Lustwerk, F., *Journal of Applied Mechanics* vol. 77, 1950, pp 299-309.

4. "Hydraulics and Its Applications", Gibson, Constable, London, 1930, p 264.

5. "The Water Jet Pump", Gosline, J.E., and O'Brien, M.P., *University of California Publications in Engineering*, vol. 3, No. 3, 1934, pp 167-190.

6. "Eductors for Hydraulic Systems Applied to Closed-Circuit Lubrication Systems," Hussman, A. W., WADC Technical Report 53-131, September 1952, Wright-Patterson AFB, Ohio.

7. "Jet mixing of Two Liquids", Folsom, R. G., and Ferguson, C. K, *Transactions of ASME*, Jan. 1949, pp 73-77.

8. "Elementary Mechanics of Fluids", Rouse, H., Wiley, 1946. p 171.

9. "Elementary Fluid Mechanics", Vennard, J. K., Wiley, 1940, p 257.

10. "The Design of Jet Pumps", Kroll, A. E., *Chemical Engineering Progress*, vol. 1, Feb. 1947, pp 21-24.

11. "Centrifugal and Axial Flow Pumps", Stepanoff, A. J., Wiley, 1948, p 413.

12. "Design of Injectors for Low-Pressure Air Flow", McElroy, G. E., U. S. Bureau of Mines Tech. Paper 678, 1945.

13. "Altitude-Pressure Tables Based on the United States Standard Atmosphere", Brombacher, W. G., U.S. NACA Rept. No. 538, 1948.

14. "Friction Factors for Pipe Flow", by Moody, L. F. *Trans. ASME*, vol. 66, 1944, p 671.

15. "Gas Evalution in Liquids and Cavitation" by Schweitzer, P.H., and Szebehely, V.G., *Journal of Applied Physics* v 21 Dec. 1950, p 1218.

16. "Properties of Specification MIL-L-7808 Oil (Synthetic Oil)" by
    Margolin, E. L., Tech. Note. WCNE 52-532-487, 11 August 1952,
    Wright Air Development Center, ARDC, Wright Patterson AFB, Ohio.

17. "The Pumping Characteristics of Long Mixing Section Jet Pumps"
    by Fox, N. L., Douglas Aircraft Co. Rept. SM-14385 Sept. 1952, p 13.

18. "Investigation of the Mixing of Parallel Flowing Plane Air Streams in
    the Pressure Gradient of a Jet Eductor" by Ferguson, C. K., M.S. Thesis,
    University of California 1948.

19. "Injector-Impeller Pump", Patent No. 2,457,388, Dec. 28, 1948.
    Kenneth R. Lung.

Appendix I

Jet Pump Theory

As a jet of fluid penetrates a stagnant or slowly moving fluid, a dragging action occurs on the boundary of the jet between the high- and low-velocity particles. Mixing occurs between the surface jet fluid and the low velocity fluid; and transfer of momenta accelerates the latter in the direction of flow. As the two flows progress, the mixture stream spreads. The undisturbed high velocity core progressively decreases in diameter until it disappears. (See Fig. 1) Confined by parallel throat walls, the secondary fluid enters a region of decreasing area, that area being the annulus between the mixture stream and the throat wall. At the throat entrance the annular area is the difference between jet and throat area. At the throat exit the mixture stream has spread until it touches the wall of the throat. Then all of the side fluid has been mixed with the primary jet.

Assumptions. - In common with other solutions, the approach may be termed an "approximate" theory, since the details of the mixing process are avoided by use of impulse-momentum relations.

1. The flow streams are one-dimensional at throat entrance and exit.
2. Mixing is completed in the constant area throat, against an adverse pressure gradient.

high velocity core
secondary flow

Fig. 1.

Nomenclature. -

W   mass flow rate lb_m/sec

W'   mass flow rate lb_m/min

P   static pressure, lb/ft^2

p   static pressure, psi

$\bar{P}$ total pressure, lb/ft^2

V   velocity, ft/sec

E   energy ft lb_f/sec

ρ density, lb_m/ft^3

A   area, ft^2

D   diameter, ft

d   diameter inches

L   throat length, in.

g   gravitational constant $\dfrac{lb_m ft}{lb_f sec^2}$

b   area ratio, $\dfrac{A_N}{A_m}$

ϕ flow ratio, W_S/W_N

K_1 nozzle coefficient

K_2 throat entry coefficient

K_3 throat wall friction coefficient

K_4 diffuser friction coefficient

N   dimensionless pressure ratio

R   Reynolds number

ν viscosity, centistokes

η efficiency, $= \phi N$

e   slope, N vs. ϕ

s.g.   specific gravity

Subscripts:

N   primary nozzle fluid

S   secondary or pump fluid

T   total flow

o   side flow entry to jet pump

i   nozzle entry

a   throat entry

m   throat exit, diffuser entry

d   diffuser exit

jl   jet loss

ml   mixing loss

fl   friction loss

l   total losses

mep   maximum efficiency point on η vs. ϕ plot

<u>Continuity Relations</u>. - The continuity relations are based on an incompressible fluid; the densities of primary and secondary streams are equal.

$$W = \rho A V$$

The annular area available to the side flow stream at throat entry is,

$$A_{Sa} = A_m - A_{Na} = A_m - A_N^*$$

hence
$$V_{Sa} = \frac{W_S}{\rho A_{Sa}} = \frac{\phi b}{1-b} \; V_{Na} = \frac{\phi b}{1-b} \; V_N^* \tag{1}$$

The throat flow is the sum of the nozzle and side flows, $W_T = W_N + W_S$

$$V_m = \frac{W_T}{\rho A_m} = b(1+\phi) \; V_N \tag{2}$$

Nozzle energy equation. -

$$\frac{P_i}{\rho} + \frac{V_i^2}{2g} = \frac{P_a}{\rho} + \frac{V_N^2}{2g} + \frac{P_{fl}}{\rho}$$

where P_{fl} is energy lost by friction in nozzle.

Let $\bar{P}_i = P_i + \frac{\rho V_i^2}{2g}$ "total pressure"

$$P_{fl} = K'_1 \frac{\rho V_N^2}{2g}$$

The nozzle energy equation becomes,

$$\bar{P}_i - P_a = (1+K'_1) \frac{\rho}{2g} \; V_N^2 \tag{3}$$

<u>Side Flow Energy Equation</u>. -

$$\frac{P_o}{\rho} + \frac{V^2_{So}}{2g} = \frac{P_a}{\rho} + \frac{V^2_{Sa}}{2g} + \frac{P_{fl}}{\rho}$$

similarly, this may be written

$$\bar{P}_o - P_a = (1 + K_2) \; \frac{\rho V^2_{Sa}}{2g}$$

*Hereafter the location subscript a will be dropped, i. e., N in place of N_a.

Inserting the continuity relation, Eq. 1,

$$\bar{P}_o - P_a = (1 + K_2) \frac{\phi^2 b^2}{(1-b)^2} \frac{\rho V_N^2}{2g} \tag{4}$$

Momentum Equation in Throat. -

$$\frac{W_N V_N}{g} + \frac{W_S V_{Sa}}{g} - \frac{W_T V_m}{g} - F_{fl} = A_m (P_m - P_a) \tag{5}$$

The term F_{fl} refers to wall friction drag accompanying the flow of a real fluid in a tube.

$$F_{fl} = f A_{wall} \frac{\rho}{2g} V_m^2$$

where f is the friction factor and $A_{wall} = \pi D_m L$ is the wall surface area of the tube, L and D_m are length and diameter of the throat. Introducing the throat cross-sectional area A_m,

$$F_{fl} = f \frac{L A_m}{D_m} \frac{V_m^2}{2g}$$

let

$$K_3 = \frac{f L}{D_m}$$

then

$$F_{fl} = K_3 A_m \frac{\rho}{2g} V_m^2 \tag{6}$$

Inserting the continuity Eqs. 1 and 2 and Eq. 6 into the momentum Eq. 5, there results

$$P_m - P_a = \frac{\rho}{2g} V_N^2 \left[2b + \frac{2\phi^2 b^2}{1-b} - (2 + K_3) b^2 (1+\phi)^2 \right] \tag{7}$$

Diffuser Energy Equation. -

$$\frac{P_m}{\rho} + \frac{V_m^2}{2g} = \frac{P_d}{\rho} + \frac{V_d^2}{2g} + \frac{P_{fl}}{\rho}$$

let

$$\bar{P}_d = P_d + \frac{\rho V_d^2}{2g}$$

$$P_{fl} = K_4 \frac{\rho V_m^2}{2g}$$

then,

$$\bar{P}_d - P_m = (1 - K_4) b^2 (1+\phi)^2 \frac{\rho}{2g} V_N^2 \tag{8}$$

By combining Eqs. 3, 4, 7 and 8, the three significant pressure-difference expressions may be obtained:

$$\bar{P}_i - \bar{P}_o = \frac{\rho}{2g} V_N^2 \left[1 + K'_1 - (1+K_2) \frac{\phi^2 b^2}{(1-b)^2} \right] \tag{9}$$

$$\bar{P}_d - \bar{P}_o = \frac{\rho}{2g} V_N^2 \left[2b + \frac{2\phi^2 b^2}{1-b} - (1+K_3+K_4) b^2 (1+\phi)^2 \right.$$
$$\left. - (1+K_2) \frac{\phi^2 b^2}{(1-b)^2} \right] \tag{10}$$

$$\bar{P}_i - \bar{P}_d = \frac{\rho}{2g} V_N^2 \left[1 + K'_1 - 2b - \frac{2\phi^2 b^2}{1-b} + (1+K_3+K_4) b^2(1+\phi)^2 \right] \tag{11}$$

<u>Jet Pump Efficiency.</u> - Pump efficiency, η , is obtained as the ratio of energy output to energy input.

$$E_{out} = \frac{W_S}{\rho} (\bar{P}_d - \bar{P}_o) \quad \text{ft lb}_f/\text{sec}$$

$$E_{in} = \frac{W_N}{\rho} (\bar{P}_i - \bar{P}_d)$$

$$\eta = \frac{E_{out}}{E_{in}} = \phi \frac{\bar{P}_d - \bar{P}_o}{\bar{P}_i - \bar{P}_d} = \phi N, \text{ where N is the dimensionless pressure ratio:} \tag{12}$$

$$N = \frac{2b + \frac{2\phi^2 b^2}{1-b} - (1+K_3+K_4) b^2(1+\phi)^2 - (1+K_2) \frac{\phi^2 b^2}{(1-b)^2}}{1 + K'_1 - 2b - \frac{2\phi^2 b^2}{1-b} + (1+K_3+K_4) b^2 (1+\phi)^2} \tag{13}$$

The pressure characteristic is thus a function of area ratio b, flow ratio ϕ, and the friction loss coefficients K_1, K_2, K_3, K_4. Those coefficients must be measured experimentally or estimated from existing information on nozzle, tube, and diffuser friction losses.

Although the method employed, and the final N equation are somewhat different in form, the relations between N and the above noted variables are identical with those established by Gosline and O'Brien (5).

The Friction Loss Coefficients

The four K coefficients, assumed zero in the ideal case above, are of finite value in the case of the actual jet pump. The values of the coefficients may be determined by three methods:

(a) Use established coefficients from the literature, handbooks, etc., for nozzle, short tube, and diffuser losses.

(b) Measure the coefficients by tests on individual parts of the pump. For example, obtain the nozzle coefficient by free-discharge tests.

(c) Calculate the K values from actual tests of the jet pump.

The latter method has been selected for this investigation of viscosity effects. The analysis and correlation of coefficients computed from pump test data are discussed in detail in Chapter III.

<u>Definitions of Coefficients.</u> - The pressure-difference equations for $\bar{P}_i - \bar{P}_o$ and $\bar{P}_d - \bar{P}_o$, (Eqs. 9 and 10 respectively) are sufficient to define the necessary coefficients when one simplifying assumption is made. The throat-entrance coefficient K_2 covers losses in the side-flow stream in entering the throat, assuming one-dimensional flow. Such a coefficient approaches zero for a well-rounded entry such as is used in these pumps. Accordingly, K_2 will be assumed equal to zero and dropped from the basic equations. A further justification for neglecting K_2 are the unknown departures from the assumed one-dimensional flow pattern. Comparison of theoretical N vs. $\emptyset$ curves with experimental data showed that reasonable value of K_2 exerted essentially no effect on the N - $\emptyset$ characteristic curve.

<u>Throat-Diffuser Coefficient, K_{34}.</u> - It will be noted in the pressure difference Eqs. 10 and 11 that the throat coefficient K_3 and the diffuser coefficient K_4 appear together as a sum. This is of course the result of defining both losses as proportional to the throat velocity, V_m. Hence it is convenient to lump these friction factors together; $K_{34} = K_3 + K_4$.

Given the performance data on a jet pump, the throat-diffuser loss coefficient K_{34} may be calculated from Eq. 10 rearranged as,

$$K_{34} = \frac{2}{b(1+\emptyset)^2} + \frac{1-2b}{(1-b)^2} \frac{\emptyset^2}{(1+\emptyset)^2} - 1 - \frac{\bar{P}_d - \bar{P}_0}{\frac{\rho}{2g} V_N^2 b^2 (1+\emptyset)^2} \quad (14)$$

where all quantities are known from the pump dimensions and the performance test data: P_i, P_o, P_d and the two flows, W_N and W_S. V_N is calculated from:

$$V_N = \frac{W_N}{\rho A_N}$$

Total pressures $\bar{P}_i$, $\bar{P}_o$, $\bar{P}_d$, are obtained by adding the respective velocity heads to the static pressures. In this work velocity heads were, with few exceptions, negligible compared with static pressures, permitting direct use of the latter. Using Eq. 14 a large number of throat-diffuser coefficients were calculated from test data and correlated vs. throat Reynolds number. (Chapter III).

Nozzle Coefficient, K'_1, K_1. - With $K_2 = 0$, Eq. 9 yields

$$K'_1 = \frac{\overline{P}_i - \overline{P}_o}{\frac{\rho}{2g} V_N^2} \quad -1 + \frac{\phi^2 b^2}{(1-b)^2} \qquad (15)$$

The analytical solution was originally based on the assumption that the pressure at the nozzle tip was equal to that in the plane of the entrance to the throat. An annular area A_m-A_N is available for the side flow. As the side flow W_S increases, the throat entry pressure - which was theoretically also the nozzle discharge pressure - must of necessity decrease relative to the side port pressure P_o. The last term in Eq. 15 compensates the supposed decrease in P_i-P_o.

Thus K'_1 is theoretically unaffected by flow ratio. In practice, (a), the tip of the nozzle is withdrawn from the throat entry by as much as several nozzle diameters and (b) jet pumps used were provided with large-area unrestricted side entry ports, minimizing pressure loss (Figs. 8,9). As a result, the nozzle experiences a discharge pressure higher than the throat entry pressure. In fact, it is for all practical purposes equal to P_o. The first term in Eq. 15 does not decrease at the same rate that the last term increases. It remains constant. Thus, K'_1 may be defined as,

$$K'_1 = K_1 + \frac{\phi^2 b^2}{(1-b)^2} \quad , \quad (16), \quad \text{where } K_1 = \frac{\overline{P}_i - \overline{P}_o}{\frac{\rho}{2g} V_N^2} \qquad (17)$$

K_1 is simply K'_1 at zero side flow, or, $\phi = 0$. As discussed elsewhere, K_1 reflects the effect of Reynolds number and nozzle design. The second term in Eq. 16 is a consequence of the departure in practice from the original theoretical configuration of the pump parts. Values of K_1 were calculated from Jet Pump tests and correlated vs. Jet Reynolds number. (Chapter III.)

Jet Loss Modification. - In over 200 tests with eight jet pumps, b = 0.1 to 0.6, P_i-P_o did not vary with change in ϕ, but remained quite constant. In only one case, where the nozzle was located abnormally close to the throat, did P_i-P_o respond, but with only a 5 per cent change. To accomodate this departure of experiment from theory, the following is postulated:

The jet discharges from the nozzle tip, surrounded by fluid at static pressure P_o, with velocity V_N and of area A_N. The free jet then traverses a short distance S, varing from about 0.1 to several nozzle or jet diameters, before entering the throat where the static pressure is P_a. This traverse of the constant-velocity constant-area, jet from P_o down to P_a constitutes a fluid frictional energy loss E_{j1}. The analysis is considerably simplified by this assumption that all the mixing occurs after the jet enters the throat.

This concept arises from tests on two particular designs (Figs. 8,9) of nozzle and throat-entry contour. It is quite possible that careful shaping of the throat entry would achieve some utilization of this so-called "jet-loss" energy.

This energy loss is,

$$E_{jl} = \frac{W_N}{\rho} (P_o - P_a), \quad \frac{ft\ lb}{sec}$$ (18)

Combining Eqs 18 and 4,

$$E_{jl} = W_N \frac{\rho\ V_N^2}{2g} (1+K_2) \frac{\phi^2 b^2}{(1-b)^2}$$ (19)

The last factor in Eq. 19 is simply the difference between K'_1 and K_1. By thus recognizing the flow of the jet from P_o to P_a as a loss distinct from the nozzle loss proper, K_1 values may be extracted from jet pump performance tests for correlation.

Revised Basic Equations

Equations 9, 10, 11, and 13 are the basic equations describing jet pump behavior. These are repeated below incorporating the jet loss factor described above.

The nozzle pressure difference (formerly Eq. 9):

$$\overline{P}_i - \overline{P}_o = \frac{\rho}{2g} V_N^2 \left[1 + K_1\right]$$ (20)

The output pressure rise (same as Eq. 10):

$$\overline{P}_d - \overline{P}_o = \frac{\rho V_N^2}{2g} \left[2b + \frac{2\phi^2 b^2}{1-b} - (1+K_{34}) b^2 (1+\phi)^2 - (1+K_2)\frac{\phi^2 b^2}{(1-b)^2}\right]$$ (21)

The overall pressure drop (formerly Eq. 11):

$$\overline{P}_i - \overline{P}_d = \frac{\rho V_N^2}{2g} \left[1+K_1 - 2b - \frac{2\phi^2 b^2}{1-b} + (1+K_{34}) b^2 (1+\phi)^2 + (1+K_2)\frac{\phi^2 b^2}{(1-b)^2}\right]$$ (22)

The pressure ratio N is found from Eqs. 21 and 22:

$$N = \frac{\overline{P}_d - \overline{P}_o}{\overline{P}_i - \overline{P}_d},$$

or,

$$N = \frac{2b + \frac{2\phi^2 b^2}{1-b} - (1+K_{34})b^2(1+\phi)^2 - (1+K_2)\frac{\phi^2 b^2}{(1-b)^2}}{1 + K_1 - numerator}$$ (23)

Through recognition of the jet loss concept, Eq. 23 is an improved arrangement of Eq. 13. Friction factors are constants, independent of $\emptyset$, whereas K'_1 in Eq. 13 had to be computed as the sum of K_1 and $(1+K_2)\ \emptyset^2 b^2/(1-b)^2$ for each $\emptyset$ value in question. Identical numerical results are obtained with either form. As shown in Chapter II theoretical N vs. $\emptyset$ characteristic curves agree quite well with test results.

ENERGY ANALYSIS

The mixing of two streams of different velocities in a jet pump demands that an energy loss occur, even if all four friction coefficients and the jet loss are zero. Separation of the mixing loss, jet loss, and friction losses through an energy analysis is helpful in understanding the jet pumping mechanism and the limitations therein imposed.

The Mixing Loss

The momentum equation 5 provides the following expression for pressure difference across the throat section:

$$P_m - P_a = \frac{W_N V_N}{g A_m} + \frac{W_S V_{Sa}}{g A_m} - \frac{2 W_T V_m}{g A_m} - \frac{F_{fl}}{A_m} \tag{5}$$

The energy equation between throat entrance and exit is:

$$\frac{W_N P_a}{\rho} + \frac{W_N V_N^2}{2g} + \frac{W_S P_a}{\rho} + \frac{W_S V_{Sa}^2}{2g} = \frac{W_T P_m}{\rho} + \frac{W_T V_m^2}{2g} + E_{ml} + E_{fl}$$

$$P_m - P_a = \frac{W_N}{W_T} \frac{\rho V_N^2}{2g} + \frac{W_S}{W_T} \frac{\rho V_{Sa}^2}{2g} - \frac{\rho V_m^2}{2g} - \frac{\rho E_{ml}}{W_T} - \frac{\rho E_{fl}}{W_T} \tag{24}$$

Noting that $\quad \dfrac{F_{fl}}{A_m} = \dfrac{\rho E_{fl}}{W_T}$,

the mixing loss is obtained by eliminating the pressure difference between Eqs. 5 and 24. By rearranging terms and simplifying, the following equation is obtained:

$$E_{ml} = W_N \frac{(V_N - V_m)^2}{2g} + W_S \frac{(V_{Sa} - V_m)^2}{2g} \tag{25}$$

Combining Eq. 25 with the continuity relations Eqs. 1 and 2,

$$E_{ml} = W_N \frac{V_N^2}{2g} \left[1 - 2b(1+\emptyset) + b^2(1+\emptyset)^3 + \frac{\emptyset^3 b^2}{(1-b)^2} - 2\emptyset^2 b^2 \frac{1+\emptyset}{1-b} \right] \tag{26}$$

It is interesting to note that at zero side flow, ($\emptyset = 0$), Eq. 23 reduces to

$$E_{ml} = \frac{W_N V_N^2}{2g} (1-b)^2$$

which is simply the expression for a "sudden enlargement" loss in a pipe line.

The Friction Losses

The friction loss terms are all expressed as constants multiplied times the kinetic energy expression of the stream in question. These plus the continuity relations yield the following:

Nozzle Loss: $E_1 = K_1 W_N \dfrac{V_N^2}{2g}$

Side Flow Loss: $E_2 = K_2 W_S \dfrac{V_{Sa}^2}{2g} = K_2 \dfrac{\emptyset^3 b^2}{(1-b)^2} W_N \dfrac{V_N^2}{2g}$

Throat Loss: $E_3 = K_3 W_T \dfrac{V_m^2}{2g} = K_3 b^2 (1+\emptyset)^3 W_N \dfrac{V_N^2}{2g}$

Diffuser Loss: $E_4 = K_4 W_T \dfrac{V_m^2}{2g} = K_4 b^2 (1+\emptyset)^3 W_N \dfrac{V_N^2}{2g}$

Total friction loss is the sum of the four equations above:

$$E_{fl} = W_N \frac{V_N^2}{2g} \left[K_1 + K_2 \frac{\emptyset^3 b^2}{(1-b)^2} + K_{34} b^2 (1+\emptyset)^3 \right] \qquad (27)$$

The Jet Loss

The jet loss term was derived above in the course of establishing Eq. 23, the modified basic characteristic equation for the jet pump. It is,

$$E_{jl} = W_N \frac{V_N^2}{2g} (1+K_2) \frac{\emptyset^2 b^2}{(1-b)^2} \qquad (19)$$

Again, this term represents the loss in available energy resulting from the constant area and velocity flow of the jet stream from the nozzle tip at P_o, to the throat entrance at P_a.

Total energy loss is the sum of equations 26, 27, and 19, $E_{ml} + E_{fl} + E_{jl}$,

$$E_1 = W_N \frac{V_N^2}{2g} \left[1 + K_1 - 2b(1+\phi) - 2\phi^2 b^2 \frac{1+\phi}{1-b} + (1+K_2)(1+\phi) \frac{\phi^2 b^2}{(1-b)^2} \right. $$
$$\left. + (1+K_{34}) b^2 (1+\phi)^3 \right] \tag{28}$$

It is noted that Eq. 28 could also be found by the following steps:

$$E_1 = E_{in} - E_{out}$$

$$= \frac{W_N}{\rho} (\bar{P}_i - \bar{P}_d) - \frac{W_S}{\rho} (\bar{P}_d - \bar{P}_o)$$

where the pressure differences involved have been derived above as Eqs. 21 and 22. In addition to Eq. 12, pump efficiency is expressed by

$$\eta = \frac{E_{in} - E_1}{E_{in}} = 1 - \frac{E_1}{E_{in}} \tag{29}$$

Dimensionless Energy Factors. - Note that for analysis purposes, mixing loss E_{ml}, friction loss E_{fl}, jet loss E_{jl}, and total energy loss E_1, can be expressed dimensionlessly by dividing the respective equations 26, 27, 19 and 28, through by

$$W_N \frac{V_N^2}{2g} .$$

Losses are then expressed only in terms of ϕ, b, and the friction factors.

Comparison of Characteristic Curves

The energy relations developed above permit comparison of three theoretical characteristic curves. These are for,

A. The ideal pump, mixing loss only.
B. The frictionless pump, but with jet loss (nozzle withdrawn from throat entry).
C. The actual jet pump, with mixing, jet, and friction losses included.

The design area-ratio b determines the head characteristic of a jet pump as discussed in Chapter I. Theoretically it may have any value $0 < b < 1.0$. For the mid-value of b = 0.5, the pressure ratio N, and efficiency $\eta = \phi N$, curves are shown in Fig. 2 for the above three theoretical solutions.

A. Ideal Jet Pump. - Examination of the mixing loss Eq. 25 shows that the mixing loss decreases as the side-flow throat-entry velocity V_{Sa} approaches the jet velocity V_N. The mixing loss is zero when these are equal. This requires that,

$$\phi = \frac{1-b}{b}$$

and for $b = 0.5$, this flow ratio is $\phi = 1.0$. Fig. 2 shows that here the efficiency is 100 per cent - but output and input are zero for this case. Two high velocity jets simply pass through the throat together and in the diffuser the kinetic energy is recovered as a pressure equal to the inlet pressure, i.e., $P_i = P_d = P_o$. If the jet pump doesn't actually "pump" at 100 per cent efficiency, what is the maximum obtainable efficiency for frictionless flow? If the ratio for the maximum energy output is selected,(to minimize pump size) curve A shows $\eta_{max} = 72.4$ per cent; here the flow ratio is $\phi = 0.534$. Higher efficiencies can be obtained only at the expense of energy output, and lowered pressure ratio, or N value.

For flow ratios greater than that for zero mixing loss ($\phi > 1.0$ in Fig. 2) the side-flow throat velocity exceeds the jet velocity, and the role of the two streams is interchanged.

B. Frictionless Flow, with Jet Loss. - Curves B show the considerable effect of jet loss on efficiency and pressure ratio. It should be added here that A and B are two extremes; either no jet loss occurs, or 100 per cent of the energy represented by jet flow from P_o to P_a (in the throat entry) is assumed lost. An intermediate case could well be postulated, wherein a part of this energy is considered utilized in the pumping process. Efficiency curve B reaches a maximum of 42 per cent at $\phi = 0.35$ as shown. This (B) represents a sort of ultimate in improvement, through reduction of friction losses.

C. Actual Jet Pump. - The lowest curves, C, are constructed assuming that $K_1 = 0.1$, $K_2 = 0$, $K_{34} = 0.3$, thus introducing friction losses. From test experience these values represent nearly the minimum obtainable in practice. Efficiency and pressure curves are lowered and the maximum flow ratio is reduced as indicated. The C curves are essentially identical with performance curves measured in the laboratory. In Chapter II theory and experimental curves are compared directly.

Appendix 2

Sample Calculations

In most of the experimental work, pump performances were measured versus flow ratio. This test consisted of operating the pump at a fixed primary flow W_N and fixed suction port pressure p_o. For each test, discharge pressure p_d was varied for approximately 14 runs, yielding a series of secondary flow rates W_S from 0 to the maximum for each pump (with the control valve wide open.)

Two flow rates W'_N and W'_S and three pressures p_i, p_o and p_d were recorded for each run. These data were employed to calculate the pressure ratio N and flow ratio, $\emptyset$ as demonstrated below. Flow rates were set approximately by rotameter and then measured by weighing against a stop watch for best accuracy (except during "altitude" testing). A portable pump was used to pump the weighed sample from a tank on a balance, back to the oil tank on the top of the test stand. A desk calculator was used in computing data.

Test Data:

Test No. 190, Run No. 8, 4/19/54

Pump No. 141/316/308, b = 0.2

Barometer 28.85 in. Hg. corr.

Room temperature 82 F

Oil: MIL-L-7808, Synthetic

Oil Temp. 150 F: from Fig. 43, s.g. = 0.892
from Fig. 44, ν = 5.7 centistokes

W'_N = 44.64 lbs/min

W'_S = 31.88 lbs/min

$\emptyset = \dfrac{31.88}{44.64} = \underline{0.714}$

p_i = 100.0 psig, corrected for gage calibration error

p_o = -0.5 in Hg or -0.24 psig relative to barometer pressure

p_d = 48.5 in Hg or 23.7 psig

$P_d-P_o = 23.94$ psi

$P_i-P_d = 76.3$ psi

$P_i-P_o = 100.24$ psi

$$N = \frac{23.94}{76.3} = \underline{0.314}$$

The calculated N values were then plotted versus flow ratio $\emptyset$, and a smooth curve faired through the points--facilitated by the nearly linear nature of the N - $\emptyset$ relation. An efficiency curve $\eta = \emptyset N$ was plotted by multiplying N values from the curve by the corresponding $\emptyset$ value.

Calculation of Friction Factors. - The experimental N - $\emptyset$ curve was used to calculate K_1 and K_{34}. At about $\emptyset = 2/3\ \emptyset_{mep}$, 0.90 for Test 190, the value of N was read from the smoothed curve:

$$N = 0.276 \text{ at } \emptyset = 0.9$$

$$b = \left(\frac{0.141}{0.316}\right)^2 = 0.199$$

$$P_d-P_o = \frac{N}{N+1}(P_d-P_o) = \frac{0.276}{1.276}(100.24) = \underline{21.68} \text{ psi}$$

From continuity, and with d_N as nozzle diameter in inches,

$$\frac{\rho V_N^2}{2g} = \frac{0.002326\ W'_N{}^2}{s.g.\ d_N^4}$$

$$\frac{\rho V_N^2}{2g} = \frac{0.002326\ (44.64)^2}{0.892\ (0.141)^4} = 13,175 \text{ lb}_f/\text{ft}^2$$

From Eq. 14, Appendix 1 or Chapter II,

$$K_{34} = \frac{10.04}{3.61} + \frac{1-0.398}{0.641} \times \frac{0.81}{3.61} -1- \frac{21.68 \times 144}{0.0396 \times 3.61 \times 13,175}$$

$$K_{34} = \underline{0.337}$$

From Eq. 17,

$$K_1 = \frac{100.24 \times 144}{13,175} - 1 = \underline{0.0956}$$

From Eqs. 38 and 39, Chapter III, the jet or nozzle and the throat Reynolds numbers are,

$$RN = \frac{379.1 \times 44.64}{0.892 \times 5.7 \times 0.141} = \underline{20,150}$$

$$R_m = \frac{0.141}{0.316} (1 + 0.9) \, 20,150 = \underline{17,100}$$

These friction factors and Reynolds numbers appear in Table 4 in Chapter III, and are plotted in Figs. 16 and 17.

Cavitation-Limited Flow Data. - As shown by Figs. 10 to 14, or Fig. 19, secondary flow, and hence, flow ratio $\emptyset$, are independent of discharge pressure when limiting flow occurs: N varies, but $\emptyset_L$ remains fixed. To measure limiting-flow rates, W_{SL}, versus absolute suction port pressure, the back pressure valve was opened wide and p_0 was reduced in a series of about 12 runs from atmospheric to the minimum obtainable (less than 1 psig). This was accomplished by evacuating the oil storage tank with an electric vacuum pump. Nozzle flow rate was held constant; nozzle gage pressure, of course, decreased as the system was evacuated. The flow rates and pressure data were reduced for plotting as limiting-flow function Y, vs p_0, as shown below.

Cavitation Test Data:

      Test No. 141, Run No. 8, 3/13/54

      Pump No. 141/316/308, b = 0.2

      Barometer 28.70 in Hg, uncorrected, 14.0 psia corrected

      Room Temperature 76 F

      Oil: MIL-L-6081 A, Grade 1005

      Oil Temperature 100 F; from Fig. 43, s.g. = 0.863

      $W'_N = 55.0$ lb/min

$W'_{SL} = 30.0$ lb/min

$p_i = 142$ psig, corrected, relative to barometric pressure, or 156 psia

$p_{tank} = -18.56$ in Hg or 4.96 psia
(multiplying in Hg at 76 F by 0.489 to convert to psi)

$p_o = -21.05$ in Hg. or 3.74 psia, representing 33,340 ft. (13).

$p_i - p_o = 156 - 3.74 = 152.3$ psia

$p_d = 4.5$ psig or 18.5 psia

$p_d - p_o = 14.8$ psi

Eq. 42, Chapter IV,

$$Y = \frac{\rho\, V_{SL}^2}{144 \times 2g} = \frac{W_{SL}^2\, b^2}{144\, \rho\, 2g \times A_N^2\, (1-b)^2} \quad psi$$

For $d_N = 0.141$ in., $b = 0.199$, and s.g. $= 0.863$, this reduces to

$$Y = 0.00293\, W'_{SL}^2 = 2.64\ psi$$

This value of Y is plotted versus $p_o = 3.74$ psia in Fig. 24.

Appendix 3.

Theory Compared with Experimental Results
on Water Jet Pumps

The approximate theoretical approach presented at the end of Chapter I was originally proposed by Gosline and O'Brien (5) and enlarged upon by Stepanoff (11). It assumed that N versus ϕ is a straight line, and accordingly

$$N = N_0 - \frac{N_0}{\phi_0} \phi \tag{34}$$

The theoretical Eq. 23 for N is considerably simplified when $\phi = 0$, here

$$N_0 = \frac{2b - (1+K_{34}) b^2}{1+K_1 - \text{numerator}} \tag{23a}$$

The intercept on the ϕ axis, or maximum flow ratio, ϕ_0, may be found directly from Eq. 33. This is presented graphically in Fig. 5: entering with b and K_{34}, ϕ_0 can be read from the curve.

In Fig. 45 the theoretical curves N_0 versus b and ϕ_0 versus b are presented for comparison with experimental values for N_0 and ϕ_0 from Stepanoff (11) for water jet pumps. With $K_1 = 0.1$ and $K_{34} = 0.3$, assuming a high Reynolds number situation, the theory agrees well with water jet pump data. Later (unpublished) data from the same author have further verified this agreement. Thus, the N_0 and ϕ_0 relations may be applied to water jet pump design.

Examination of the family of theoretical N - ϕ curves, Fig. 3, shows that at b = 0.1 and 0.2, the lines are nearly linear. But at high b values particularly 0.5 and 0.6, the N - ϕ lines are definitely concave up. Thus, use of a linear approximation would tend to be dangerously optimistic at high b values. Here the full theoretical N - ϕ relation (Eq. 23) should be used for precise work.

ENERGY ANALYSIS OF JET PUMP
## THEORETICAL CHARACTERISTIC CURVE FOR b=0.5
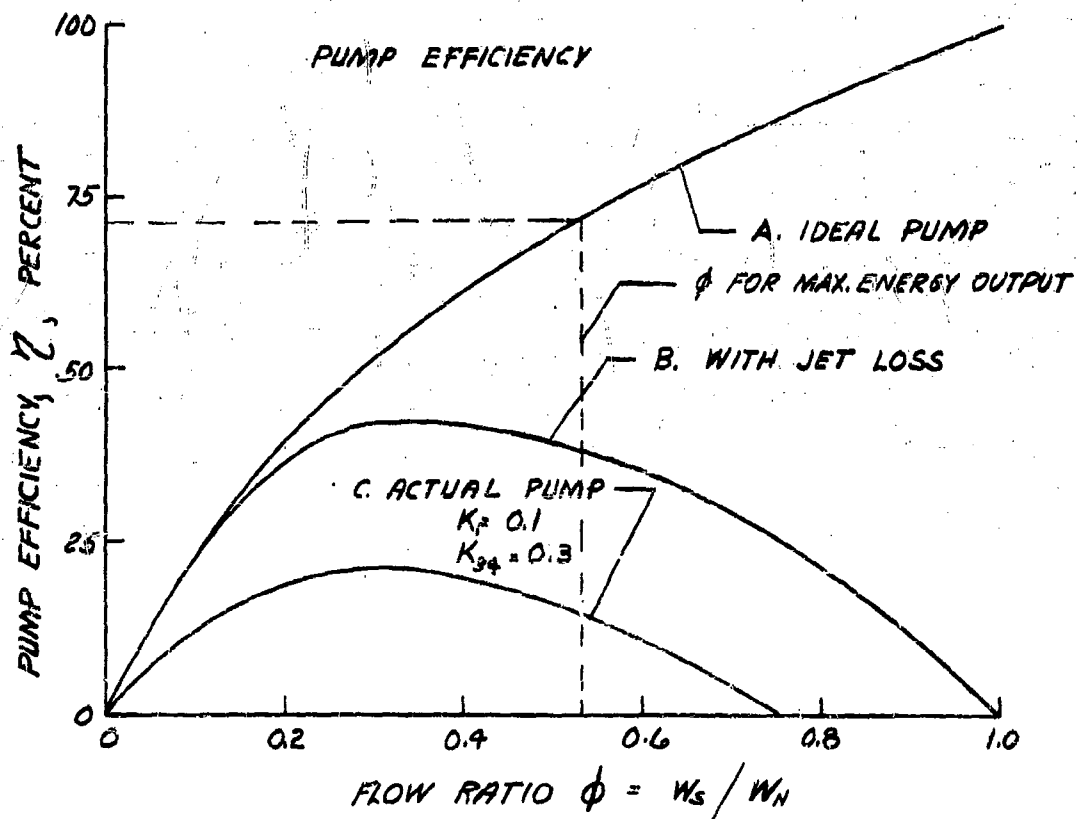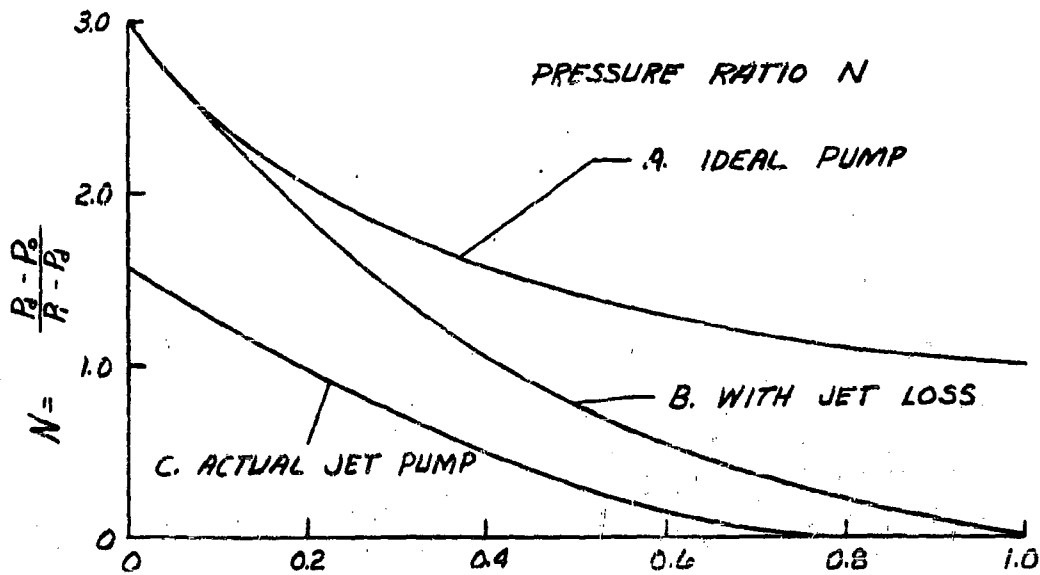
FIG 2. CHACTERISTIC CURVE SHOWING EFFECTS
OF A. MIXING, B. JET, AND C. FRICTION
LOSSES.

JET PUMP CHARACTERISTIC CURVES
FROM THEORY WITH $K_1 = 0.1$, $K_{SM} = 0.3$
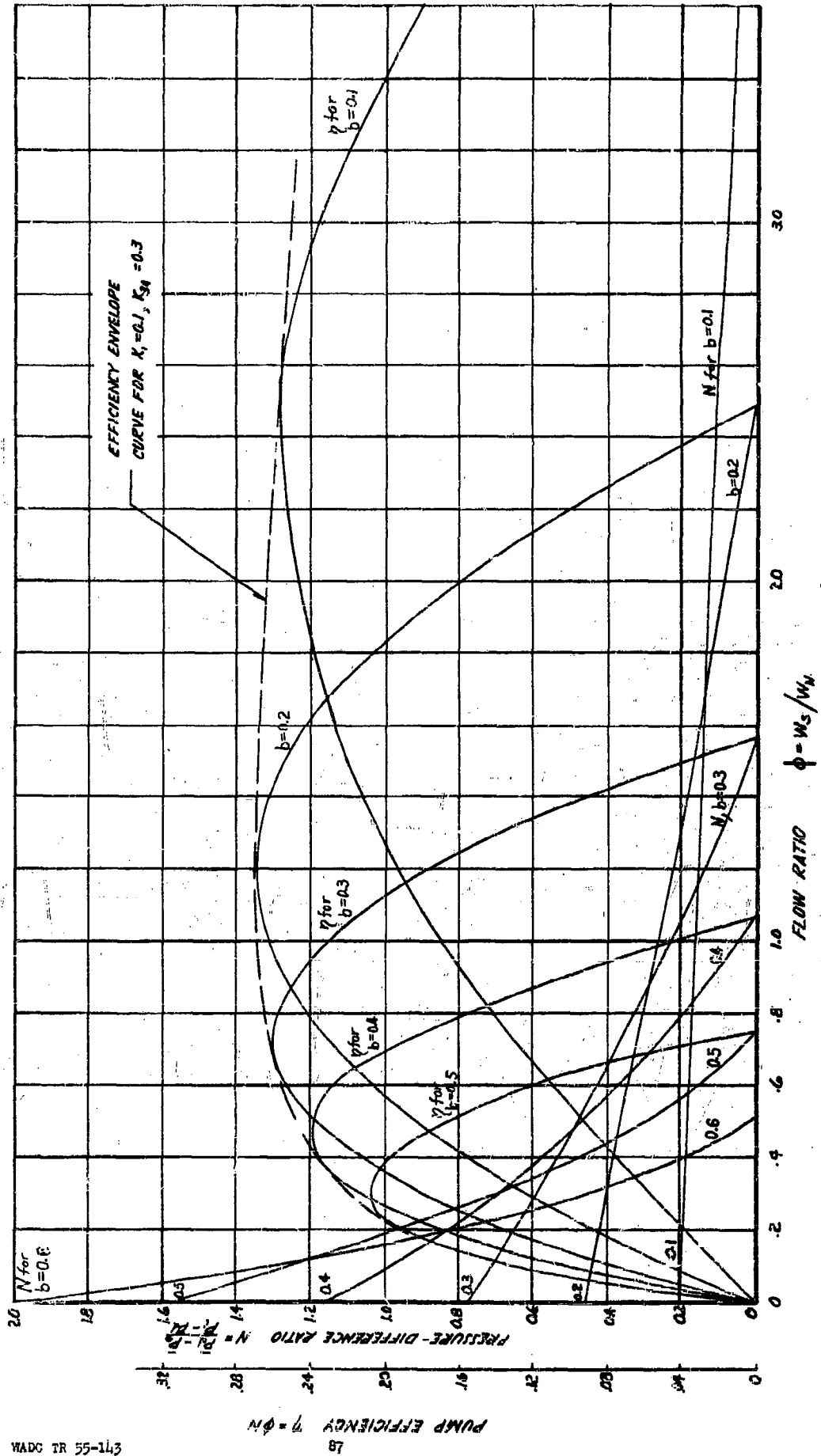
FIG. 3 PRESSURE-DIFFERENCE RATIO AND EFFICIENCY VERSUS FLOW RATIO FOR PUMPS WITH $b = 0.1$ TO 0.6.

Optimum Design Area Ratio
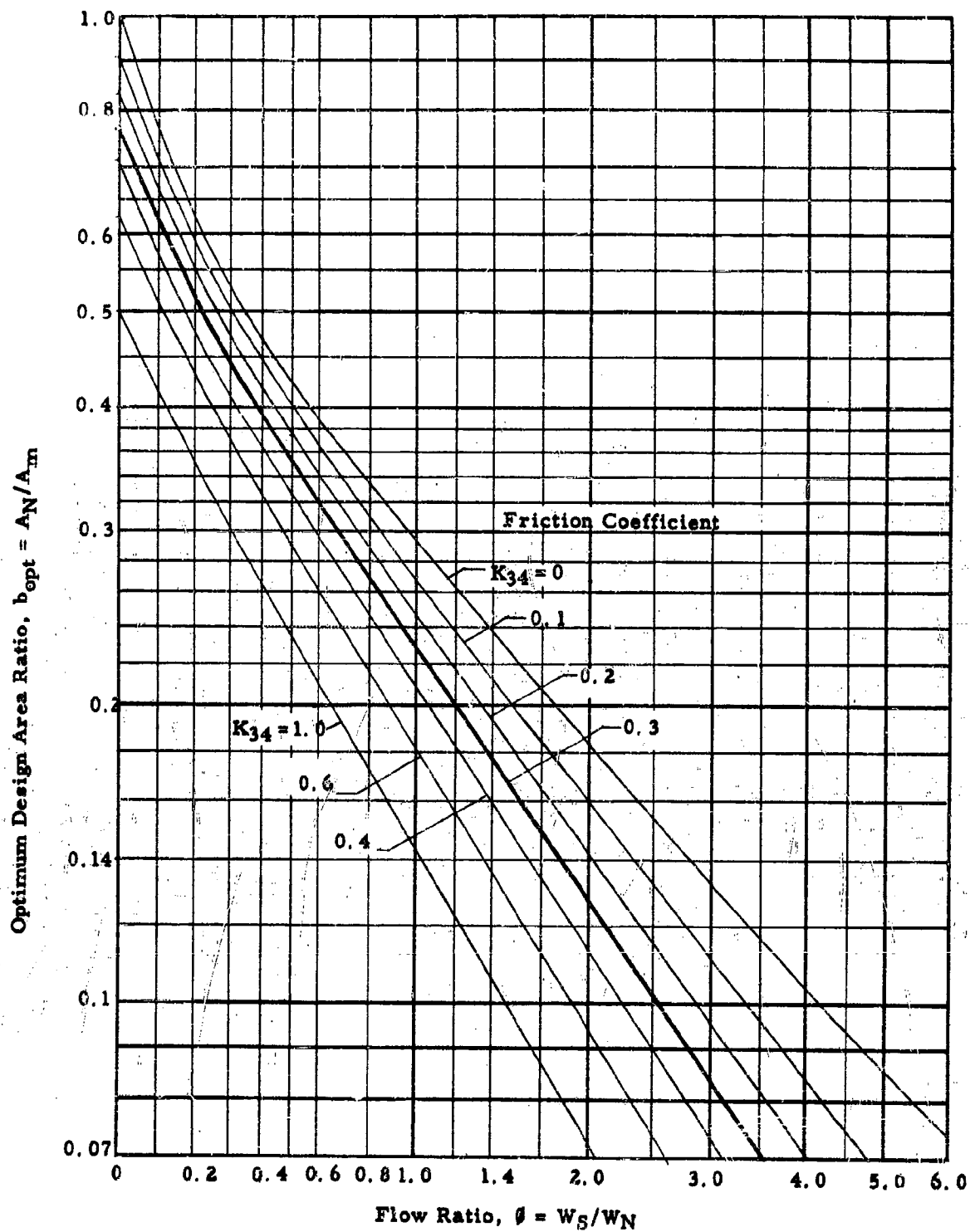
Fig. 4 Optimum Area Ratios versus Flow Ratio and Friction Factors.
From Theoretical Equation
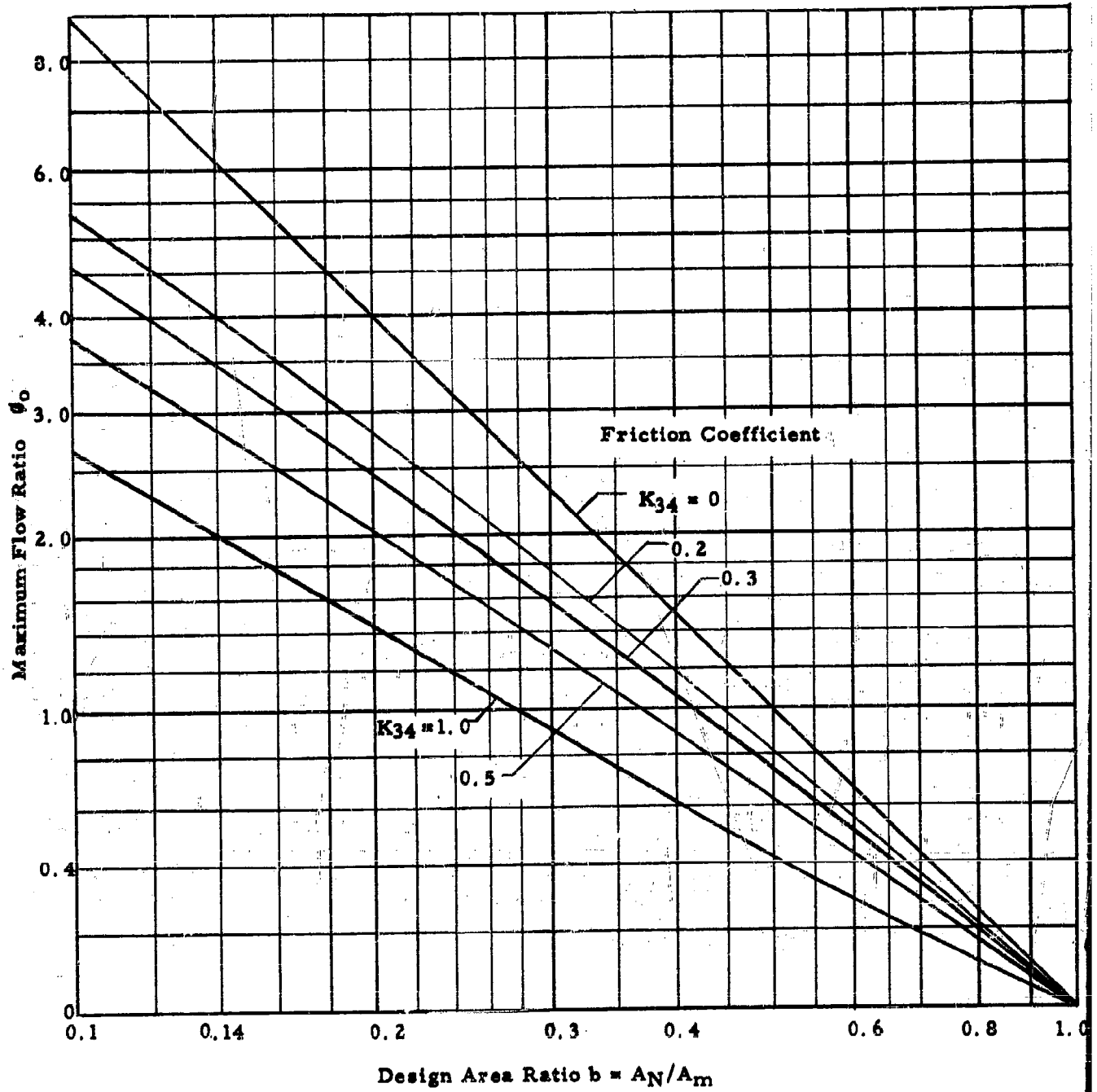
Fig. 5 Maximum Flow Ratio as a function of Area Ratio and Friction Factor.

THEORETICAL JET PUMP CHACTERISTICS
$K_1 = 0.1$, $K_{34} = 0.3$, $K_2 = 0$
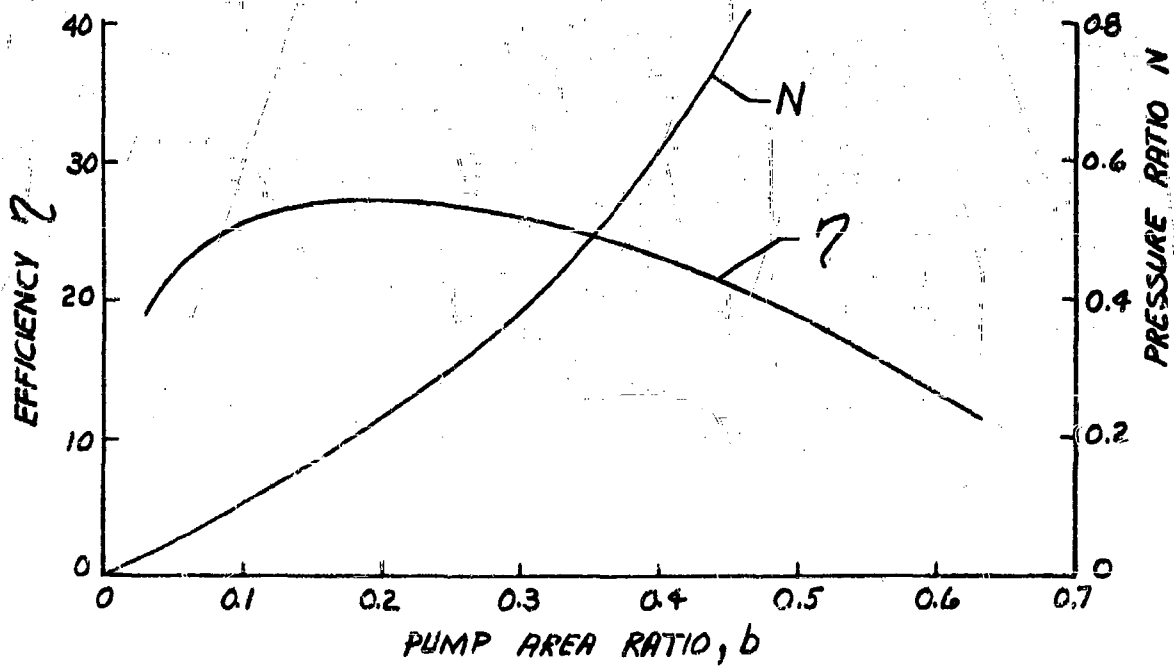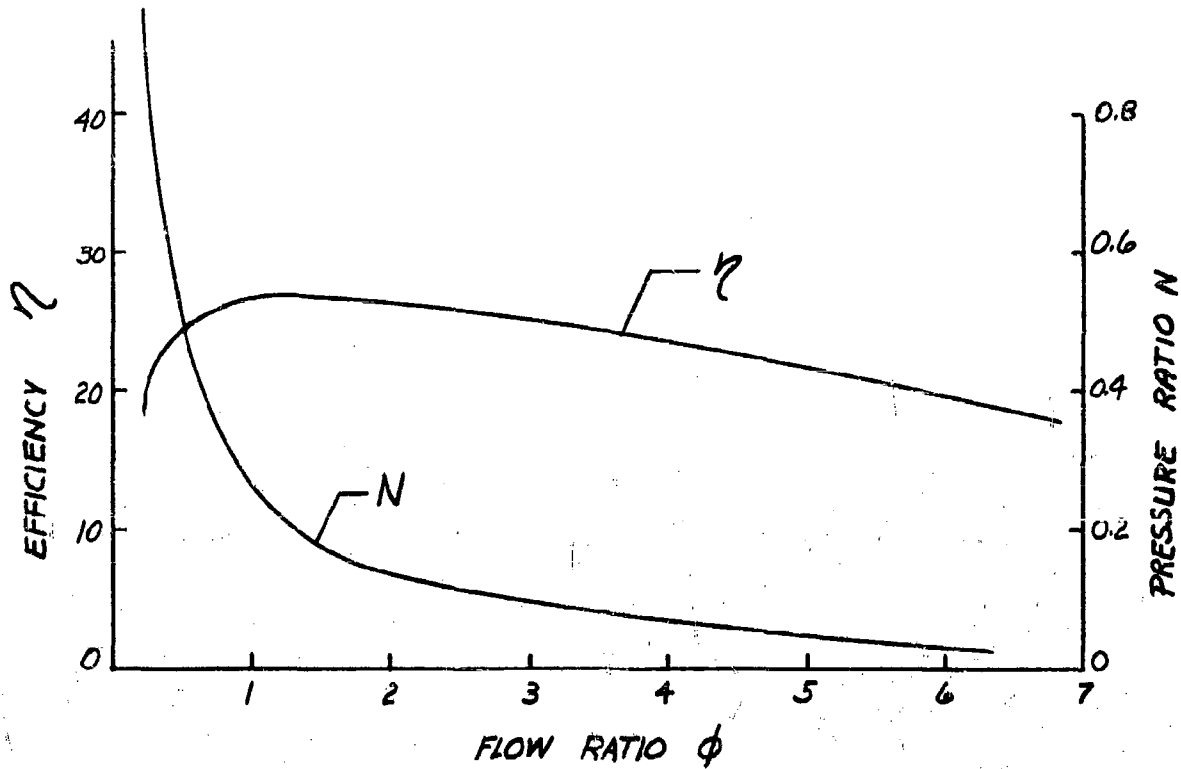
FIG 6. EFFICIENCY AND PRESSURE RATIOS vs
ϕ AND b FOR OPTIMUM CONDITIONS

VENT

OIL SUPPLY TANK

ROTAMETER (W_s)

VARIABLE SPEED PUMP

BACK PRESSURE CONTROL VALVE

MANOMETER (P_o)

ROTAMETER (W_N)

JET PUMP

GAGE (P_L)

GAGE (P_d)
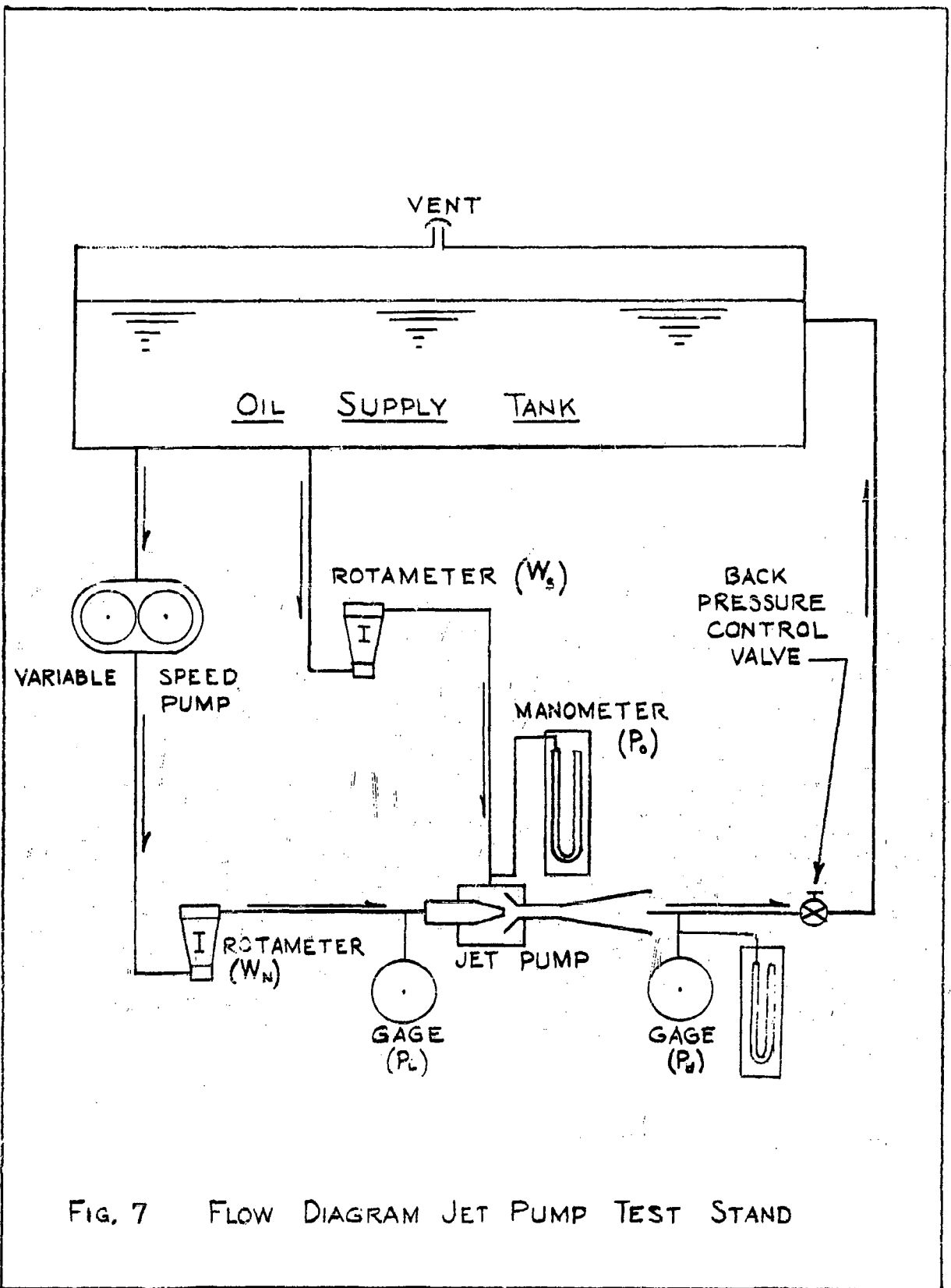
FIG. 7 FLOW DIAGRAM JET PUMP TEST STAND

THROAT-DIFFUSER SECTION

BODY SECTION

1 INCH PIPE TEE WITH RUN THREADS
CHANGED TO 1 3/8" 12 N-3 THREAD
AXIALLY ALIGNED, FIXED AND
BEVELED FOR O-RING SEALING.

NOZZLE SECTION
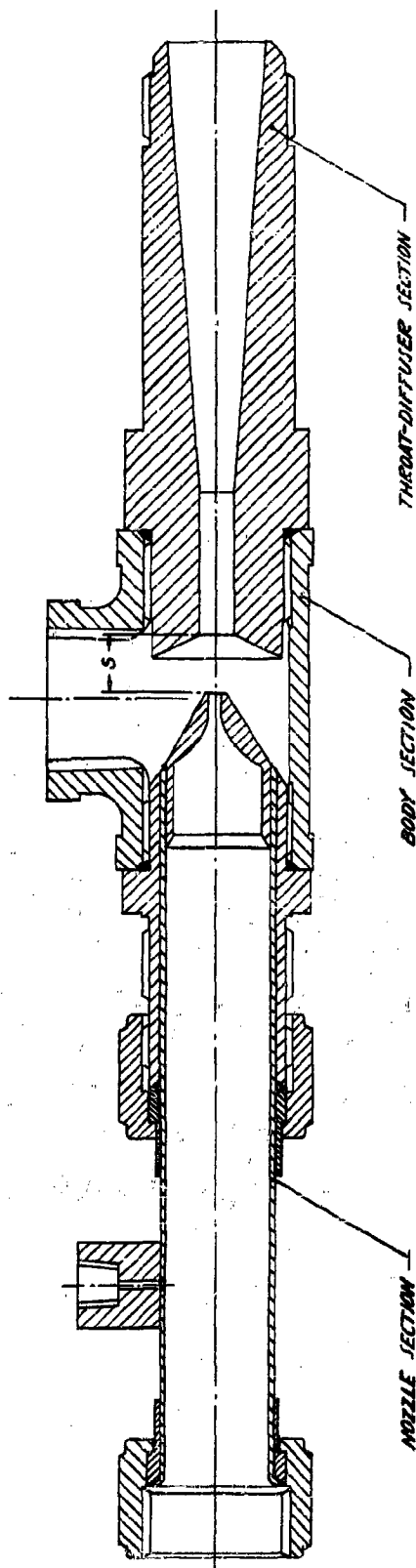
FIG. 8a

ASSEMBLY
EXPERIMENTAL JET PUMP
THE PENNSYLVANIA STATE COLLEGE
DEPARTMENT OF ENGINEERING RESEARCH

SCALE	FULL	DATE	11-5-53
DRAWN	C.F.G.		

THROAT - DIFFUSER SECTION
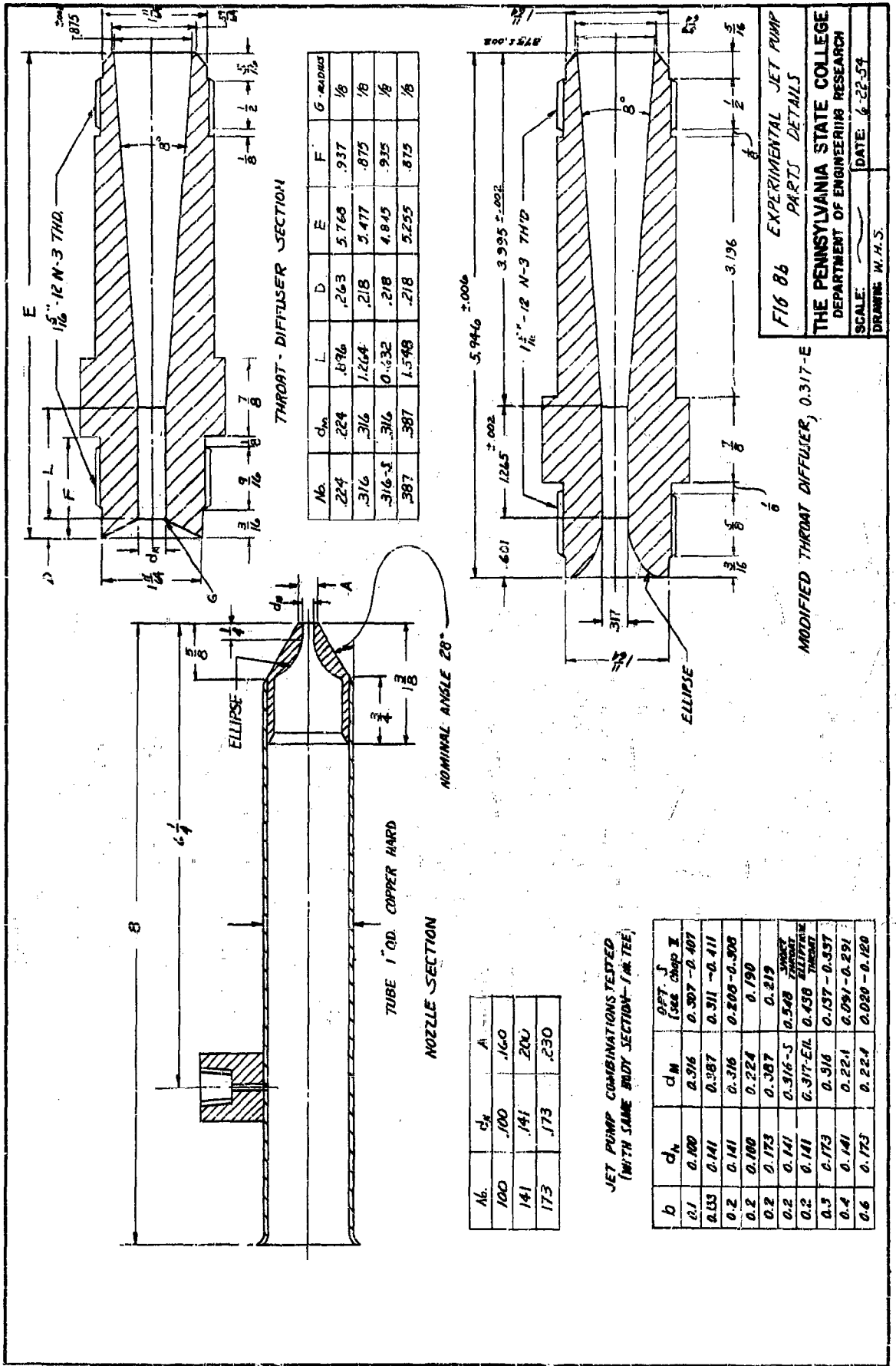
No.	d_in	L	D	E	F	G-RADIUS
.224	.224	.636	.263	5.765	.937	1/8
.316	.316	1.264	.218	5.477	.875	1/8
.316-S	.316	0.632	.218	4.845	.935	1/8
.387	.387	1.548	.218	5.255	.875	1/8

MODIFIED THROAT DIFFUSER, 0.317-E

NOZZLE SECTION

TUBE 1" OD. COPPER HARD

NOMINAL ANGLE 28°

ELLIPSE

No.	d_N	A
100	.100	.160
141	.141	.200
173	.173	.230

JET PUMP COMBINATIONS TESTED
(WITH SAME BODY SECTION - 1"x TEE)

b	d_N	d_M	OPT. S (see chap I)
0.1	0.100	0.316	0.307 - 0.407
0.133	0.141	0.387	0.311 - 0.411
0.2	0.141	0.316	0.205 - 0.305
0.2	0.100	0.224	0.190
0.2	0.173	0.387	0.219
0.2	0.141	0.316-S	0.548 SHORT THROAT
0.2	0.141	0.317-Ell.	0.456 ELLIPTIC THROAT
0.3	0.173	0.316	0.157 - 0.357
0.4	0.141	0.224	0.091 - 0.291
0.6	0.173	0.224	0.020 - 0.120

FIG 86 EXPERIMENTAL JET PUMP PARTS DETAILS

THE PENNSYLVANIA STATE COLLEGE
DEPARTMENT OF ENGINEERING RESEARCH

SCALE:	DATE: 6-22-54
DRAWN: W.H.S.	

FIG. 9 CONVENTIONAL JET PUMP

THE PENNSYLVANIA STATE COLLEGE
DEPARTMENT OF ENGINEERING RESEARCH

SCALE: ~
DRAWN: W.H.S.
DATE: 7-6-54

JET PUMP CHARACTERISTIC CURVES
FOR $b = 0.60$

PUMP NO. 173/224/020 $P_1 - P_0 = 79.8$ PSI.
TEST NO. 164 $W_N = 58.6$ LB/MIN.
OIL C AT 180°F $R_N = 21,370$

THEORETICAL N

CAVITATION

EFFICIENCY $\eta = \phi N$

PRESSURE RATIO $N = \dfrac{P_2 - P_0}{P_1 - P_2}$

FLOW RATIO $\phi = \dfrac{W_S}{W_N}$
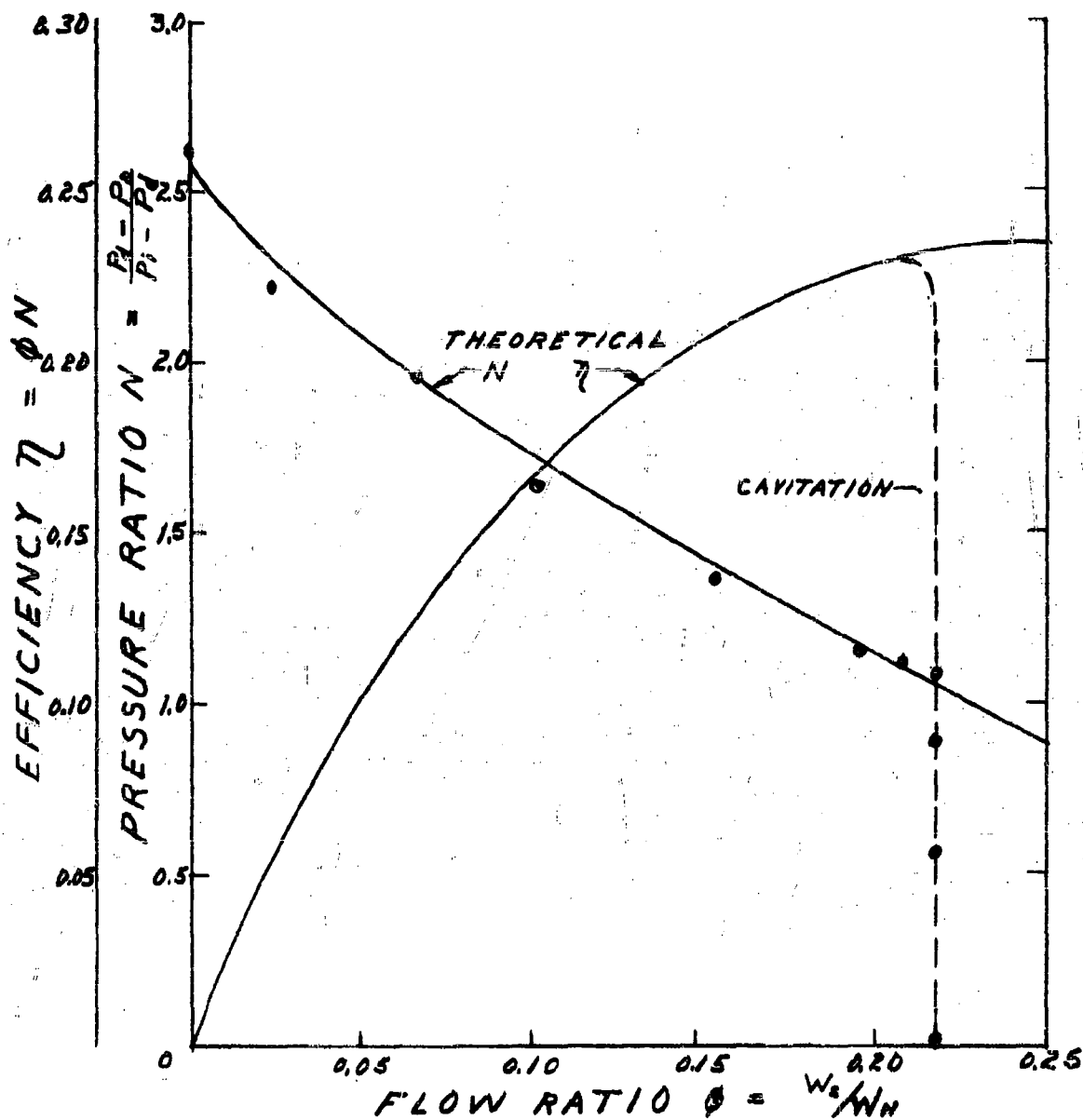
FIG. 10 EXPERIMENTAL N VALUES vs ϕ,
THEORY SHOWN AS SOLID LINE

JET PUMP CHARACTERISTIC CURVES
FOR b = 0.544

PUMP NO. 177/240/255 $P_i - P_o$ = 79.07 PSI
TEST NO. 166 W_N = 60.0 LB/MIN.
OIL C AT 180°F R_N = 21,970
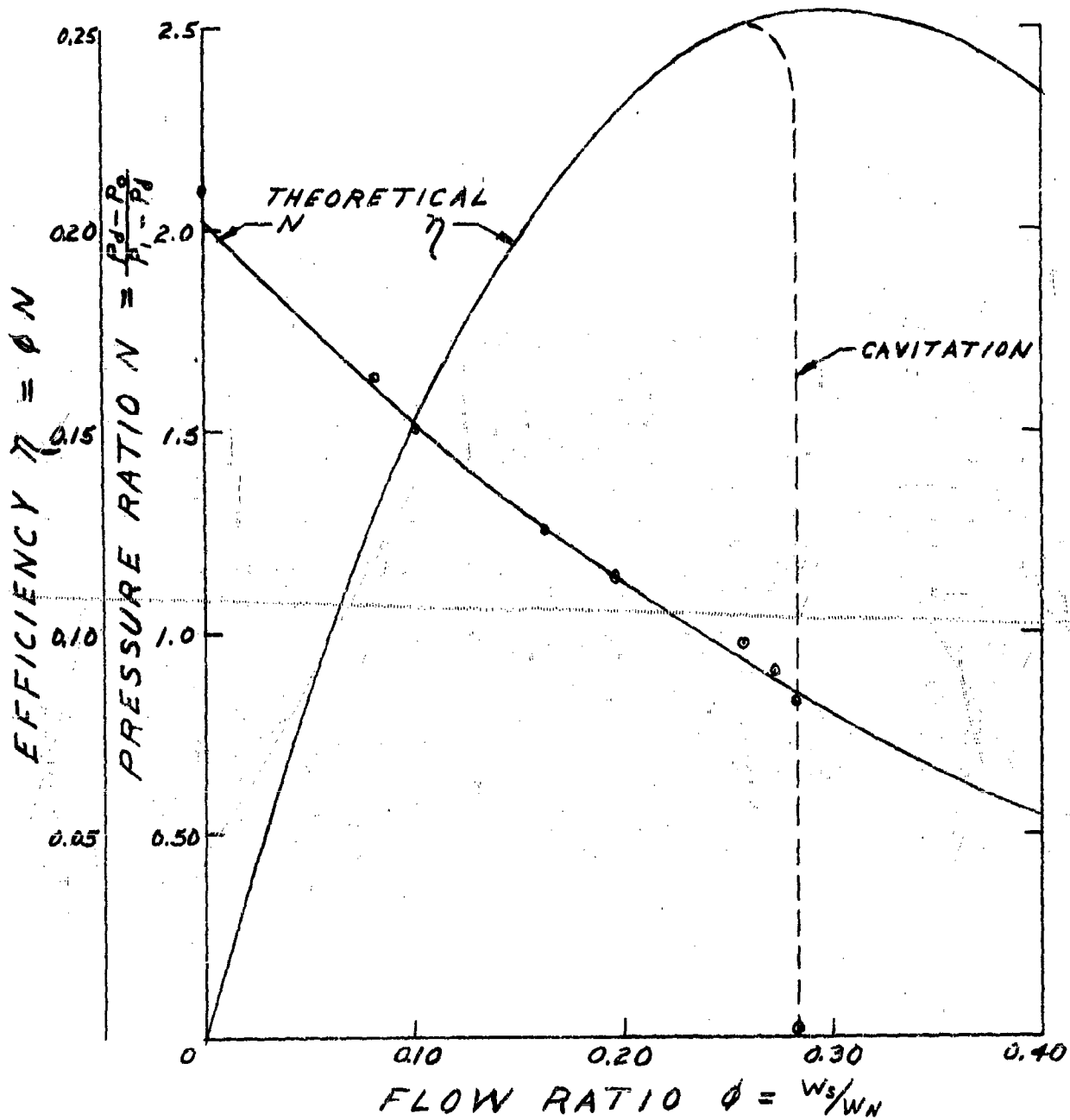
FIG. 11 EXPERIMENTAL N VALUES vs ϕ,
THEORY SHOWN AS SOLID LINE

JET PUMP CHARACTERISTIC CURVES
FOR $b = 0.4$

PUMP NO. 141/224/291 $P_i - P_o = 99.22$ PSI.
TEST NO. 148 $W_N = 44.3$ LB/MIN.
OIL 1005 AT 100°F $R_N = 25,840$
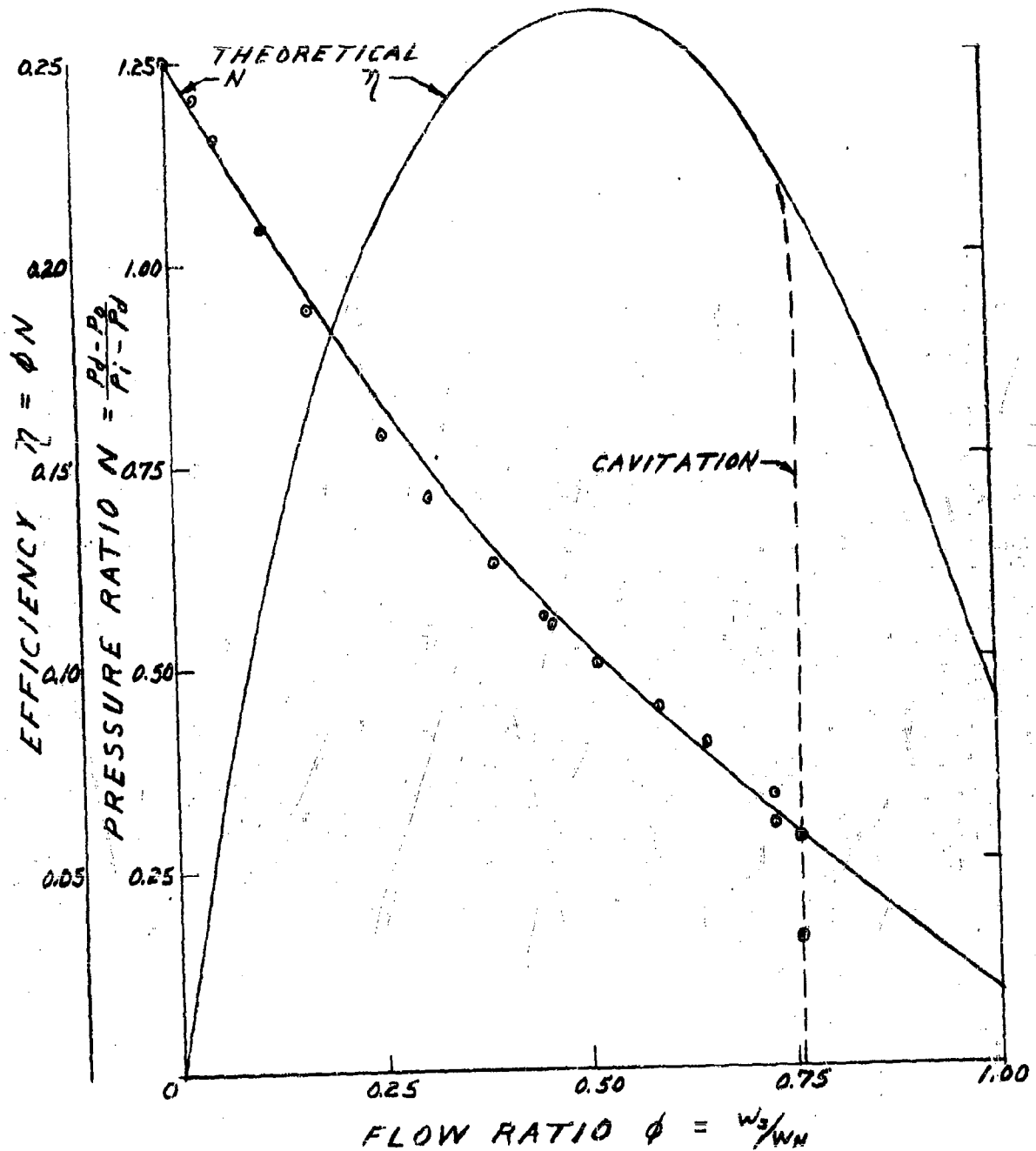
FIG. 12 EXPERIMENTAL N VALUES vs ϕ,
THEORY SHOWN AS SOLID LINE

JET PUMP CHARACTERISTIC CURVES
FOR b = 0.2

PUMP NO. 141/316/308 $P_1 - P_0$ = 100.02 PSI
TEST NO. 179 W_N = 43.1 LB/MIN
OIL C AT 180°F R_N = 19,230

THEORETICAL
N
η

CAVITATION

EFFICIENCY $\eta = \phi N$

PRESSURE RATIO $N = \frac{P_2 - P_0}{P_1 - P_1}$

FLOW RATIO $\phi = \frac{W_S}{W_N}$
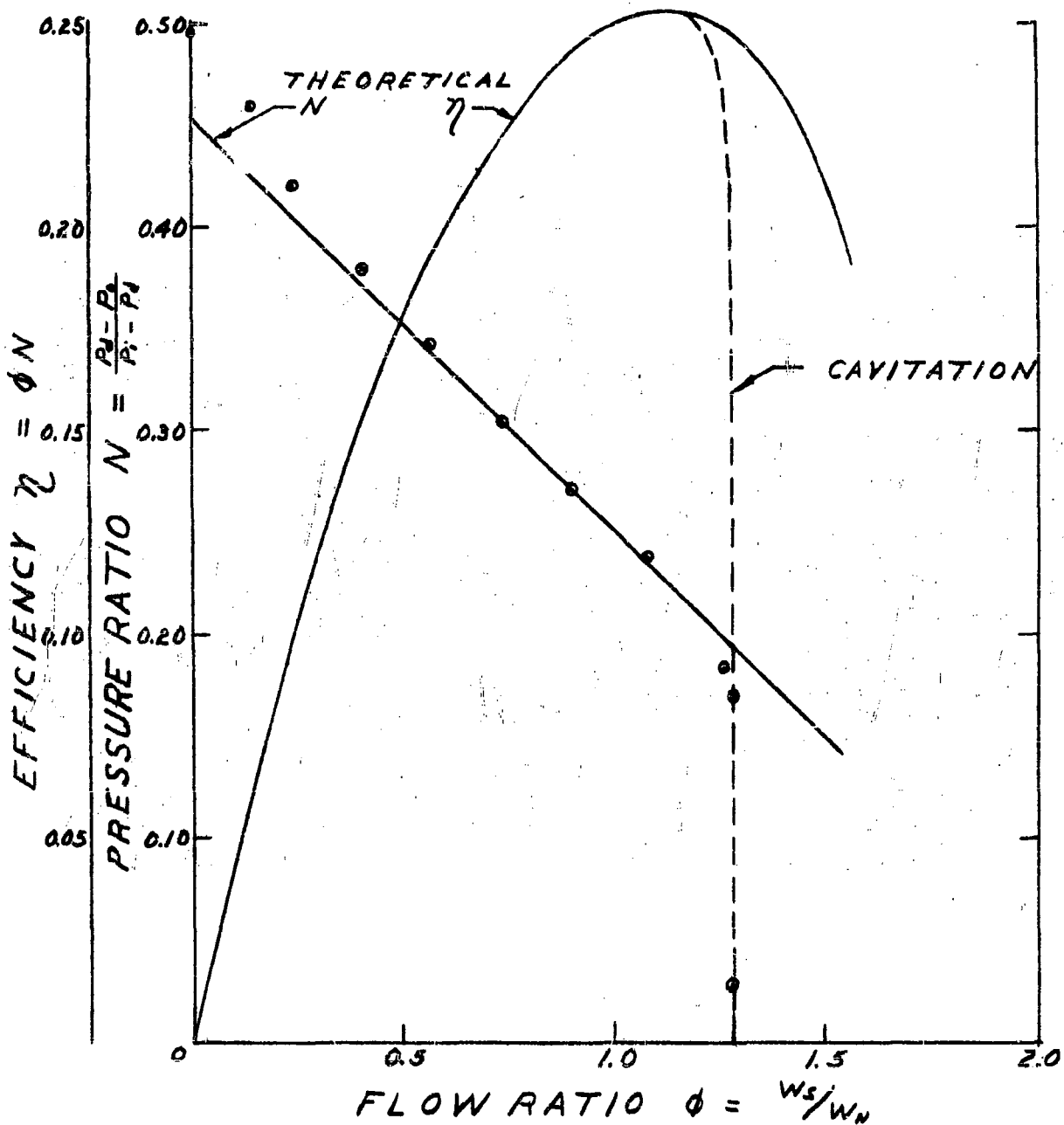
FIG. 13   EXPERIMENTAL N VALUES vs ϕ
THEORY SHOWN AS SOLID LINE

JET PUMP CHARACTERISTIC CURVES
FOR b = 0.1

PUMP NO. 100/316/307 $P_i - P_0$ = 100.24 PSI.
TEST NO. 173 W_N = 20.72 LB/MIN.
OIL C AT 180° F R_N = 13,075
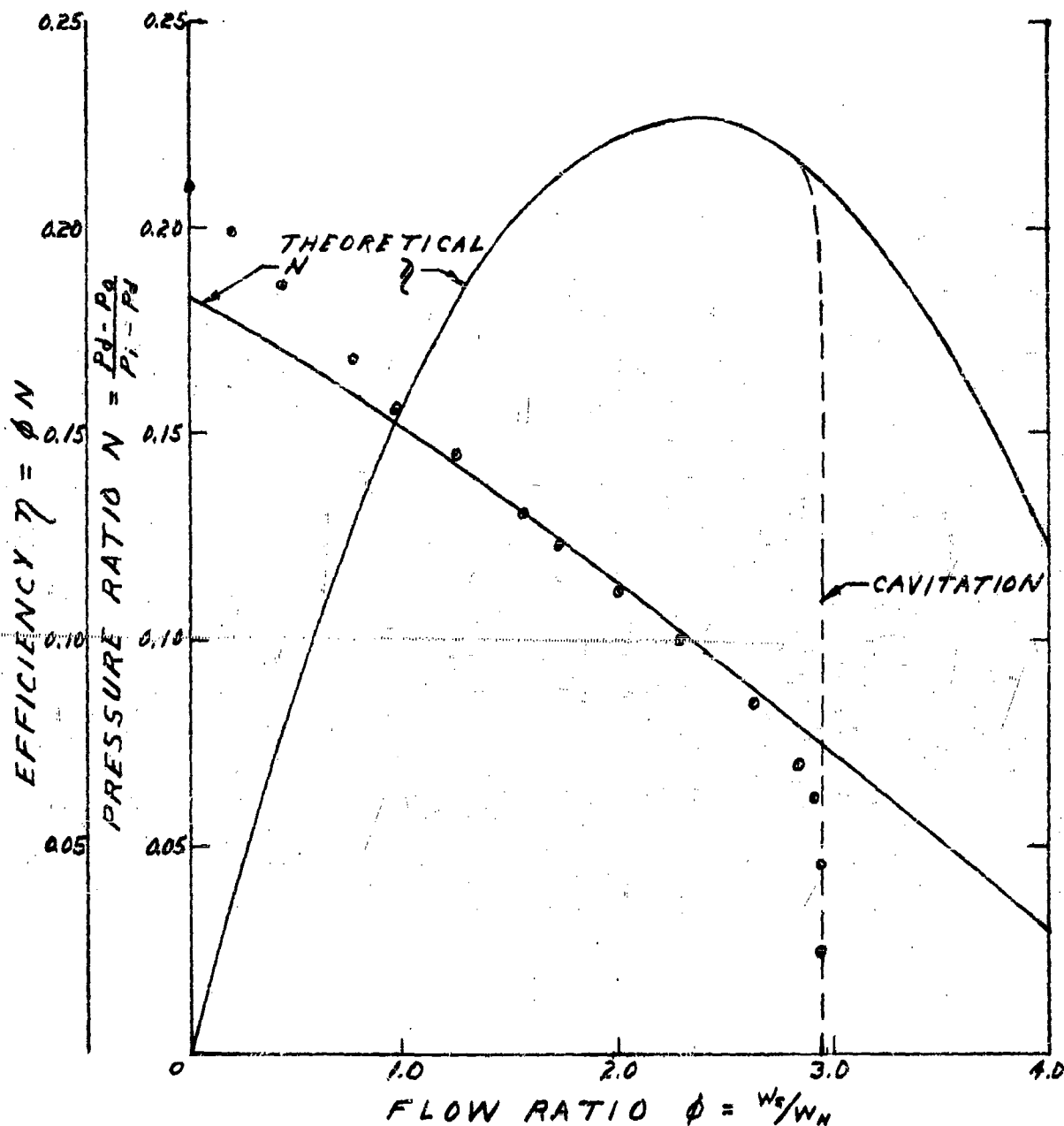
FIG. 14 EXPERIMENTAL N VALUES vs φ,
THEORY SHOWN AS SOLID LINE

JET PUMP PERFORMANCE vs FLOW RATIO

KINEMATIC VISCOSITY
V: 6.5

PUMP NO 100/240/445
b = 0.174
P₁ - P₈ = 40 PSI
NOMINAL

R_N, JET REYNOLDS NO.
— 10,340
— 3,420
— 2,480
— 2,120
— 1,720
— 437

16
19
25
31
100

TEST NOS. 38, 55-58, 60, 62.
OIL: GRADE 1005 AND BLEND A.

PRESSURE RATIO N

0.4
0.3
0.2
0.1
0

0.4   0.8   1.2   1.6   2.0

FLOW RATIO ϕ

PUMP NO. 141/316/408
b = 0.20
P₁ - P₈ = 40 PSI
NOMINAL

TEST NOS. 72, 73, 74.

V = 16
31
100

R_N
— 5,160
— 2,510
— 654

PRESSURE RATIO N

0.4
0.3
0.2
0.1
0

0.4   0.8   1.2   1.6   2.0

FLOW RATIO ϕ
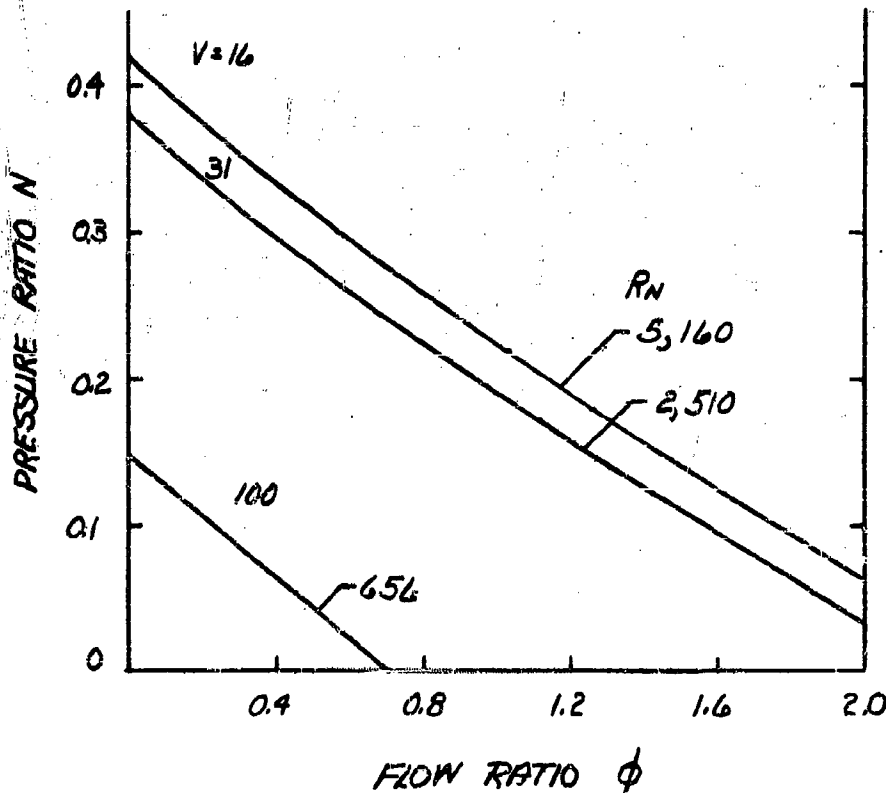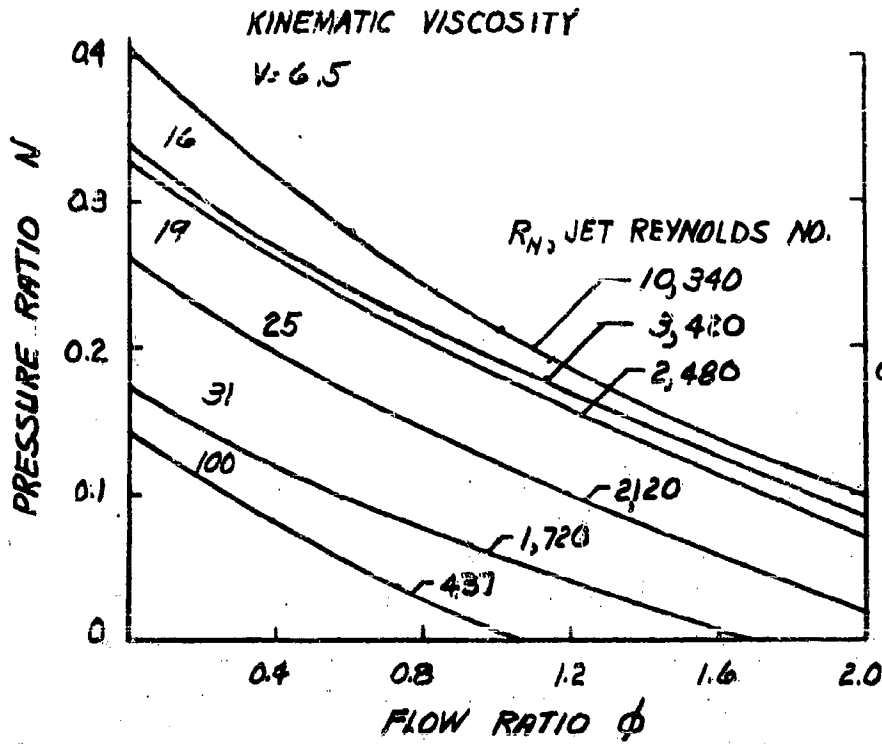
FIG. 15 EFFECT OF OIL VISCOSITY ON N CHARACTERISTIC CURVES
OILS GRADE 1005 AND BLEND A, 80 F TO 160 F

JET PUMP FRICTION COEFFICIENT K_1

DATA FROM JET PUMP
PERFORMANCE TESTS,
TABLE 4, AND NOZZLE TESTS

ELLIPTICAL NOZZLES

SYMBOL	d_N IN.	b
X	0.100	0.10
✹	0.141	0.133
●	0.141	0.20
✦	0.141	0.40
■	0.173	0.30
□	0.173	0.60

CONICAL NOZZLES

SYMBOL	d_N	b
♂	0.100	0.174
△	0.177	0.534
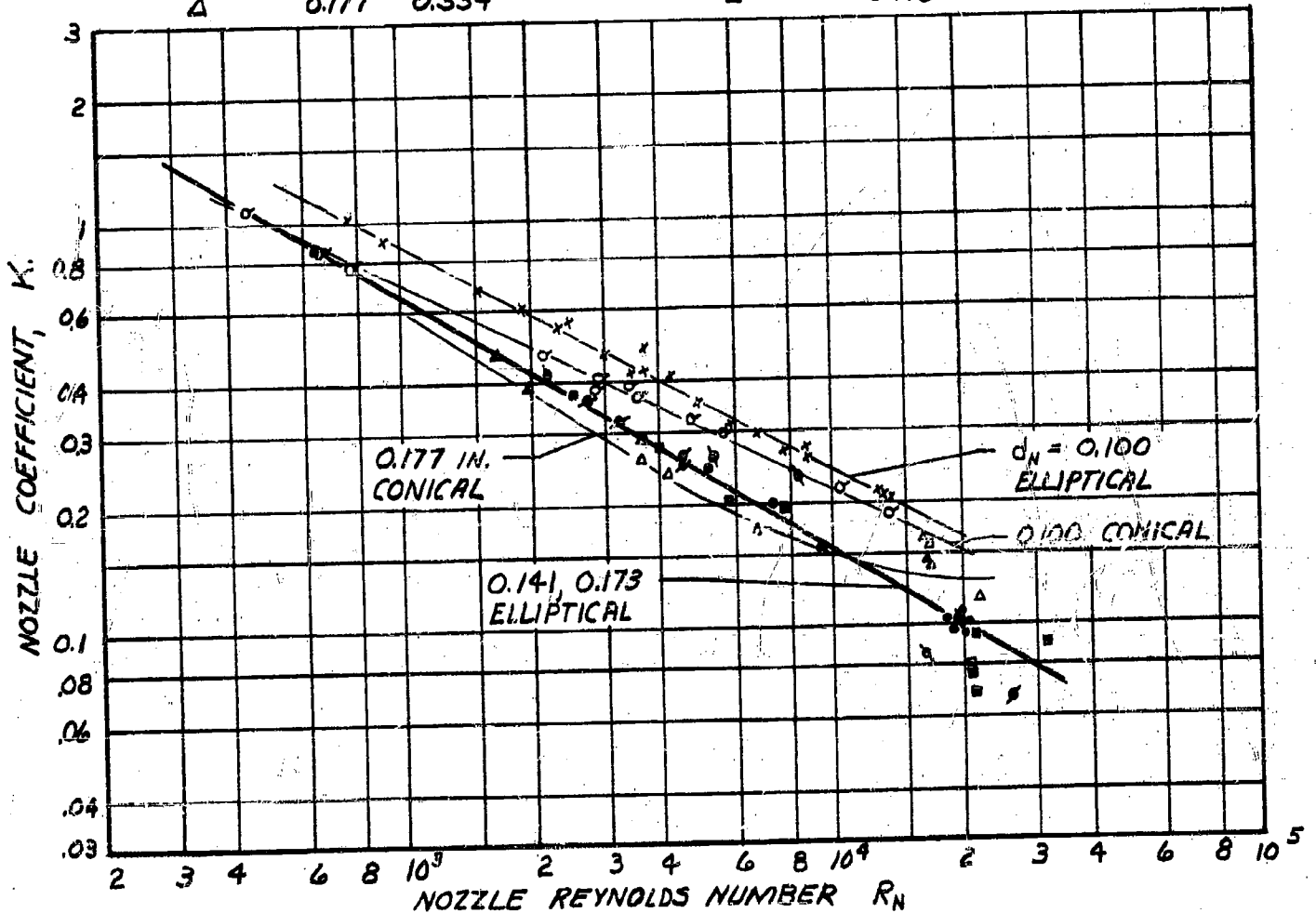
FIG 16.   EXPERIMENTAL NOZZLE COEFFICIENTS K_1
VERSUS REYNOLDS NUMBER

JET PUMP FRICTION COEFFICIENT K_{34}

DATA: TABLE 4

SYMBOL	AREA RATIO b	SYMBOL	AREA RATIO b
▓	0.30	X	0.10
▨	0.40	⚑	0.133
△	0.534	♂	0.147
□	0.60	●	0.20
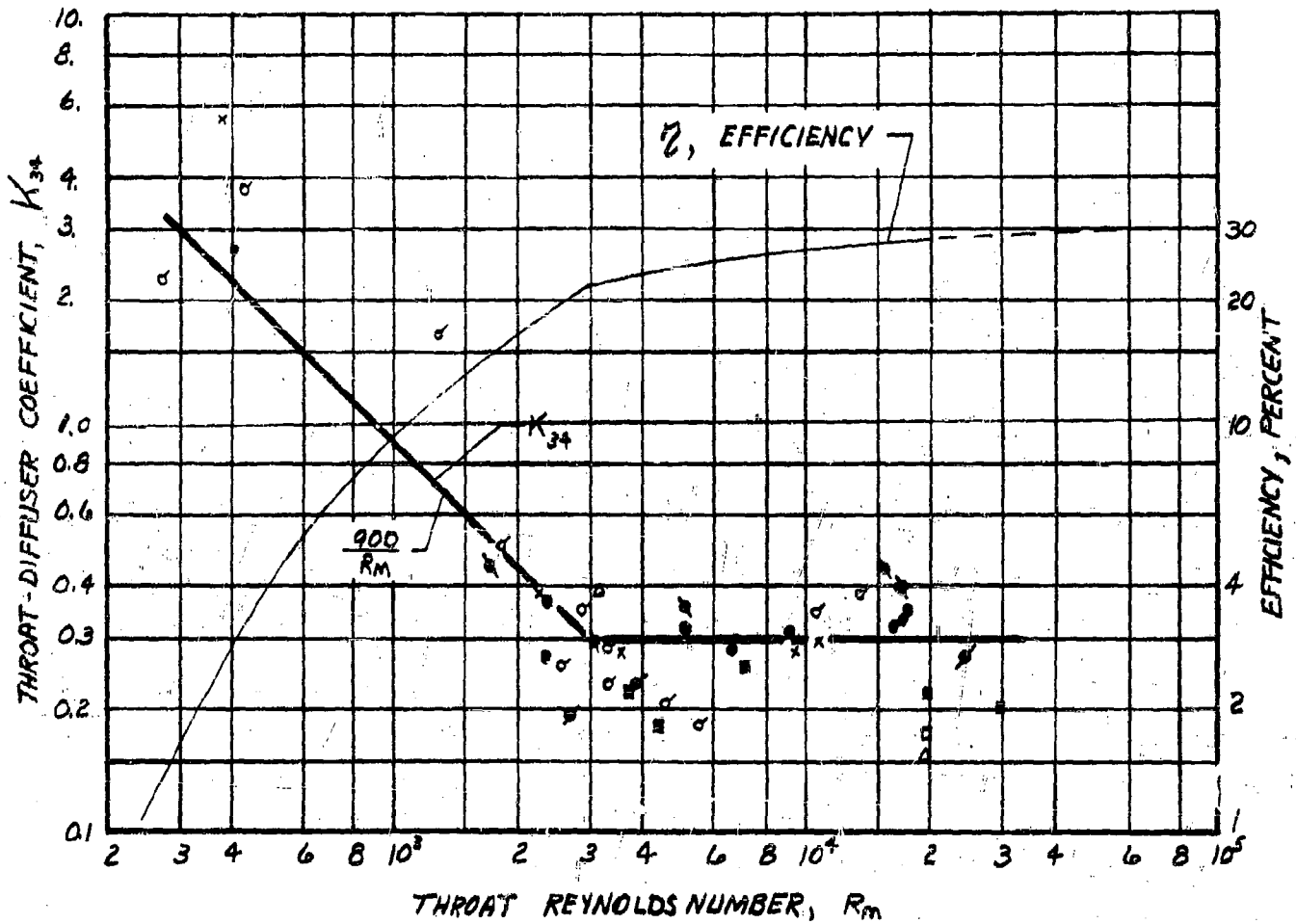
FIG 17   EXPERIMENTAL THROAT-DIFFUSER
COEFFICIENT K_{34} VERSUS REYNOLDS
NUMBER

JET PUMP CHARACTERISTIC CURVES

PUMP NO. 141/316/308 , b = 0.20
OIL : MIL-L-7808 SYNTHETIC AT 150°F
NOZZLE PRESSURE P₁ = 100 PSIG.

X   TEST NO. 190   P₀ AT 1,480 FT. ALT. , 13.9 PSIA.
                        Wₙ = 44.6 LB/MIN. Rₙ = 20,150

⊙   TEST NO. 197   P₀ AT 12,000 FT. ALT. , 9.31 PSIA.
                        Wₕ = 45.6 LB/MIN. Rₙ = 20,550
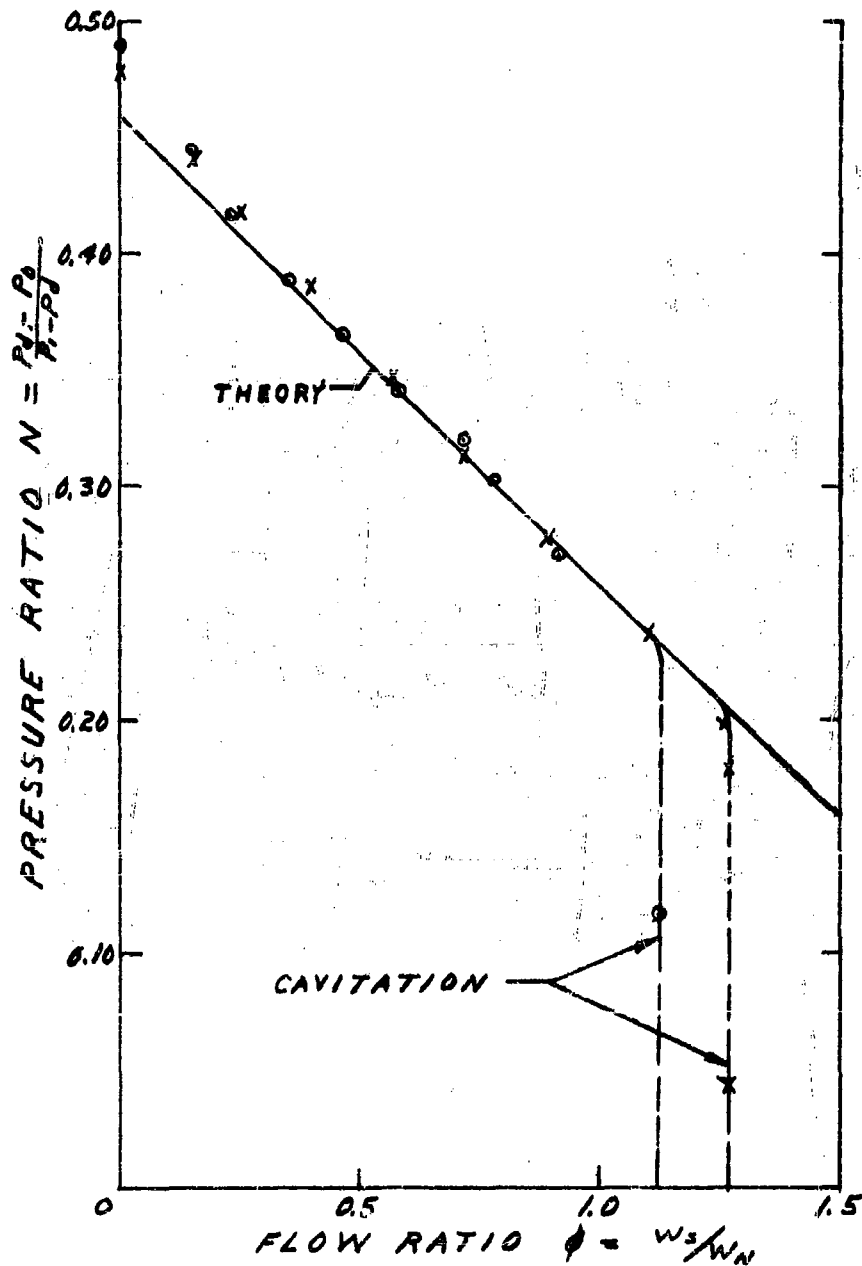
FIG. 18 EFFECT OF ALTITUDE PRESSURE

JET PUMP CHACTERISTIC CURVES
PUMP NO. 100/240/455

A. EFFECT OF JET VELOCITY
$R_N = 3,900$ NOM.
OIL: BLEND A

SYMBOL	$P_1 - P_2$	W_N	TEMP	TEST
●	39.5	12.15	160 F	57
☐	99	19.5	135 F	63

PRESSURE RATIO N

LIMITING FLOW
$P_1 - P_2 = 99$ PSI.

39.5 PSI.

B. THROTTLED SUCTION, TEST 14
$W_N = 27$, $P_1 - P_2 = 150$ PSI.
OIL 1005 @ 80 F, $R_N = 16,350$

SYMBOL	P_2	
X	14.9	PSIG.
O	9.8	
△	4.9	

PRESSURE RATIO N

$P_2 = 4.9$ PSIG.

9.8

14.9

LIMITING FLOW

FLOW RATE φ
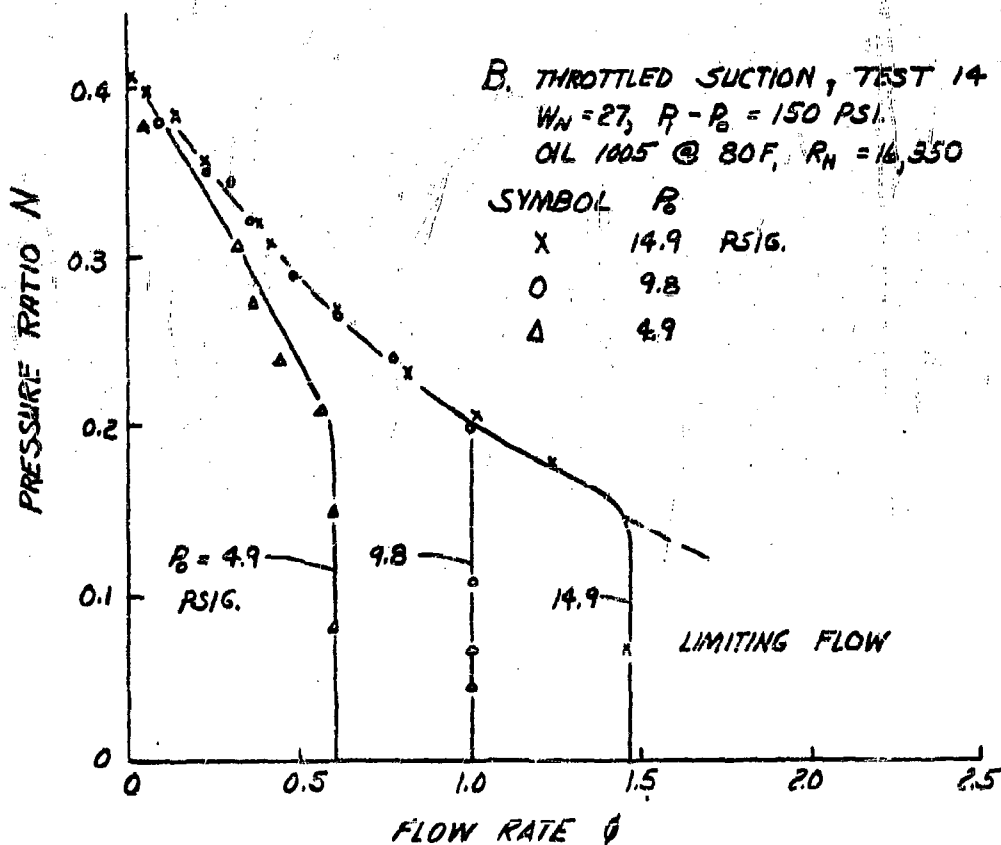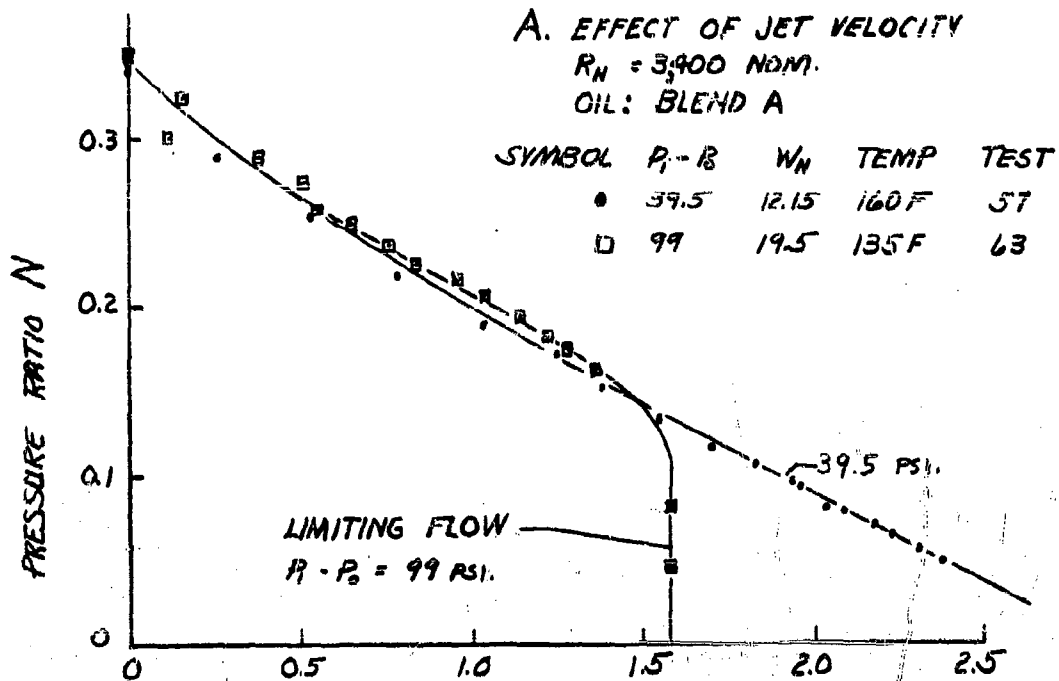
FIG 19. LIMITING FLOW CAUSED BY A. JET VELOCITY AND B. REDUCED PRESSURE P_2

SECONDARY FLOW - W_s AT P_o
(DUAL PIPE CONNECTIONS ON BACK NOT SHOWN)

TO BACK PRESSURE CONTROL VALVE

1" PIPE

$1\frac{11}{16}$

A   A'

10°

THROAT $\frac{1}{4} \times \frac{1}{4}$

DIFFUSER PRESSURE TAP P_d

END PLATE (BRASS)

12

THROAT $\frac{1}{4} \times \frac{1}{4}$

$3\frac{1}{4}$

$1\frac{5}{16}$

THROAT TAPS 1,2,3

NOZZLE FLOW IN
W_N at P_i

NO. 12
AN TUBING

END PLATE
(BRASS)

CLEAR LUCITE

$2\frac{9}{32}$

SECTION A-A'

$\frac{1}{4}$

$2\frac{1}{2}$

NOZZLE SLIT
0.05" × 0.22"

CLEAR LUCITE
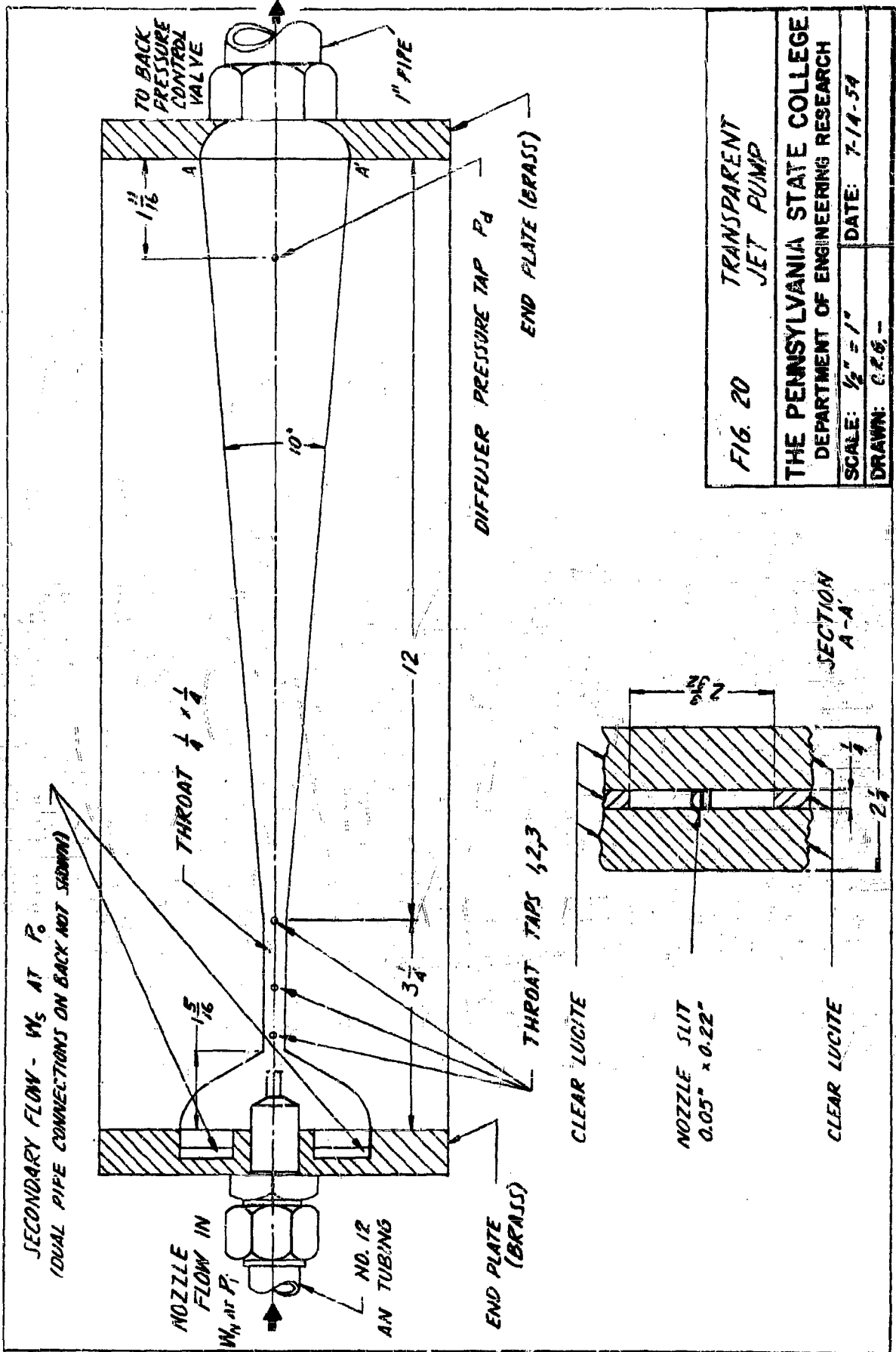
FIG. 20   TRANSPARENT JET PUMP

THE PENNSYLVANIA STATE COLLEGE
DEPARTMENT OF ENGINEERING RESEARCH

SCALE: $\frac{1}{2}$" = 1"   DATE: 7-14-54
DRAWN: C.E.G. —
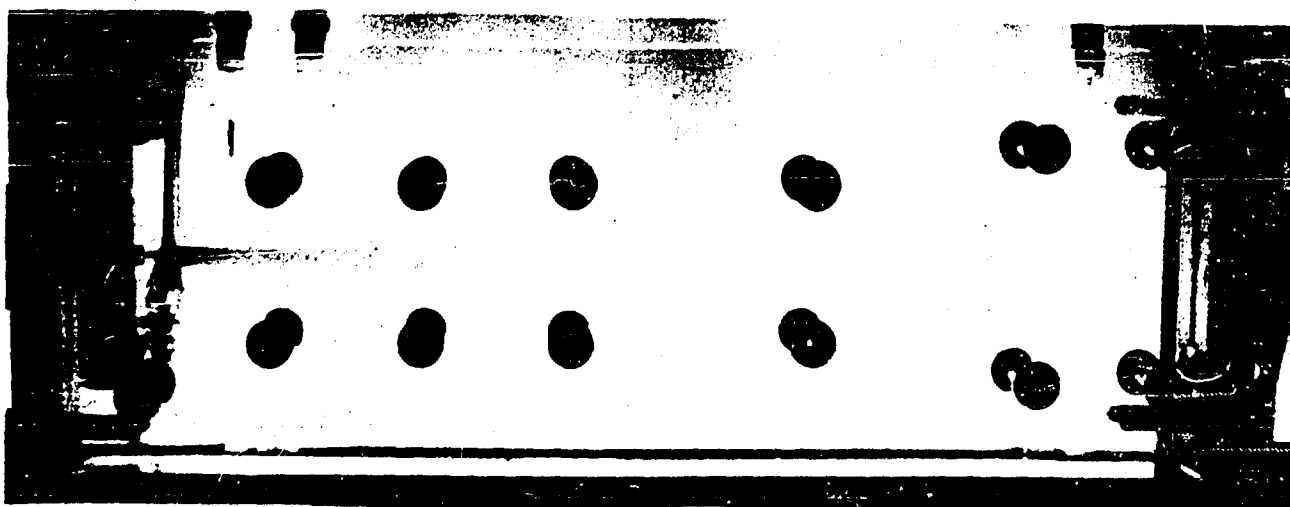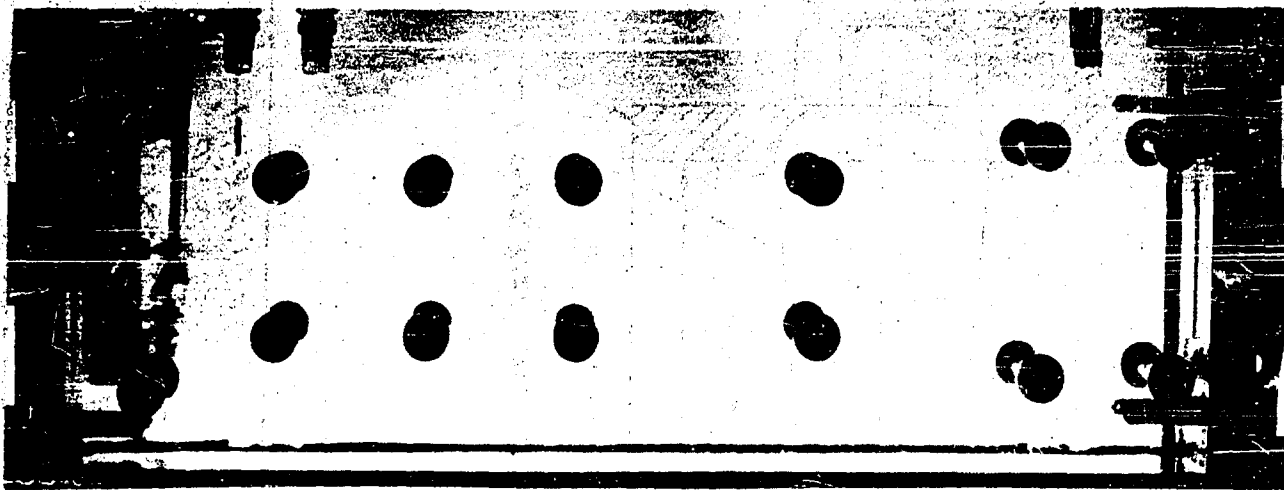
FIGURE 2i   CAVITATION IN   OIL-JET PUMP

W_N = 26.5 LB/MIN P_i = 150 PSIG

TOP: NOT CAVITATING, P_b = 37 PSIA W_s = 10 LB/MIN

BOTTOM: CAVITATION FRONT BETWEEN THROAT TAPS I AND 2.
P_b = 22.5 PSIA W_s = 40 LB/MIN
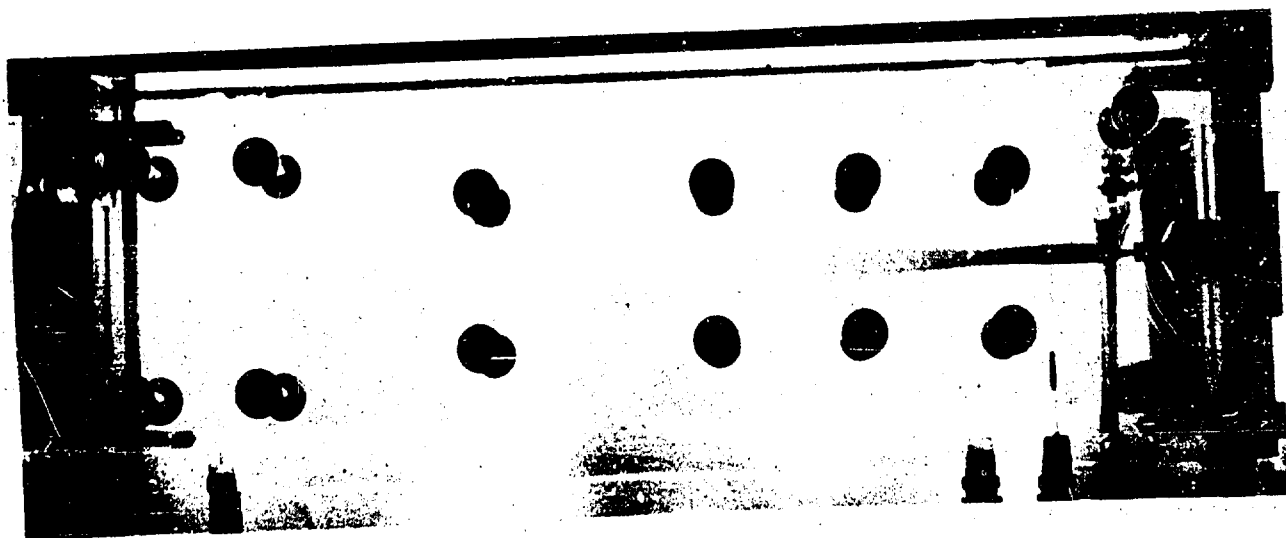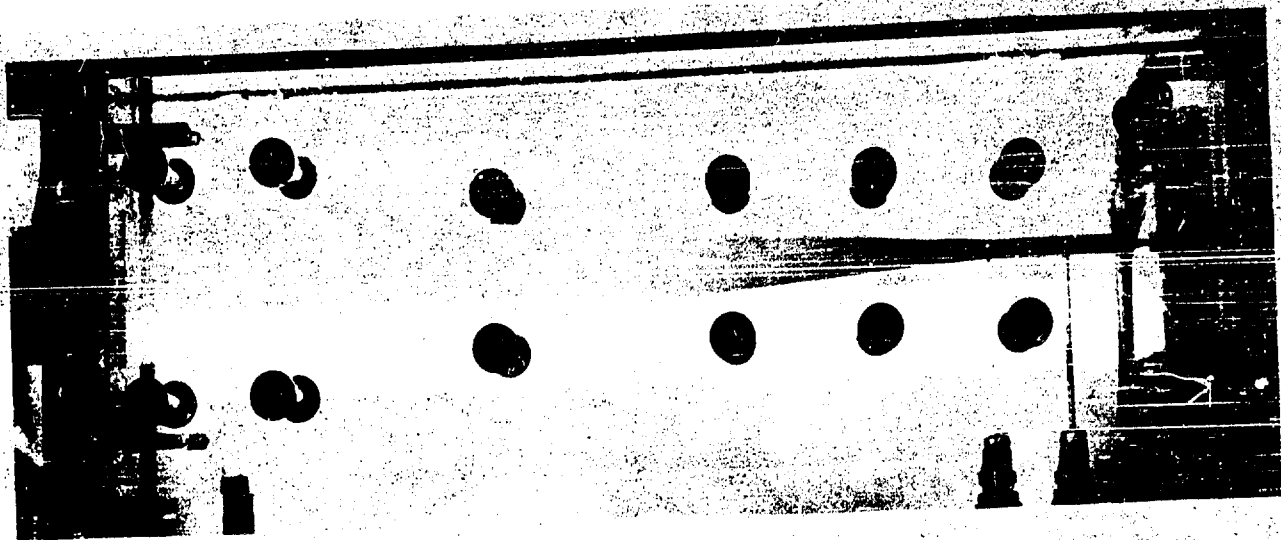
FIGURE 22   CAVITATION IN OIL-JET PUMP

W_N = 26.5 LB/MIN P_i = 150 PSIG

TOP: CAVITATION FRONT BETWEEN THROAT TAPS 2 AND 3.
P_b = 21 PSIA W_s = 40 LB/MIN

BOTTOM: CAVITATION FRONT IN DIFFUSER.
P_b = 17 PSIA W_s = 40 LB/MIN
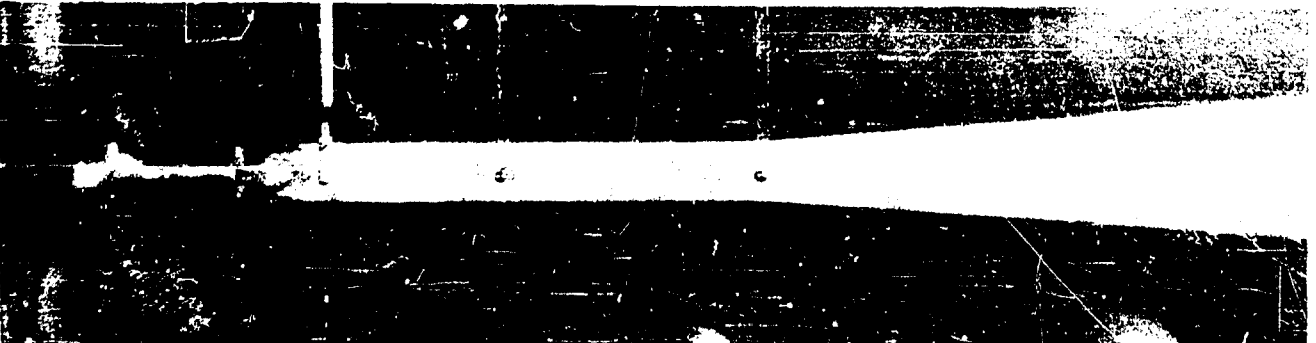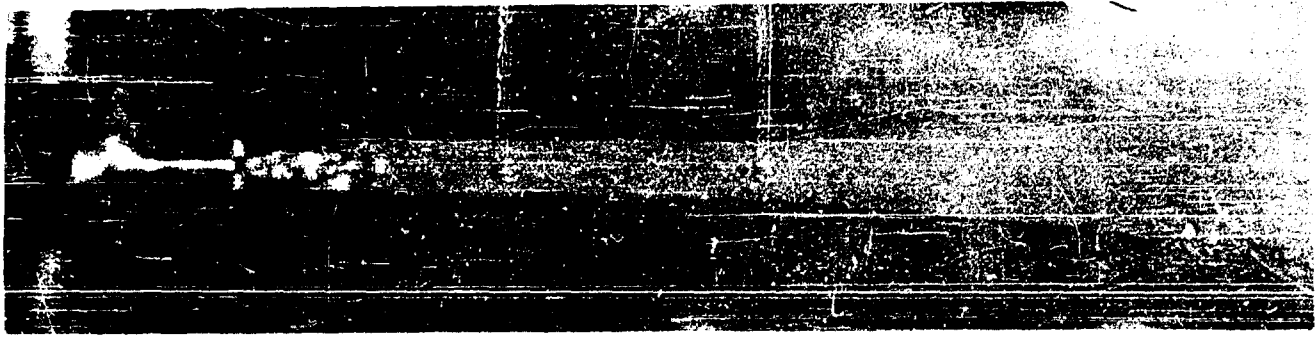
Fig. 23 High speed flash pictures of oil jet pump showing four stages
of cavitation.

JET PUMP LIMITING-FLOW FUNCTION
OIL TANK EVACUATED TO CONTROL P_0
OIL : GRADE 1005 AT 100°F

SYMBOL	$(P_1-P_0)_j$, PSI	TEST	δ	PUMP NO.
●	100	142 }	0.20	141/316/308
○	150	141		
■	100	154 }	0.30	173/316/237
□	150	155		
▲	100	140 }	0.544	177/240/455
△	150	138, 139		
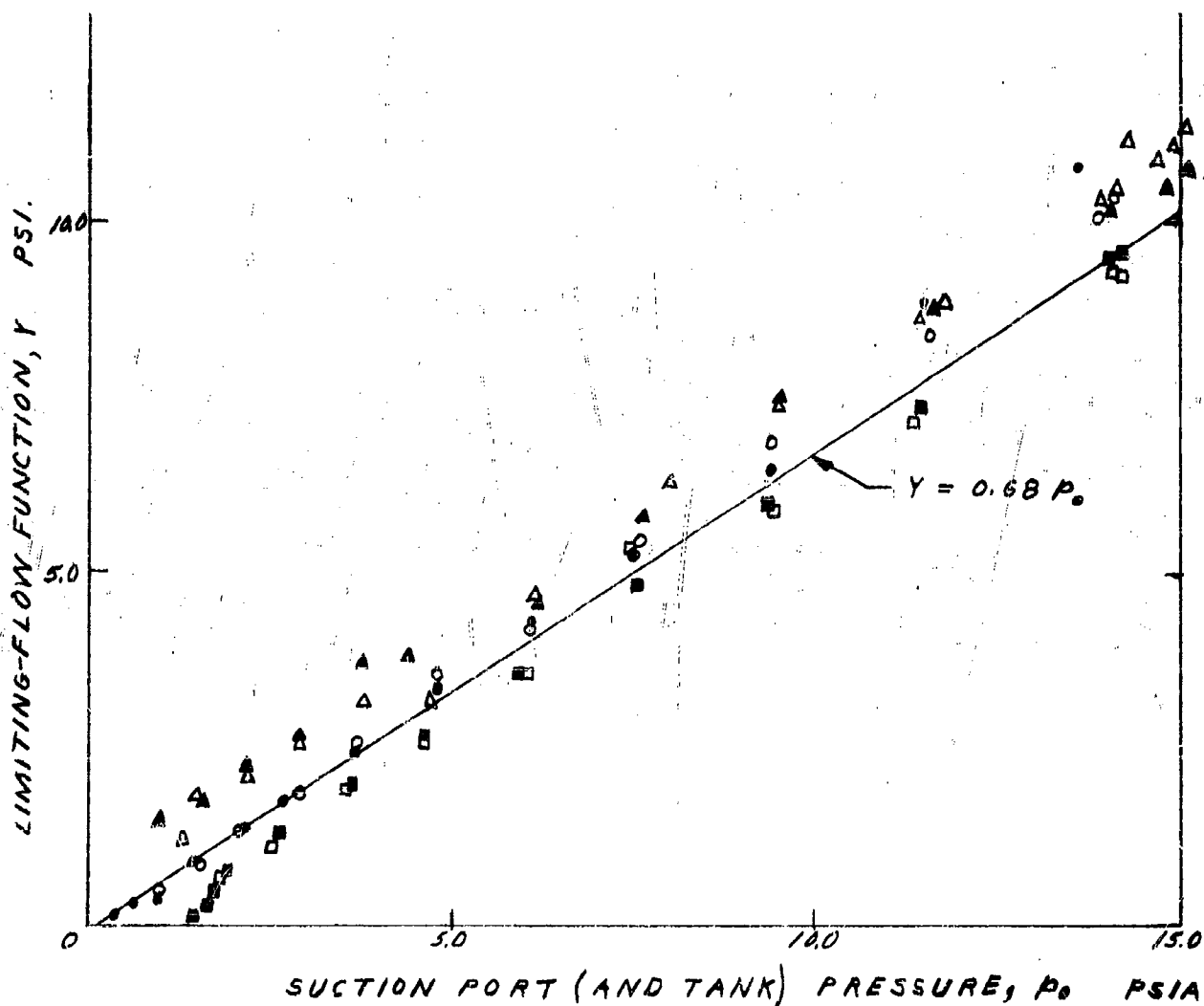
FIG. 24 LIMITING-FLOW FUNCTION Y FOR THREE
JET PUMPS

JET PUMP LIMITING - FLOW FUNCTION

SUCTION PORT THROTTLED
TANK PRESSURE : 14.7 PSIA.
OIL: GRADE 1005

SYMBOL	(A-B), PSI	TEMP, °F	PUMP NO.	b	TEST NO.
X	150	100	141/316/308	0.20	116
O	150	150	141/316/308	0.20	115
△	150	100	100/316/307	0.10	124
□	150	100	141/387/311	0.133	132
▣	100	100	141/387/311	0.133	131

WITH TANK AT ALTITUDE, PRESSURE, $Y = 0.68 P_0$

Y WITH THROTTLED SUCTION, TANK AT AMBIENT

LIMITING-FLOW FUNCTION, Y PSI

SUCTION PORT PRESSURE, P_0 PSIA
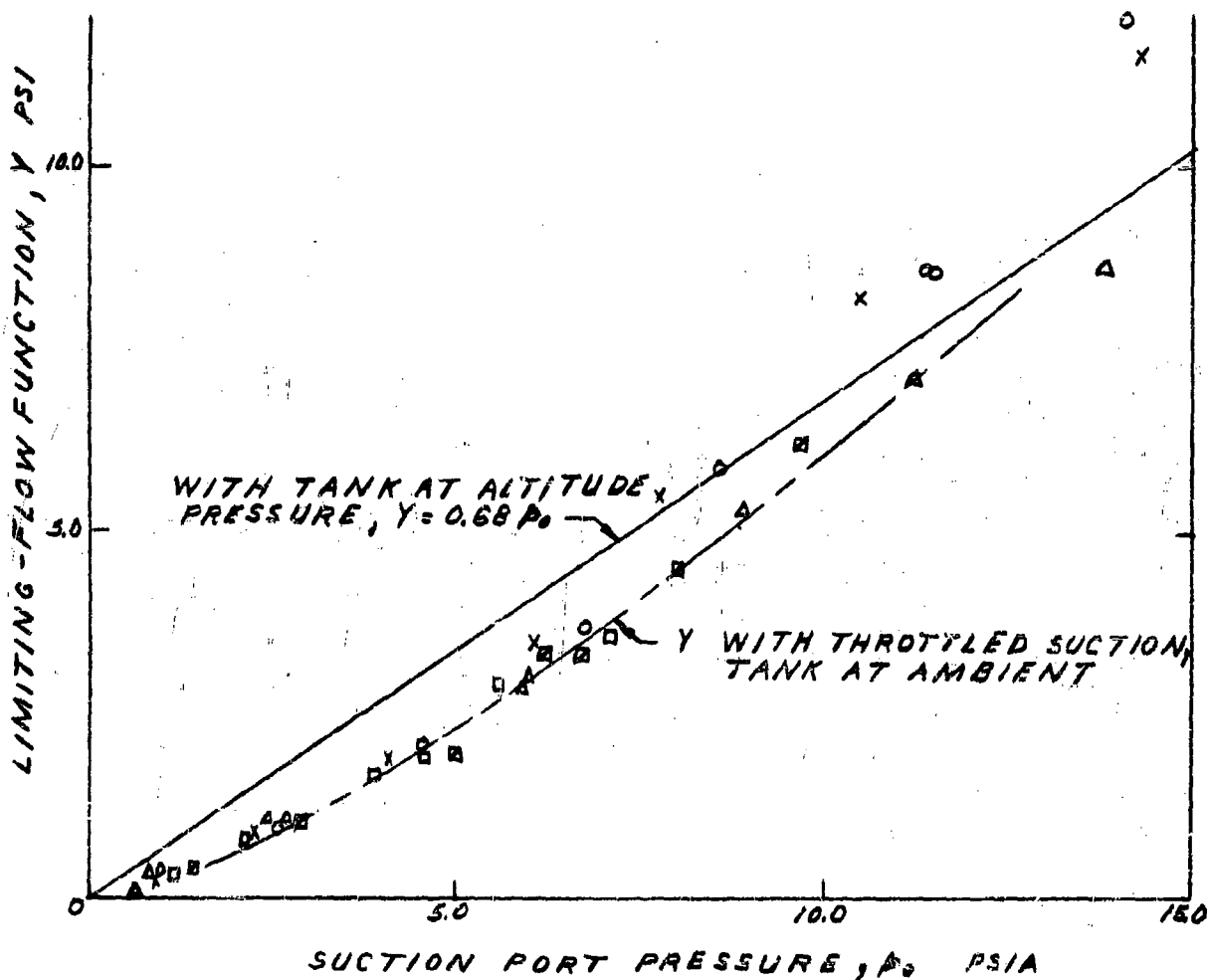
FIG. 25 LIMITING-FLOW RESULTS, OBTAINED BY THROTTLING THE SUCTION PORT TO CONTROL P_0

JET PUMP LIMITING-FLOW FUNCTION

OIL TANK EVACUATED TO CONTROL P_o
PUMP NO. 141/316/308 , b = 0.200

SYMBOL	OIL	TEMP. °F	$(P_i - P_o)$, PSI	TEST NO.
O	GRADE 1005	100	100	142, 145
X	SYNTHETIC	150°	100	189
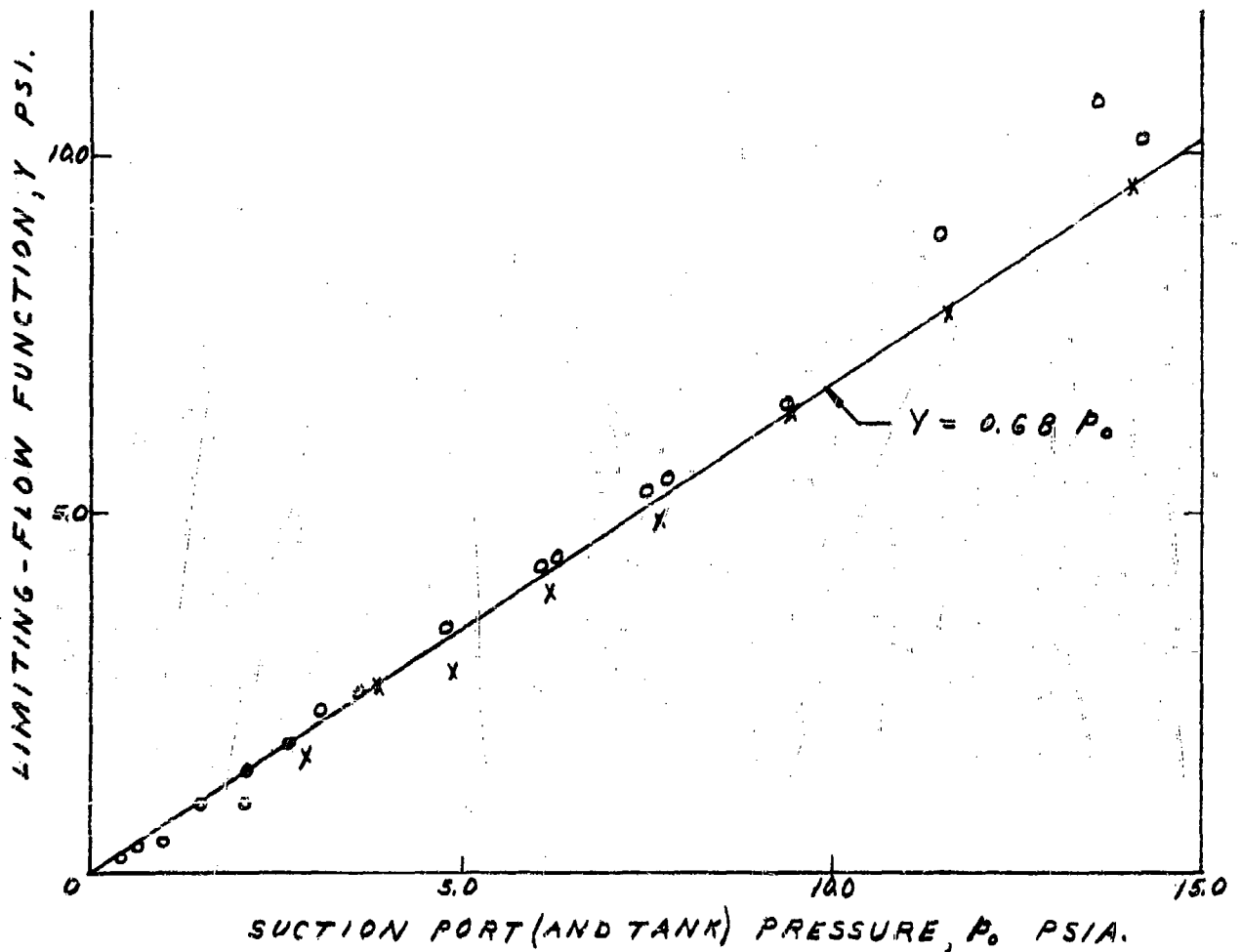
FIG. 26 LIMITING-FLOW RESULTS FOR HYDRO-
CARBON AND SYNTHETIC LUBRICATING OILS

JET PUMP LIMITING-FLOW FUNCTION

OIL TANK EVACUATED TO CONTROL P_0
PUMP NO. 141/316/308
OIL : MIL-L-7808, SYNTHETIC AT 150°F
$(P_1 - P_0) = 100$ PSI.
TESTS NO. : 189, 193
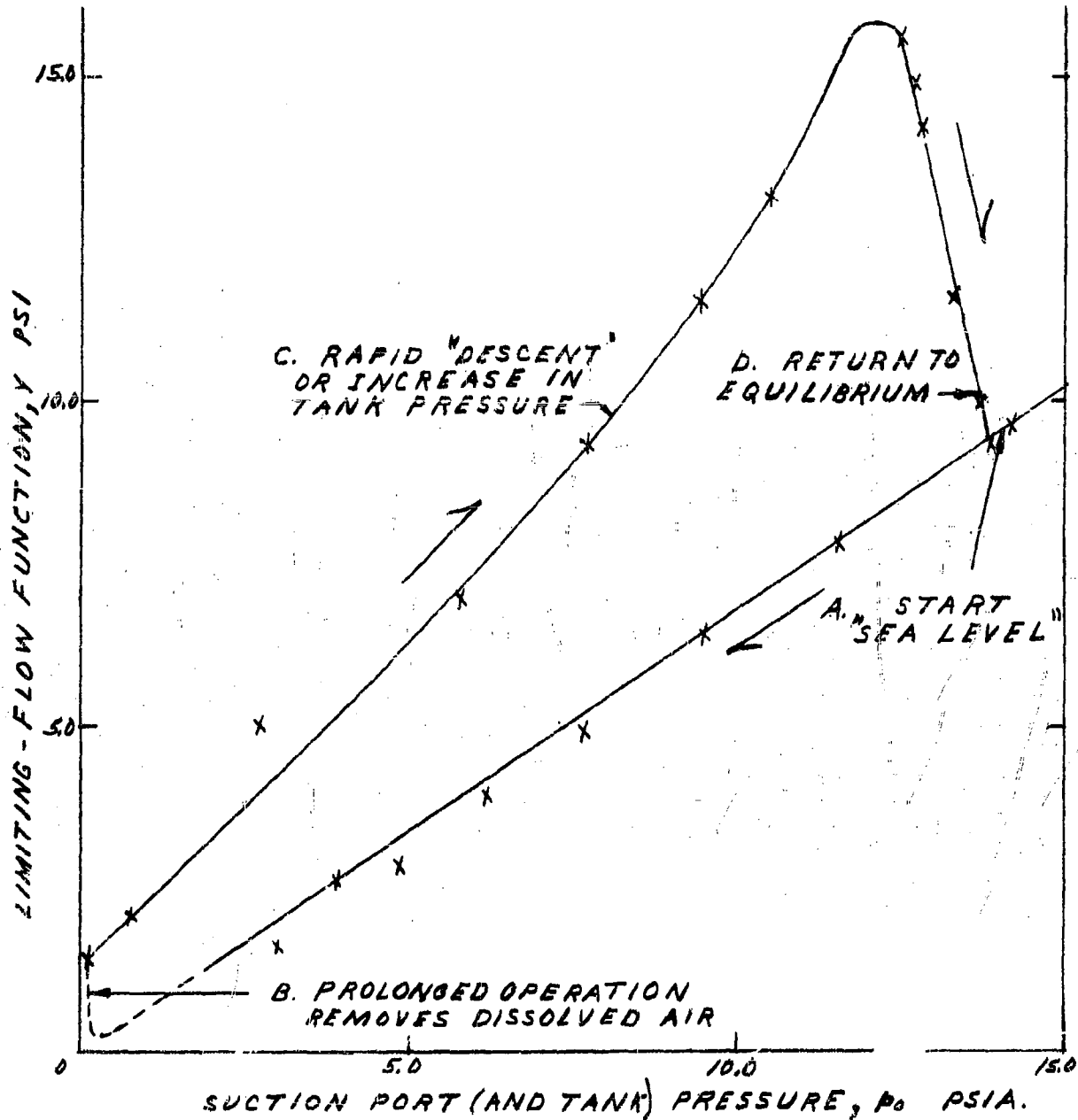
FIG. 27 INCREASE IN LIMITING FLOW AFTER
REMOVAL OF DISSOLVED AIR

JET PUMP PERFORMANCE vs NOZZLE FLOW RATE

JET PUMP NO. 100/240/455
TESTS NO. 49,50
OIL GRADE 1005; TEMPERATURE 70°F
BACK PRESSURE P_{ti} = 3.56 PSIG.
SIDE PORT PRESSURE P_o = 14.1 PSIA.
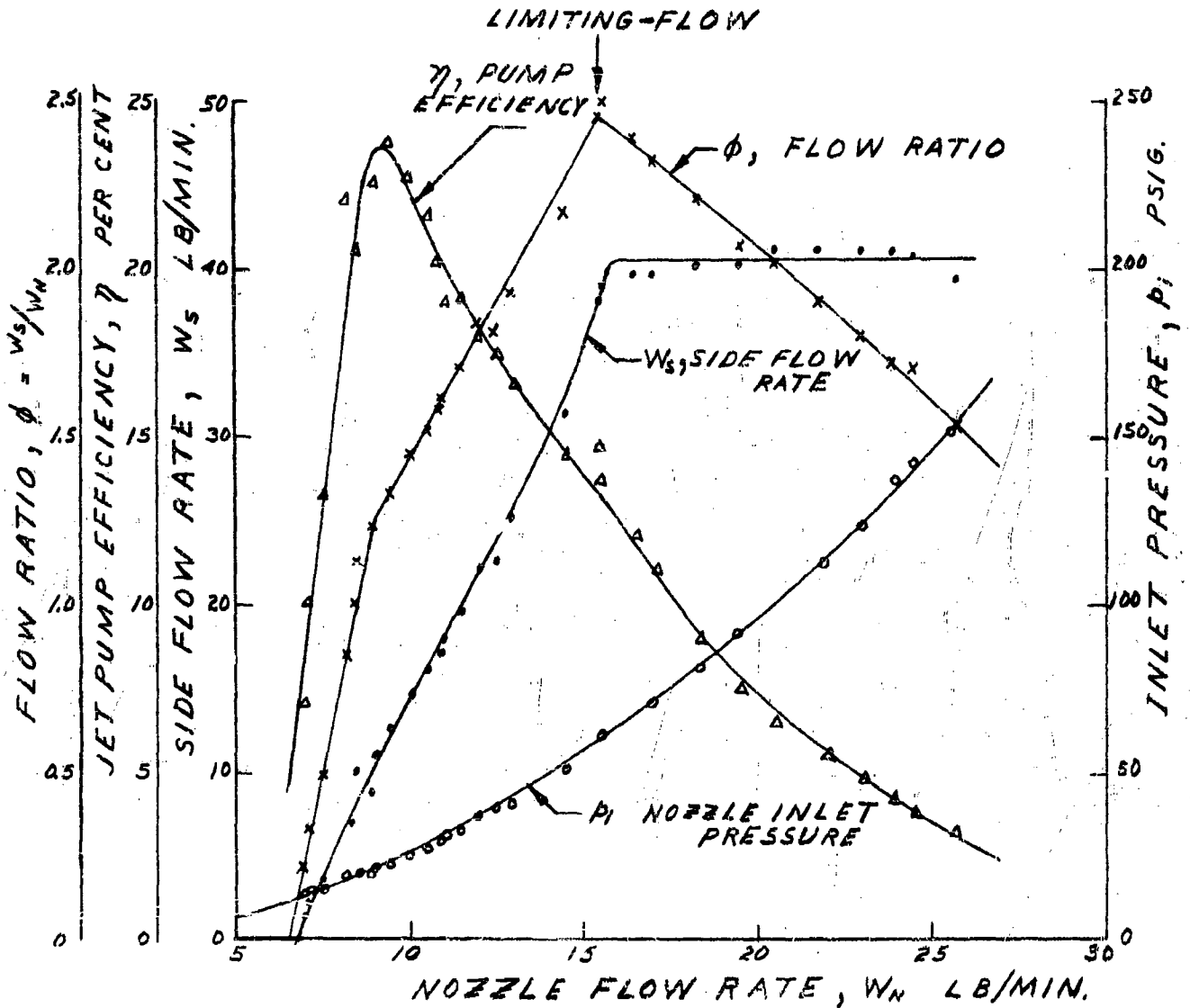
FIG. 28   SHOWING FOUR CONDITIONS OF FLOW. NOTE
RELATION OF PEAK EFFICIENCY TO LIMITING - FLOW.

JET PUMP LIMITING-FLOW FUNCTION

OIL TANK EVACUATED TO CONTROL P_o
OIL : GRADE 1005 AT 100°F.
PUMP NO. 141/316/308 , TESTS 143, 144
$(P_i - P_o) = 40$ PSIG.
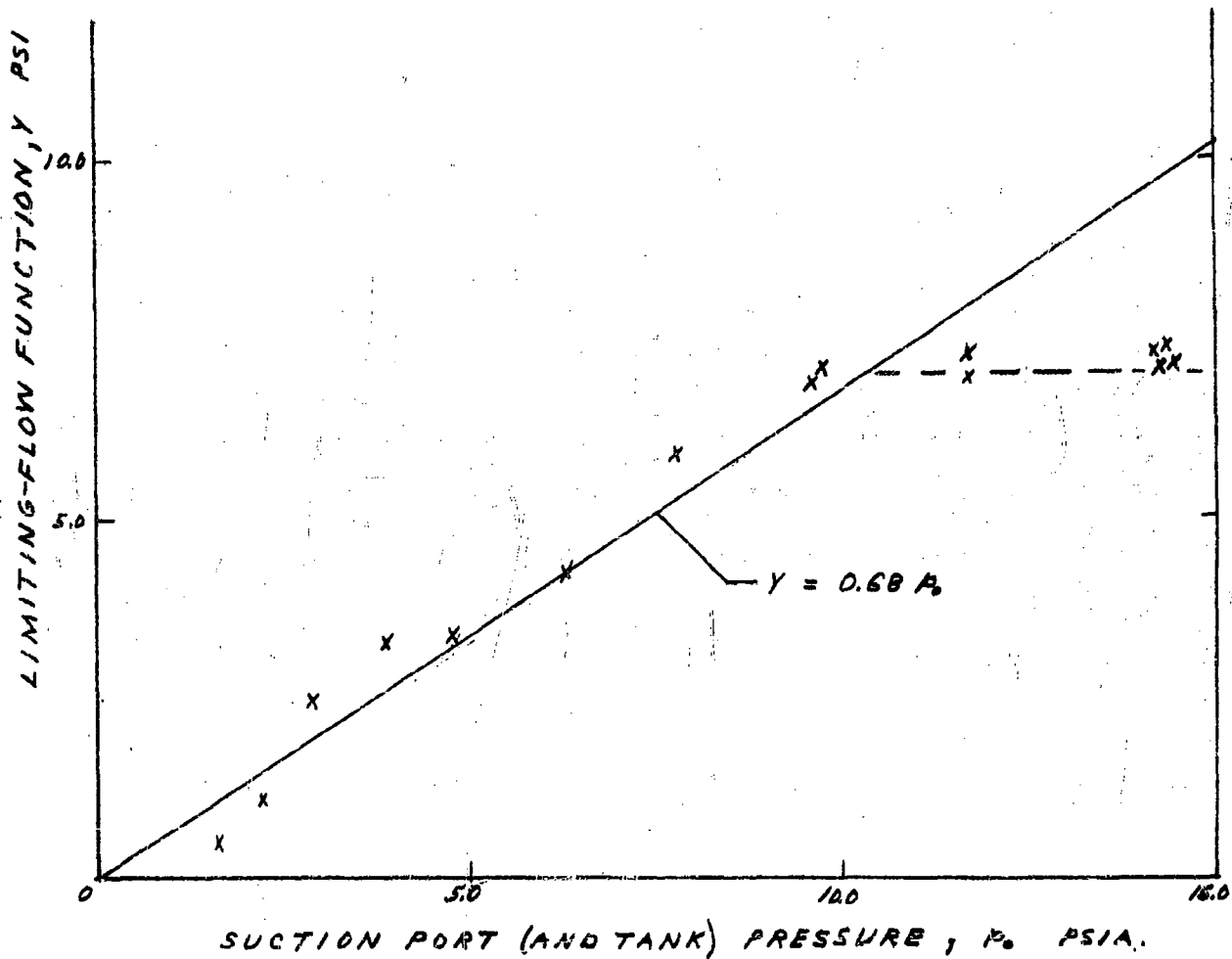
FIG. 29 Y versus P_o FROM TEST WITH LOW JET VELOCITY.
PERFORMANCE UNAFFECTED BY LIMITING-FLOW FOR $P_o > 10$ PSIA.

JET PUMP ALTITUDE CEILING

ASSUMING $\phi_{op} = \phi_L = \frac{2}{3} \phi_{MEP}$

$\eta \approx 21$ PER CENT

-b = 0.1

0.2

0.4

0.6

ALTITUDE CEILING, FT.

SUCTION PORT PRESSURE, P_o, PSIA.

70×10^3
60
50
40
30
20
10
S.L.

b = 0.1
0.2
0.4
0.6

70×10^3
60
50
40

ASSUMING:
$\phi_{op} = \phi_L = \frac{1}{4} \phi_{MEP}$
$\eta \approx 12$ PER CENT

0   50   100   150   200

NOZZLE PRESSURE DROP, $(P_2 - P_o)$ PSI.
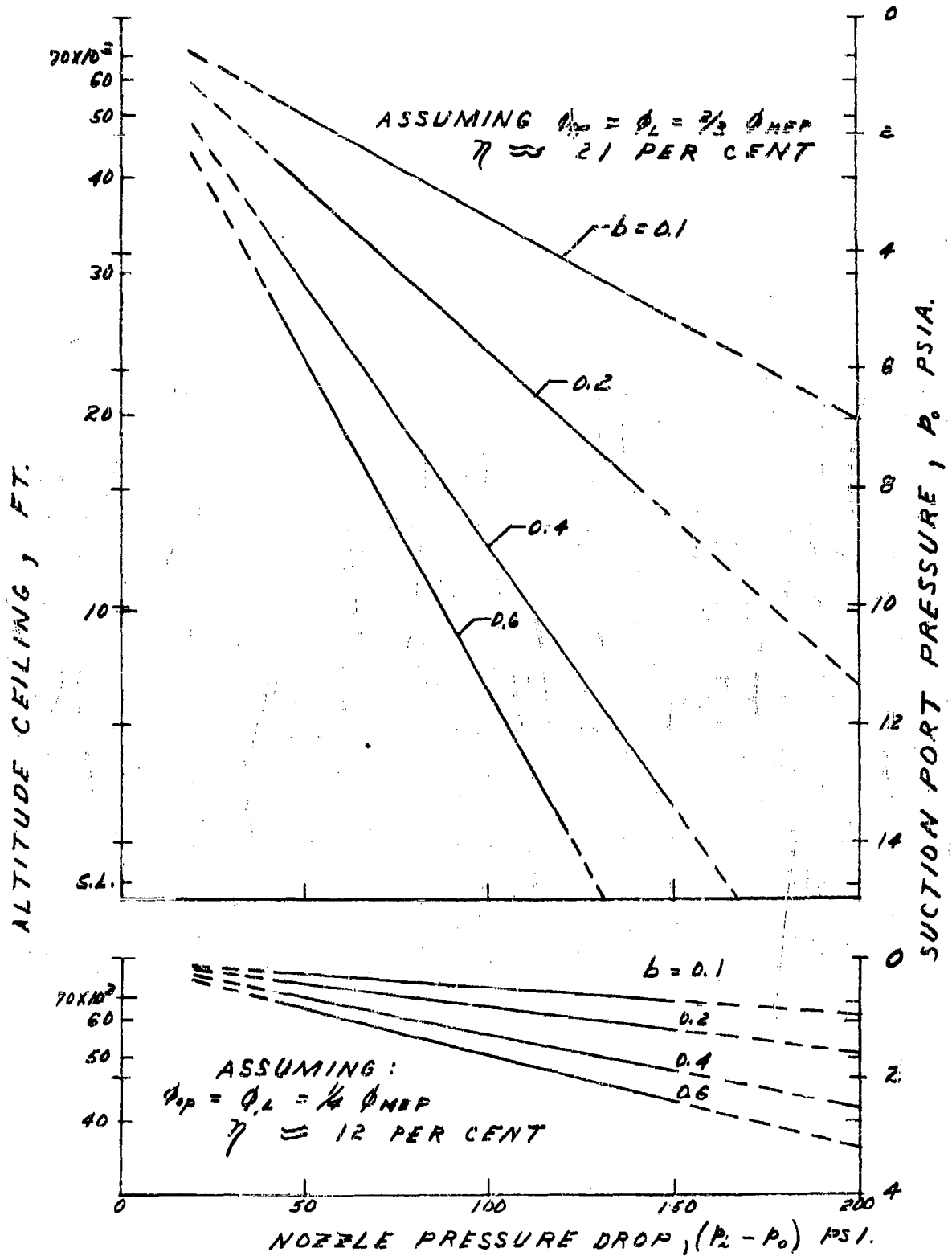
FIG. 30 ALTITUDE CEILING VERSUS NOZZLE PRESSURE DROP.
BOTTOM CURVES SHOW GAIN FROM REDUCING FLOW RATIO.

JET PUMP ALTITUDE CHARACTERISTICS

ALTITUDE : 60,000 FT.

ASSUMING : ALTITUDE = 60,000 FT., P_0 = 1.047 PSIG.

γ = 0.68 P_0

ϕ_{op} = $\frac{1}{4}$ ϕ_{MEP} , (η_{op} = 12 PER CENT)

N AND ϕ VALUES TAKEN FROM

TESTS 173, 179, 153, 148, 166, 164
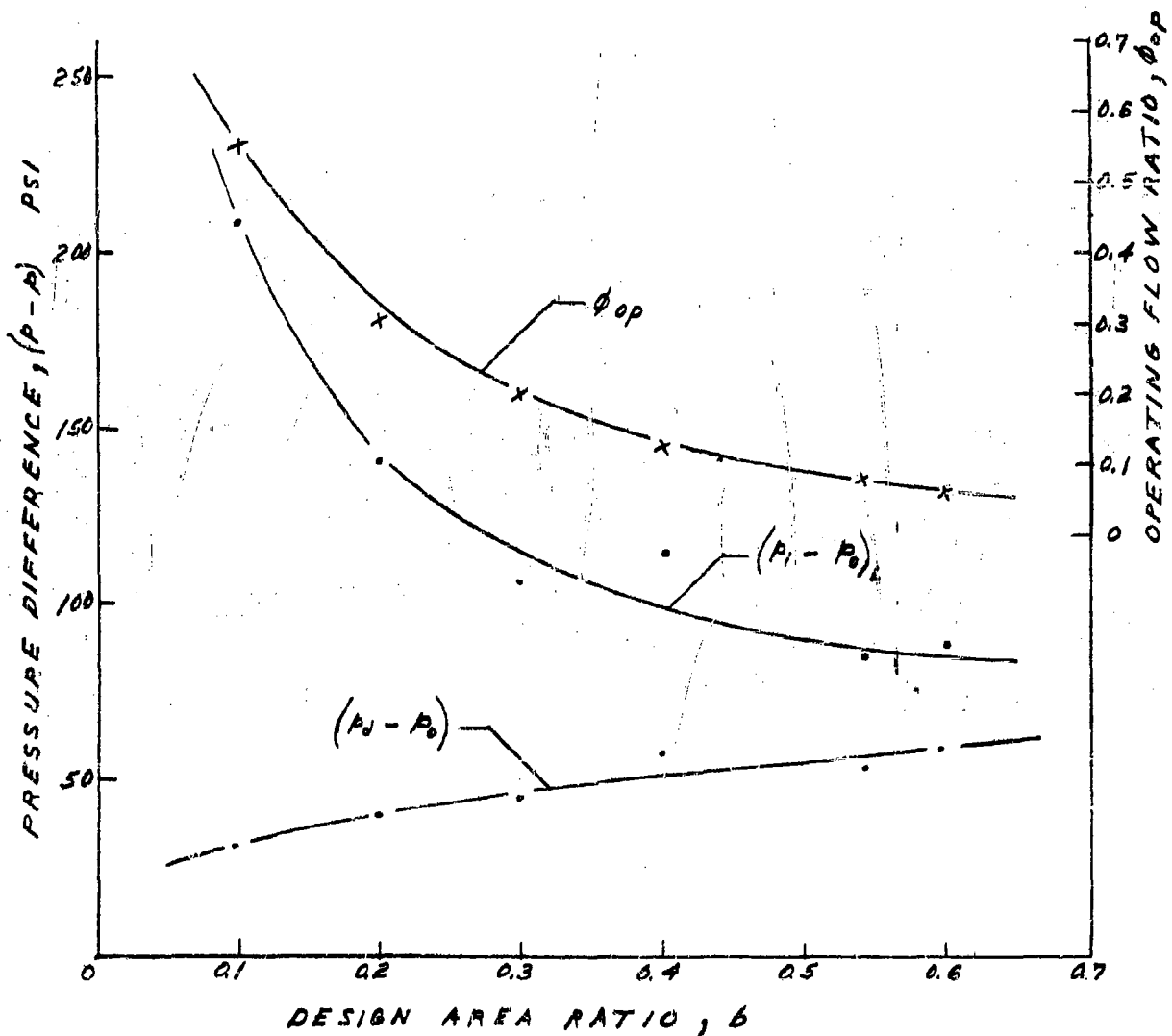
FIG. 31 FLOW RATIO AND MAXIMUM PUMP PRESSURES vs b
FOR OPERATION AT 60,000 FEET.

OPTIMUM NOZZLE-THROAT SPACING
## FOR FOUR-DIAMETER THROAT LENGTH

JET PUMP NO.	b	TEST NOS.
100/316	0.1	92
141/387	0.133	83, 128
141/316	0.2	75, 178, 179
173/316	0.3	152, 156, 158, 159
141/224	0.4	147
173/224	0.6	163

DATA FROM TABLE 7.
FOR JET PUMP DETAILS
SEE FIG. 8
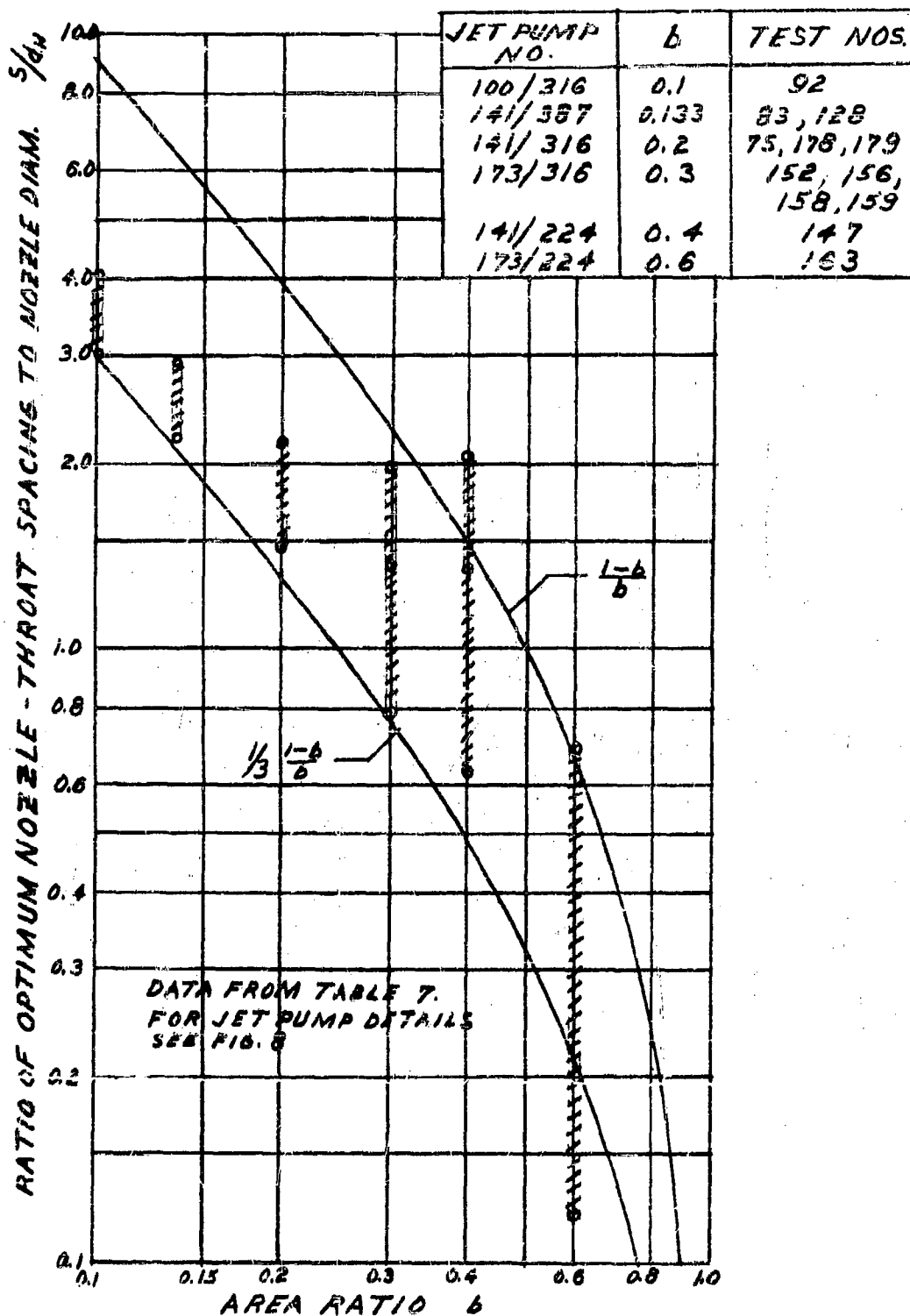
FIG. 32 OPTIMUM NOZZLE-THROAT SPACING VERSUS
AREA RATIO. HIGH JET REYNOLDS NUMBER, $\phi \approx \frac{2}{3} \phi_{MEP}$

JET PUMP LIMITING FLOW FUNCTION

OIL TANK EVACUATED TO CONTROL P_0
PUMP NO. 141/316/VAR. S, b = 0.2.
OIL: MIL-L-7808, SYNTHETIC AT 150°I
$(P_i - P_0)$ = 100 PSI.

SYMBOL	NOZZLE-THROAT SPACING, IN.	TEST NO.
o	0.108	192
x	0.308 (OPT. FOR η_{MAX})	189
Δ	0.508	191
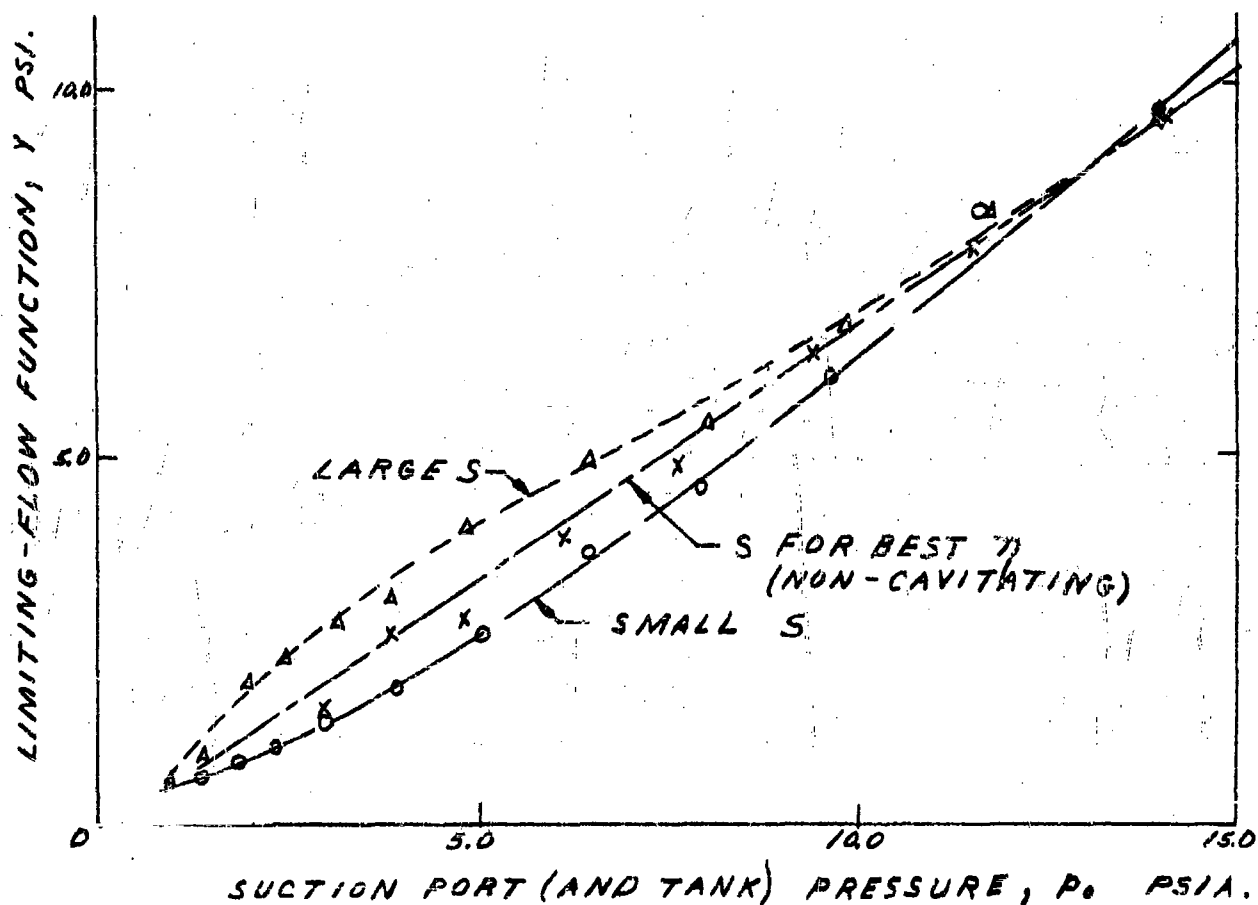


FIG. 33. EFFECT OF NOZZLE-THROAT SPACING
ON LIMITING-FLOW FUNCTION
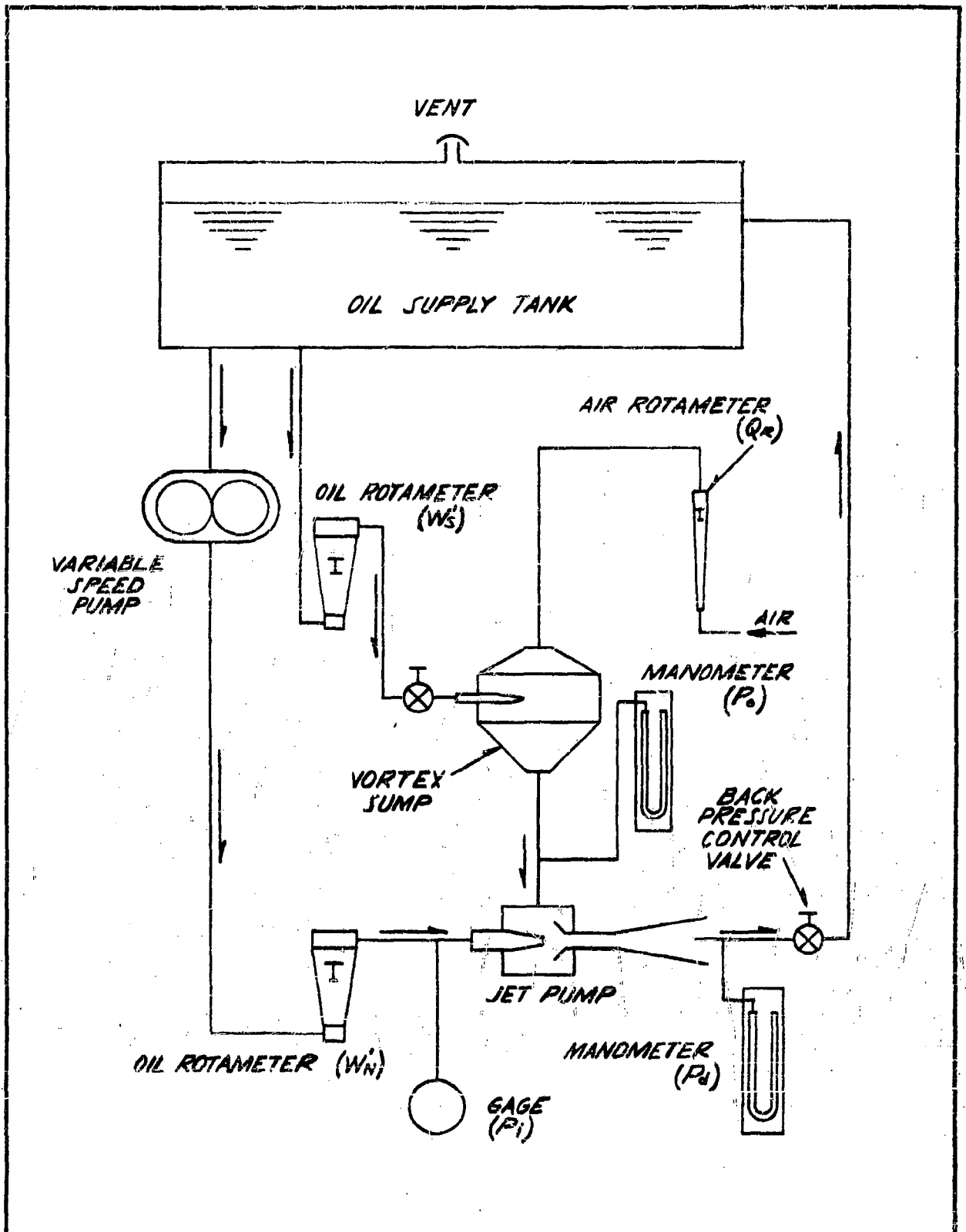
FIG. 34 JET PUMP TEST STAND MODIFIED FOR AIR TESTS

SCALE: ~	THE PENNSYLVANIA STATE COLLEGE	DATE: 2-10-54
DRAWN: CRG.	DEPARTMENT OF ENGINEERING RESEARCH	

JET PUMP PERFORMANCE
vs FLOW RATIO

JET PUMP N? 100/316/307
TEST NO. 100 JAN. 22, 1954
OIL BLEND "B" TEMP. 200°F
VISCOSITY: 6.7 CENTISTOKES
PUMP COND.: W'_N = 12.6 LB/MIN.
P_i = 41.0 PSIG.
P_o = -0.10 PSIG.

PUMP EFFICIENCY - η

PRESSURE RATIO - N

N_A VALUES DURING TEST AT ϕ = 1.58

PRESSURE RATIO-N AND PUMP EFFICIENCY - $\eta = \phi N$

FLOW RATIO - ϕ = W_s/W_N
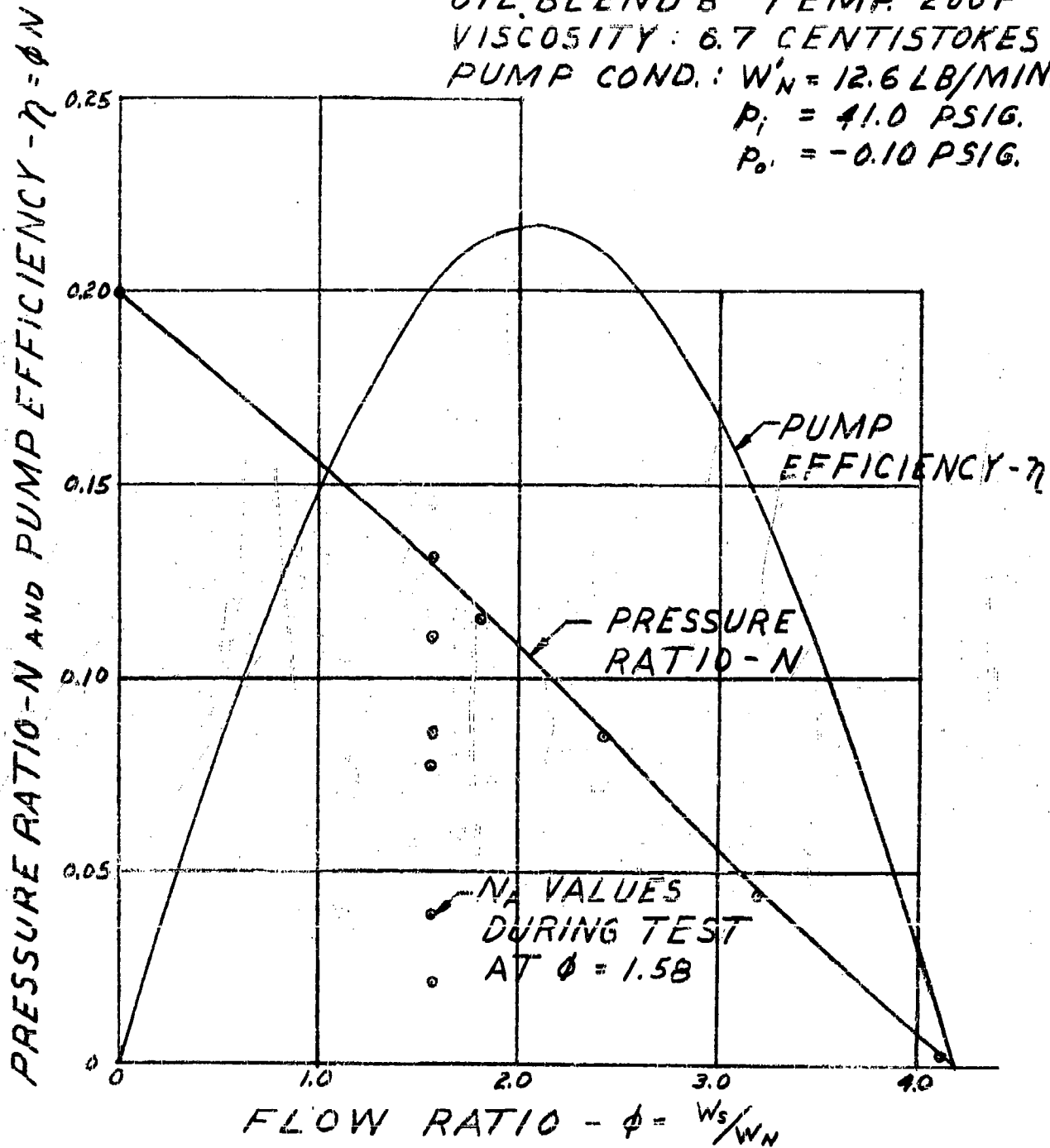
FIG. 35 PERFORMANCE CHARACTERISTIC CURVES

JET PUMP WITH TWO-PHASE
SIDE FLOW
PUMP NO. 100/316/307 , b = 0.10

TEST NO. 100
OIL : BLEND 'B' AT 200°F
W_N^i = 12.6 LB/MIN.
P_i = 40.0 PSIG. NOMINAL
W_S^i = 19.9 LB/MIN.
ϕ = 1.58 } NO AIR FLOW
N = 1.31 }

THEORY

EXPERIMENTAL
RESULTS

AIR FLOW AT SIDE PORT, Q_A, CFM,(NTP)
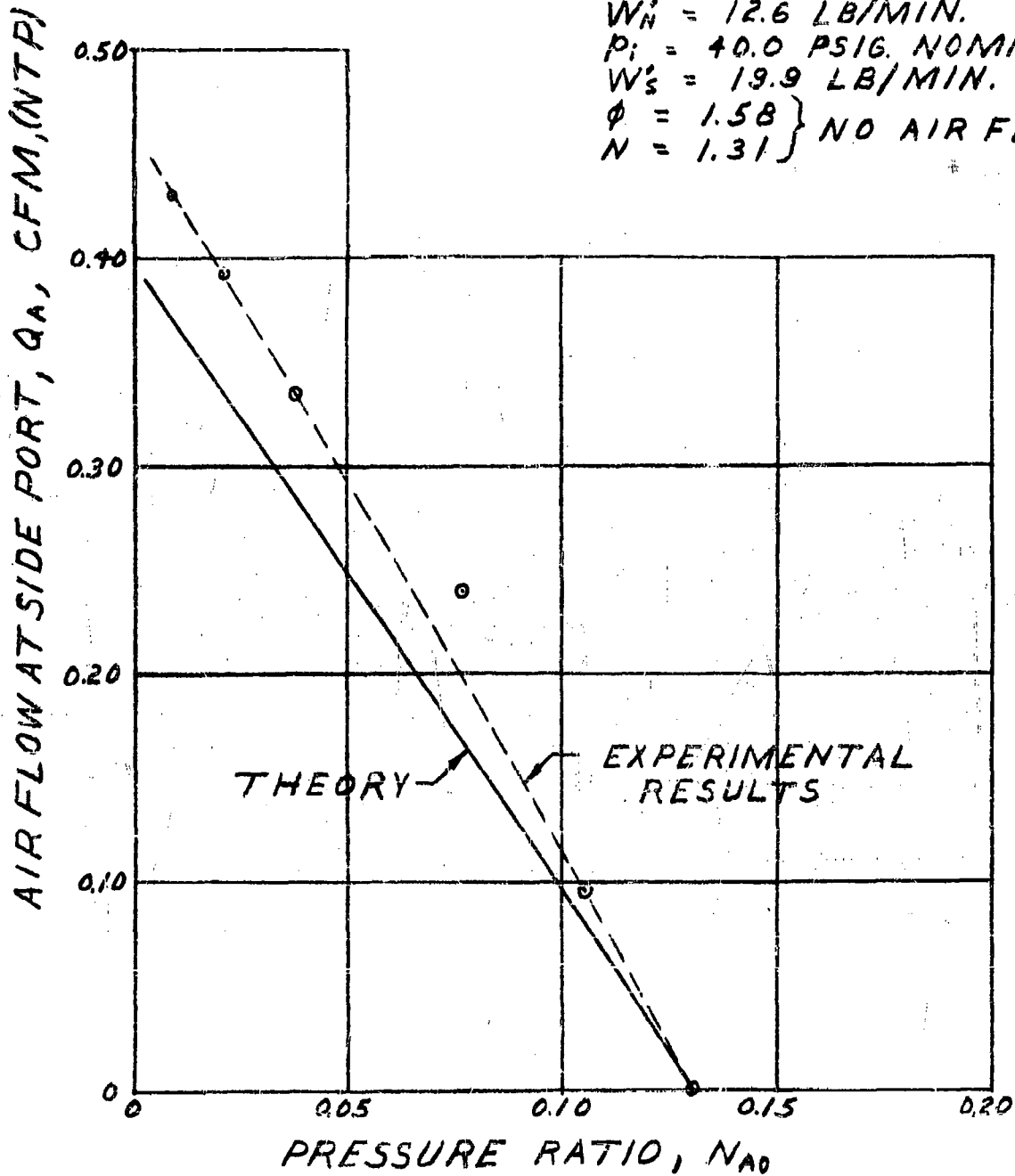
PRESSURE RATIO, N_{A0}

FIG. 36 AIR FLOW vs. PRESSURE RATIO N_A
b = 0.10

JET PUMP WITH TWO-PHASE
SIDE FLOW
PUMP NO. 100/316/307 , b = 0.10

TEST NO. 101
OIL: BLEND "B" AT 200°F
$W_N' = 20.8$ LB/MIN.
$P_i = 100$ PSIG. NOMINAL
$W_S' = 33.2$ LB/MIN.
$\phi = 1.60$ } NO AIR FLOW
$N = 0.127$

EXPERIMENTAL
RESULTS

THEORY

PRESSURE RATIO , N_{AO}

Y-axis: AIR FLOW AT SIDE PORT , Q_A ; CFM (NTP)
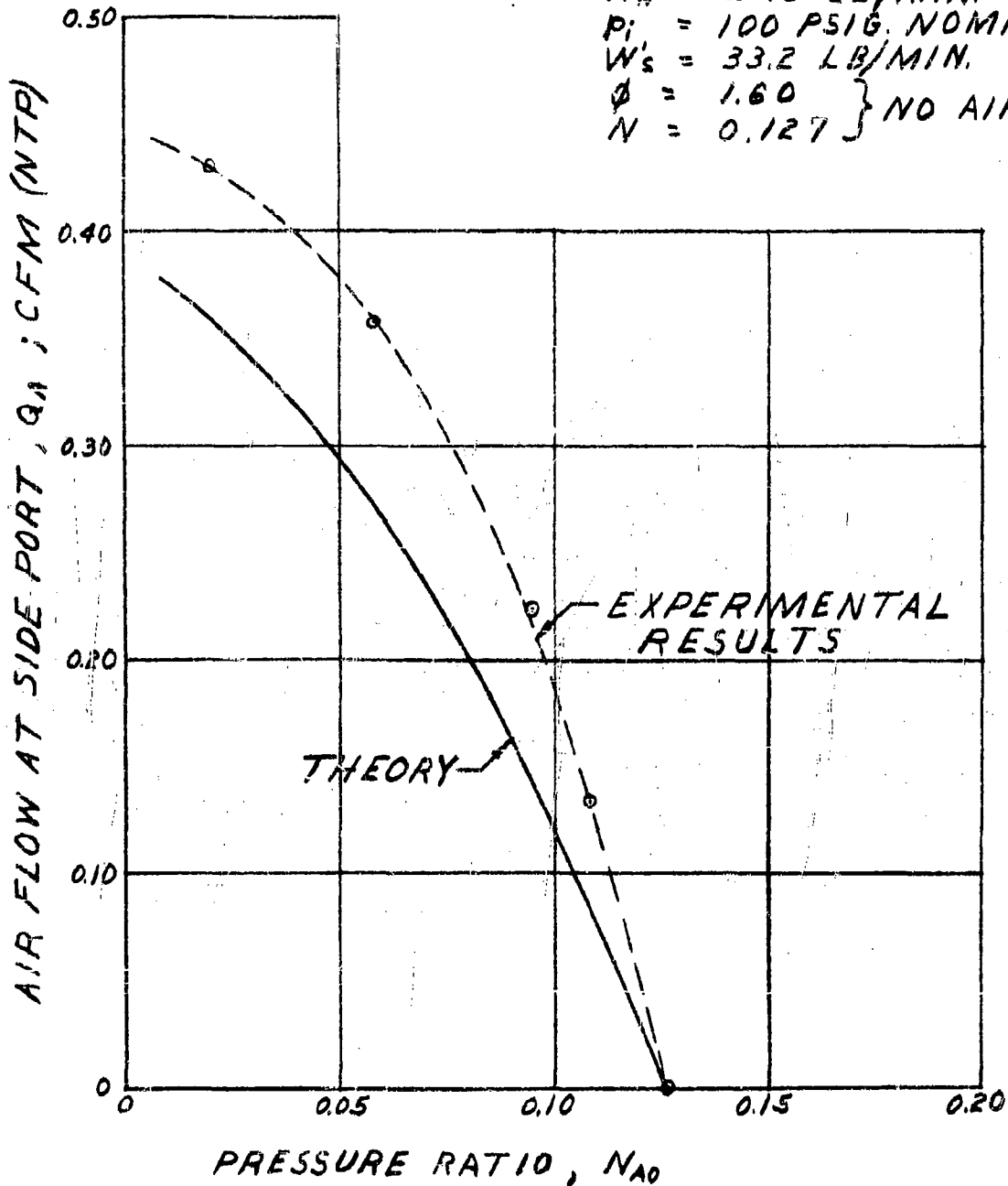
FIG. 37 AIR FLOW VS N_A , b = 0.10 , WITH
HIGH JET VELOCITY

JET PUMP WITH TWO-PHASE
SIDE FLOW

PUMP NO. 141/316/308., b = 0.20

TEST NO. 88
OIL : BLEND "B" AT 200°F
W'_N = 25.8 LB/MIN.
P_i = 40.0 PSIG. NOMINAL
W'_s = 20.3 LB/MIN.
ϕ = 0.787 } NO AIR FLOW
N = 0.156
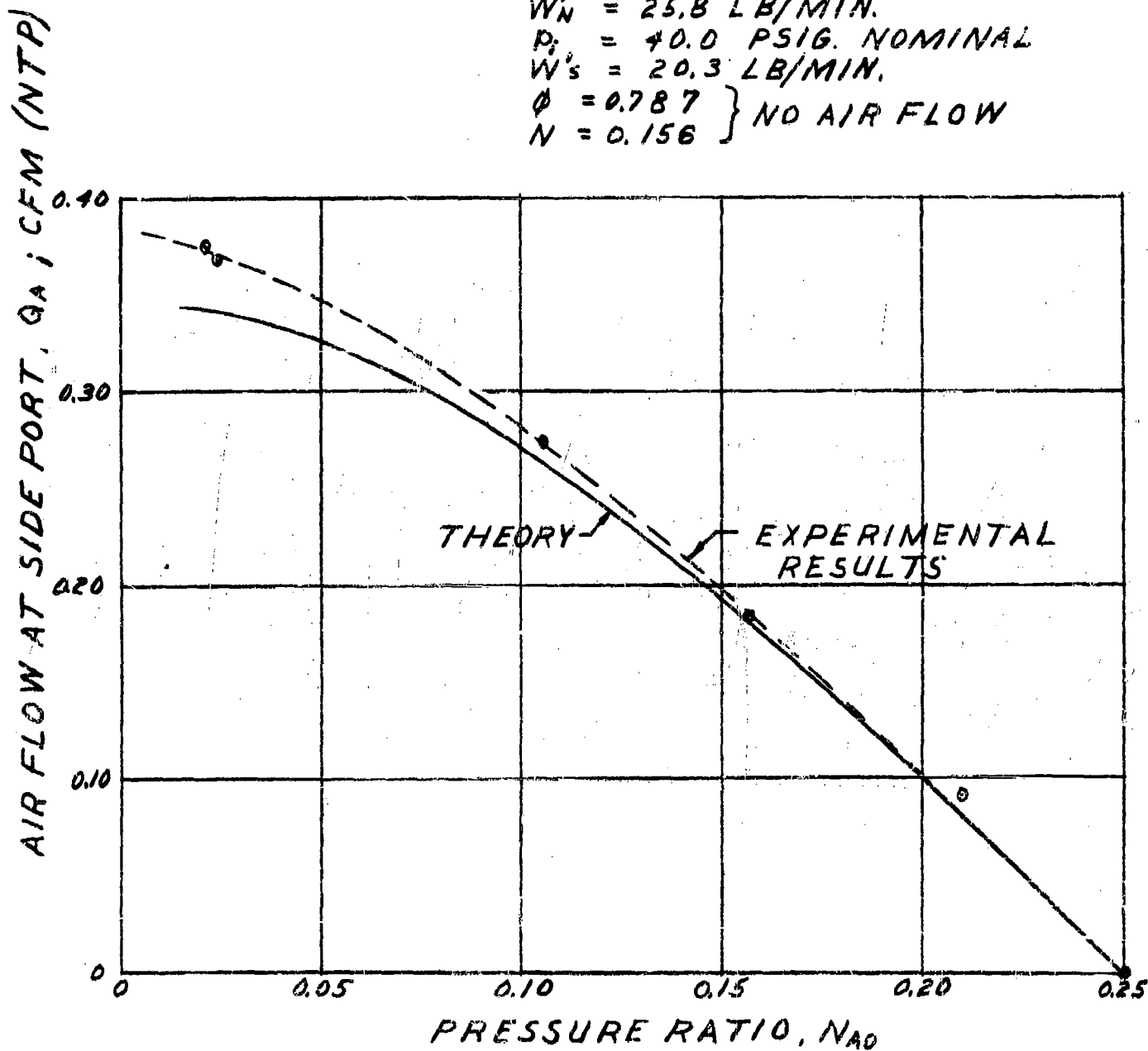
FIG. 38 AIR FLOW vs PRESSURE RATIO N_A, b = 0.20

JET PUMP WITH TWO-PHASE SIDE FLOW

PUMP NO. 177/240/455, b = 0.544

TEST NO. 104
OIL : BLEND "B" AT 200°F
W'_N = 41.67 LB/MIN.
P_1 = 40.0 PSIG. NOMINAL
W'_S = 4.02 LB/MIN.
ϕ = 0.10 } NO AIR FLOW
N = 1.10
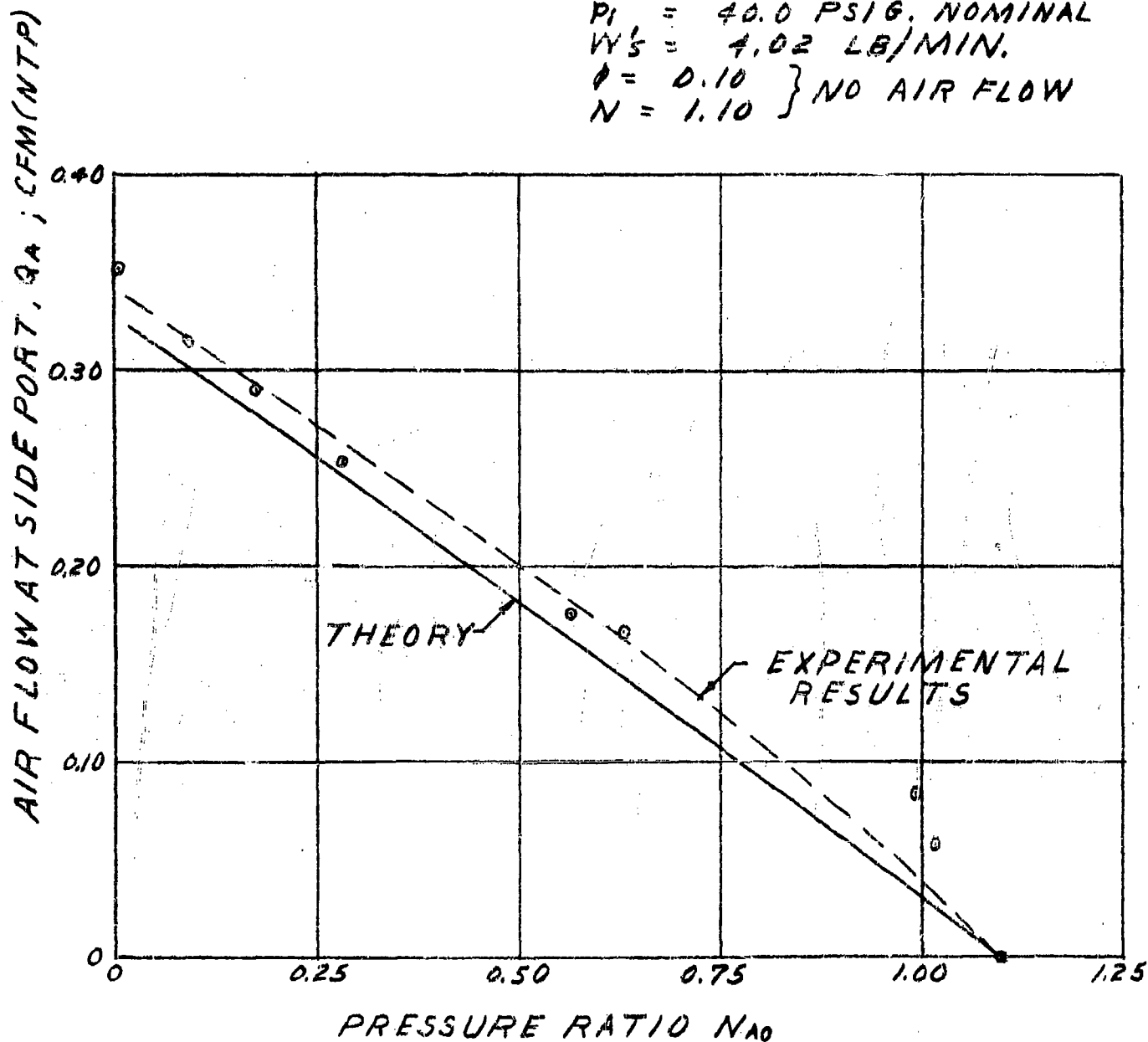
FIG. 39 AIR FLOW vs PRESSURE RATIO N_A, b = 0.544

PERFORMANCE WITH AIR ENTRAINED IN PRIMARY OIL STREAM

PUMP NO. 141/316/308 , b = 0.2

OIL : MIL - L - 7808, SYNTHETIC , AT 150°F.

NOMINAL P_0 = 13.6 PSIA.

SYMBOL	TEST NO.	$(P_i - P_0)_{A \cdot 0}$	W_N	ϕ
O	211	40	28	0.8
X	213	40	28	0
Δ	210	80	40	0.8
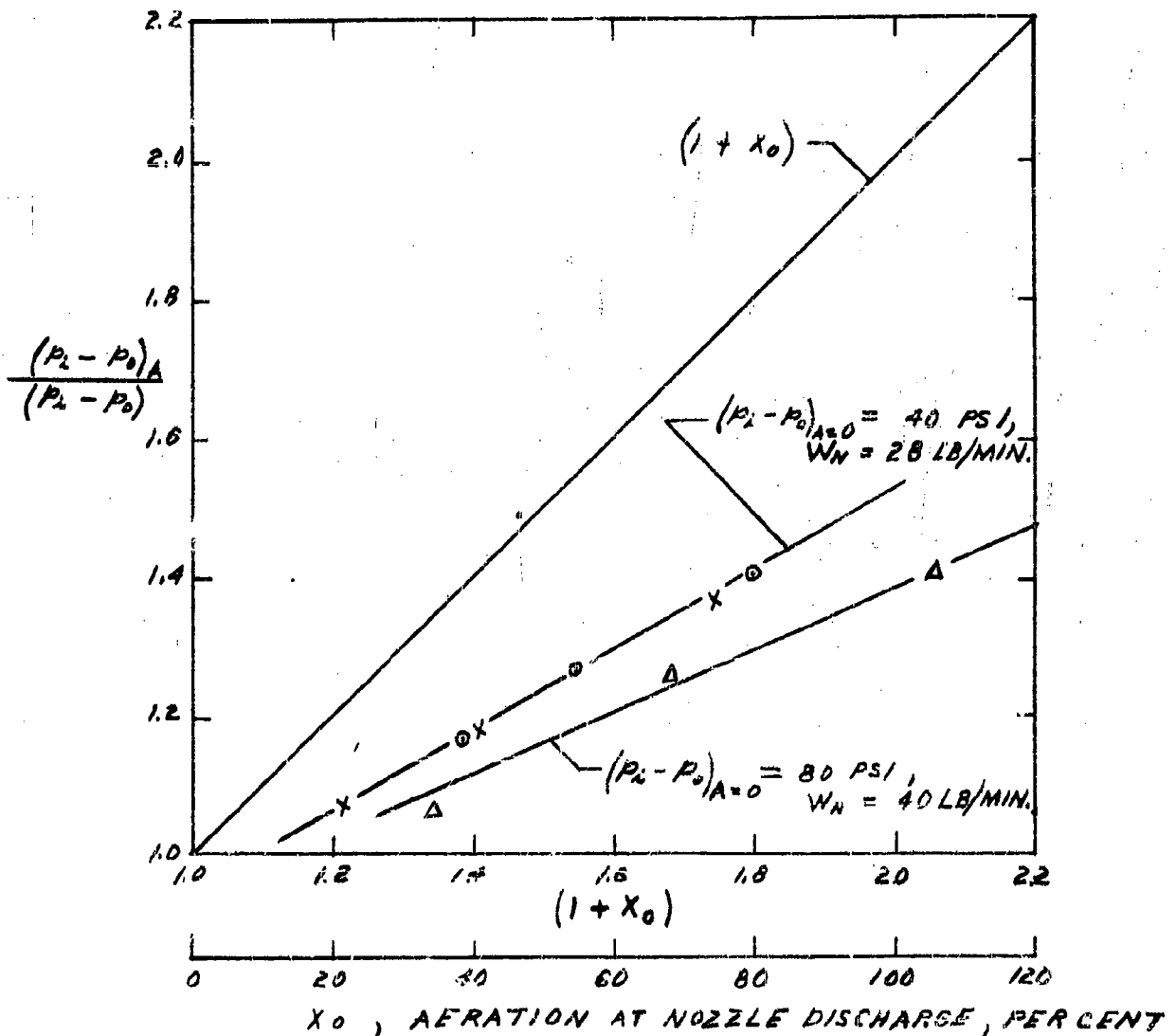
FIG. 40   EFFECT OF AERATION ON NOZZLE
PRESSURE DROP

PERFORMANCE WITH AIR ENTRAINED IN PRIMARY OIL STREAM

PUMP NO. 141/316/308, $\epsilon = 0.20$
OIL : MIL-L-7808, SYNTHETIC, AT 150°F
NOMINAL P_0 = 13.6 PSIA.

SYMBOL	TEST NO.	$(P_d - P_0)_{A=0}$ PSI	W_N	ϕ	P_0 PSIA
⊙	211	40	28	0.8	13.66
△	210	80	40	0.8	13.50
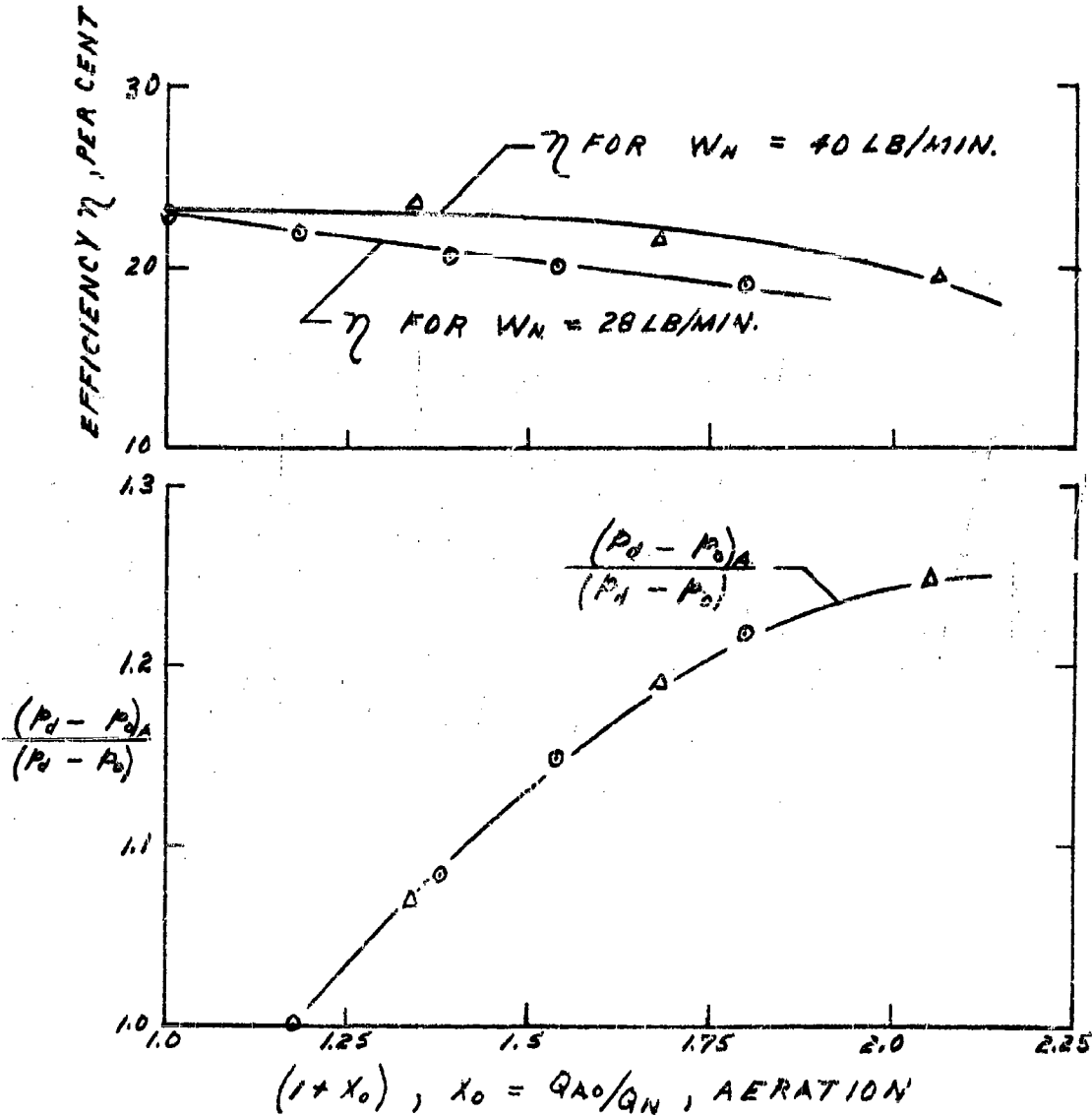
FIG. 41   EFFECT OF NOZZLE FLOW AERATION ON OUTLET PRESSURE RISE AND PUMP EFFICIENCY
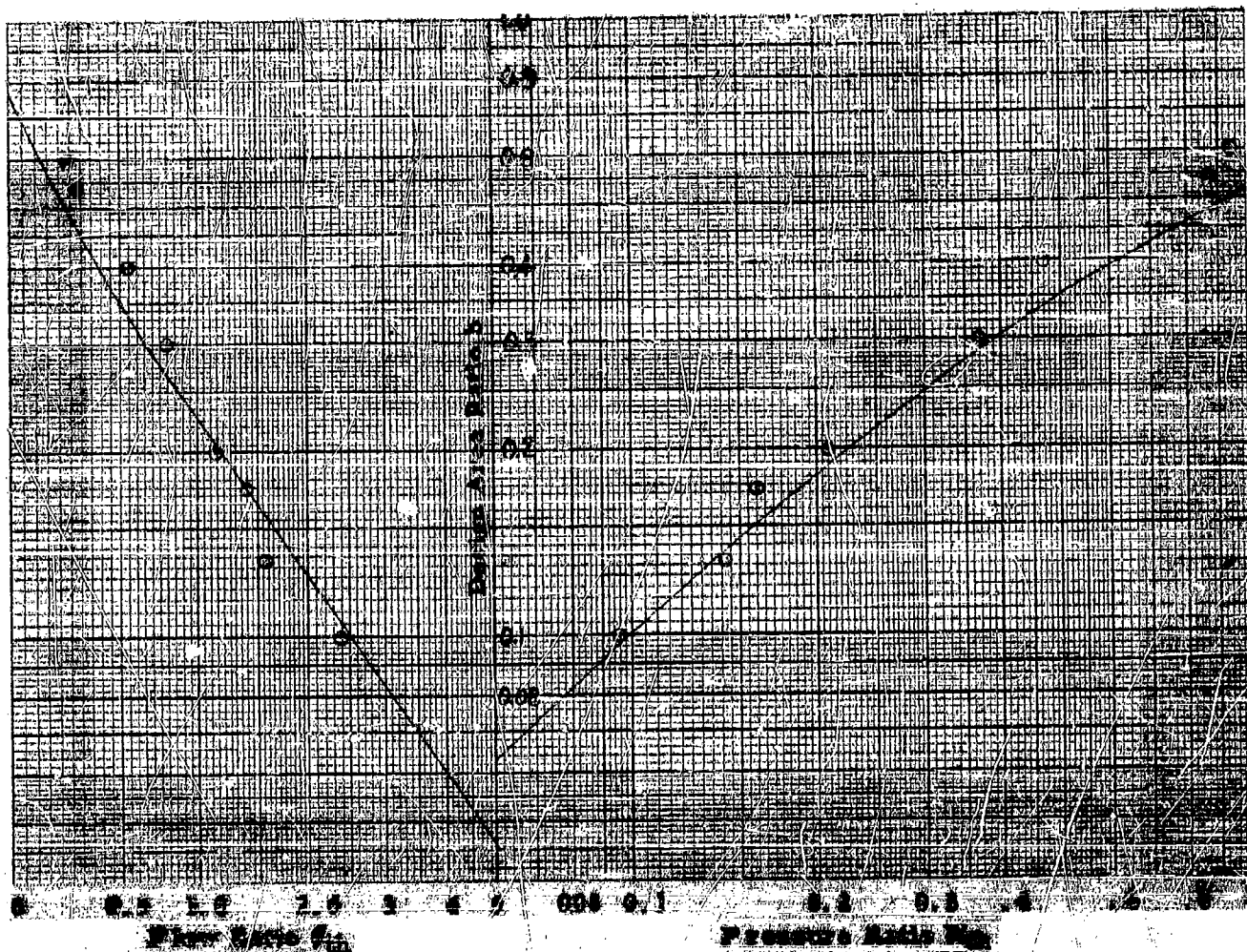
Fig. 42 Relation of Optimum Area Ratio to Flow and Pressure
Ratios. Experimental values of $\emptyset_{mep}$ and N_{mep} from
Table 3 (K_1 values 0.07 to 0.2, K_{34} 0.15 to 0.45).

SPECIFIC GRAVITY vs TEMPERATURE
FOR
MIL-L-7808 TURBINE
MIL-G-KORIA GRADE 1060
ALO BLANDS A, B & C FLUIDS WITH ONE OIL
REF 621 SPEC

FIG 45

FIG. 44 VISCOSITY vs TEMPERATURE FOR

MIL-L-7808 SYNTHETIC
GRADE 1100, MIL-O-6082 A
GRADE 1005, MIL-O-6081 A
AND 3 BLENDS OF GRADE
1100 AND 1005

A.S.T.M. STANDARD VISCOSITY-TEMPERATURE CHARTS
FOR LIQUID PETROLEUM PRODUCTS (D 341)
CHART E KINEMATIC VISCOSITY HIGH-TEMPERATURE RANGE
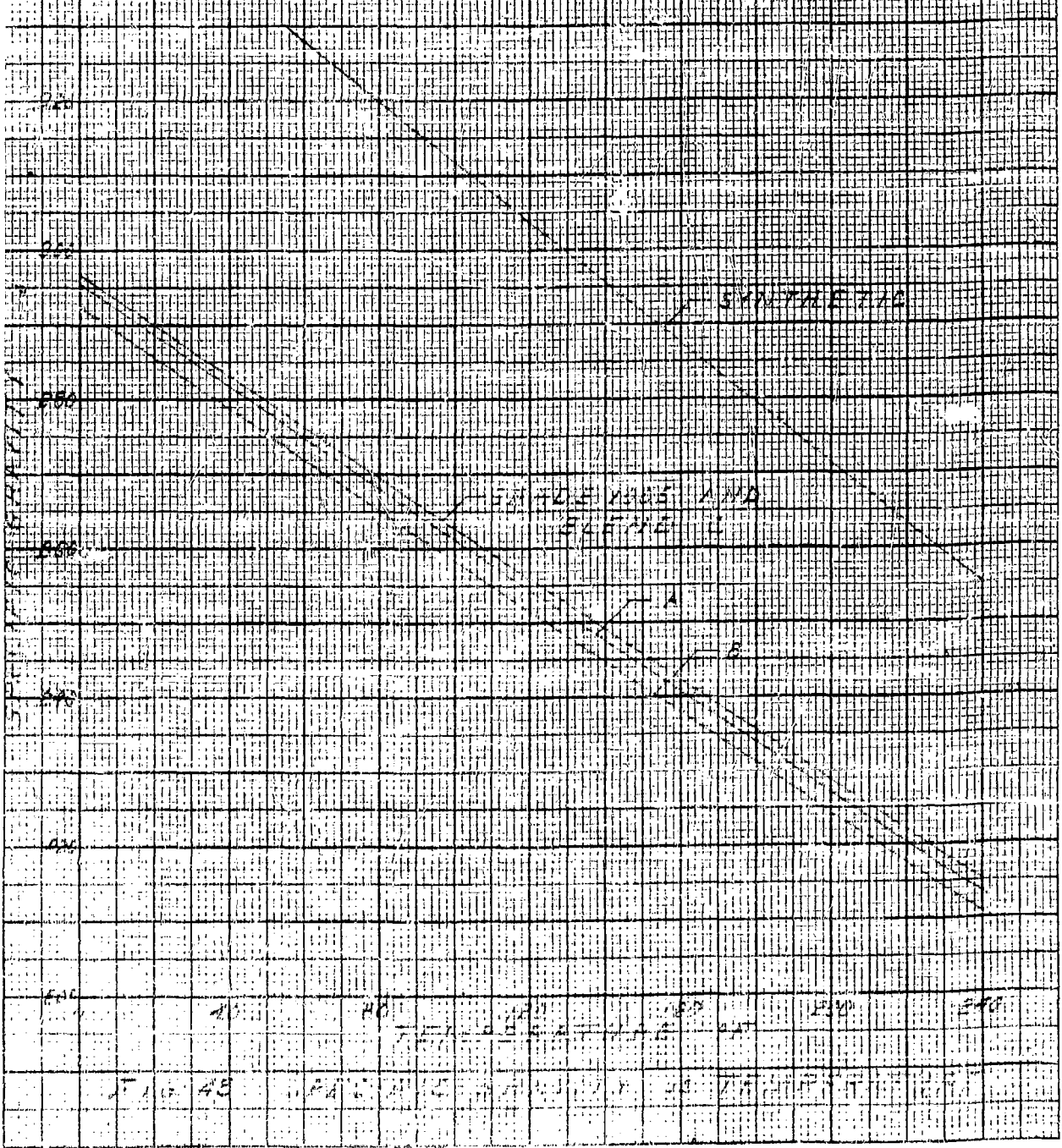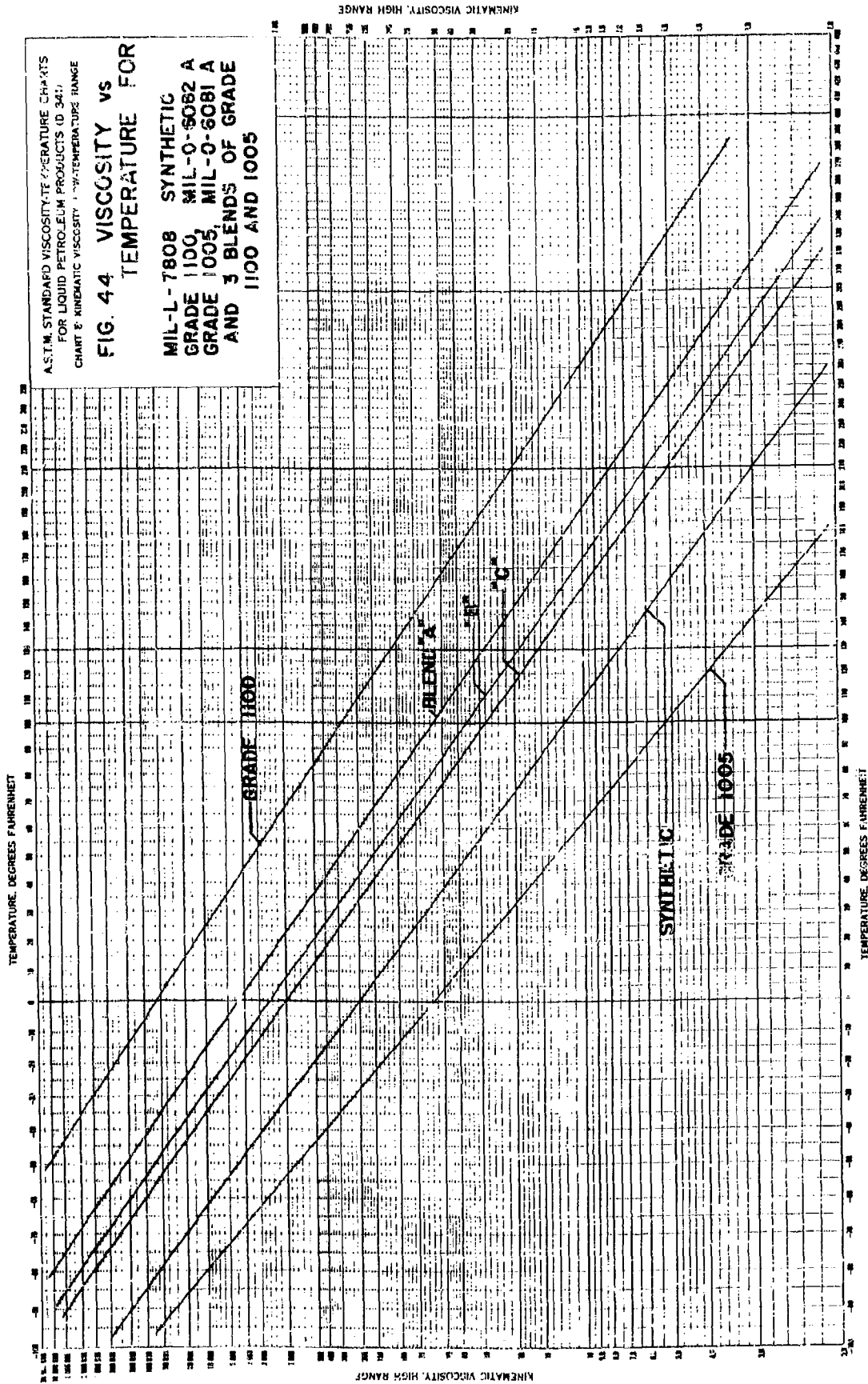
THEORY COMPARED WITH EXPERIMENTAL RESULTS
ON WATER JET PUMPS

DATA: REFERENCE 11

**Solid Line Curves Represent Theory
with $K_i = 0.1$ and $K_{th} = 0.3$**
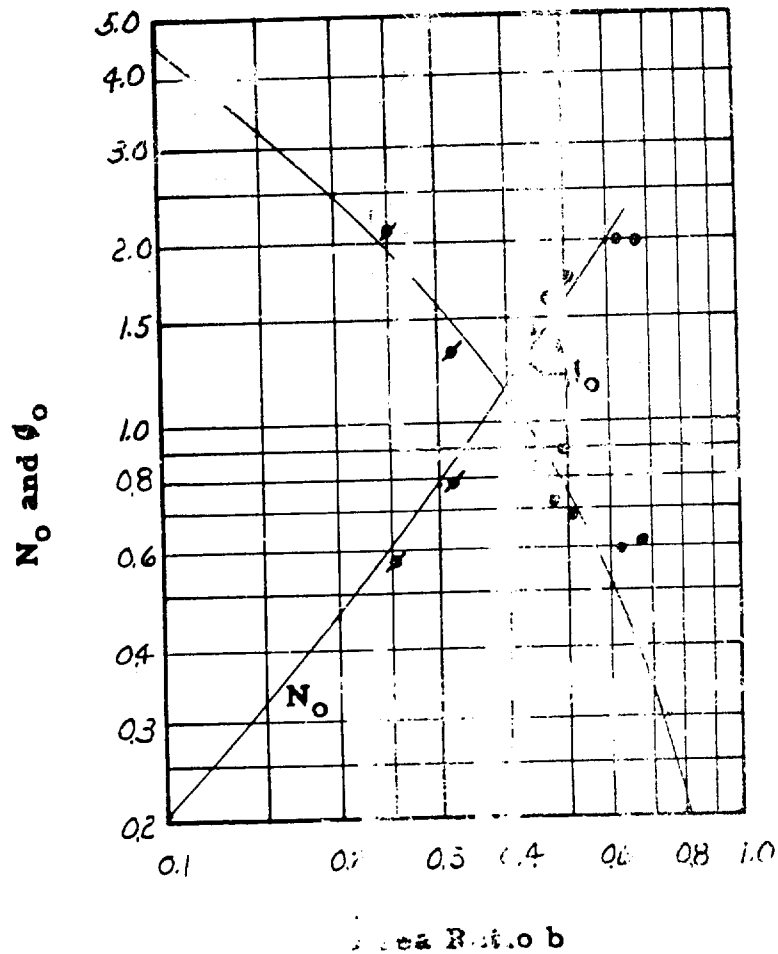
**Fig. 45**   Theoretical Pressure-Difference Ratio at Zero Flow
Ratio, N_o, and Maximum Flow Ratio, q_o, versus
Area Ratio b. Data Points from Stepanoff (11).